ESTI European Society of Thoracic Imaging

ESTI 2019

JOINT MEETING OF ESTI AND THE FLEISCHNER SOCIETY

MAY 09-11, 2019
PARIS, FRANCE

ONLINE ABSTRACT SYLLABUS

Abstracts appear as submitted to the abstract/poster submission system and have not been checked for correctness and completeness.

INVITED ABSTRACTS

Secondary pulmonary lobule anatomy and nodular pattern

H. Prosch; Vienna/AT

Body: A prerequisite for the analysis of the CT pattern in lung imaging is a knowledge of the anatomy of the architecture of the secondary pulmonary lobule. The secondary pulmonary lobule is the smallest anatomical unit of the lung bordered by connective tissue septa. Analysis of HRCT images should aim to narrow the differential diagnosis by attributing CT patterns to the components of the secondary pulmonary lobule: the interlobular septa; the centrilobular structures; or the lobular parenchyma. An understanding of the anatomy of the architecture of the secondary pulmonary lobule is particularly important for the differential diagnosis of nodular lung diseases. Nodular lung diseases are best characterized by the distribution of the nodules, which can be centrilobular, random, or perilymphatic.
Centrilobular nodules arise from the peribronchovascular bundle, and thus, the differential diagnosis includes bronchiolar diseases (i.e., hypersensitivity pneumonitis, infectious bronchiolitis, respiratory bronchiolitis, and follicular bronchiolitis) and vascular diseases (i.e., edema, vasculitis, pulmonary hypertension, and metastatic calcification). In contrast to nodules with a random or perilymphatic distribution, centrilobular nodules do not involve the pleura. A particular kind of centrilobular distribution is the so-called "tree-in-bud" sign, which is caused by a filling of small airways with cells, mucous, or blood. On CT, "tree-in-bud" manifests as branching linear opacities, which do not reach the pleural surface.
Nodules with a random distribution are the consequence of a hematogenous spreading of a disease and show a homogenous distribution all over the lung parenchyma, including the pleural surface. The differential diagnosis of nodules with a random distribution includes miliary tuberculosis, miliary metastases, and a miliary distribution of fungal infections.
Nodules with a perilymphatic distribution are, in most cases, caused by sarcoidosis, pneumoconiosis, or lymphangitis carcinomatosa. In a perilymphatic distribution, nodules are found along the pleura, the walls of the secondary pulmonary lobule, and the bronchovascular bundle.
By following such a structured approach to the distribution pattern, the list of differential diagnoses should be narrowed, and thereby, provide guidance for additional diagnostic steps with which to diagnose the underlying disease.

Take Home Points:
- The secondary pulmonary lobule is the smallest anatomical unit of the lung bordered by connective tissue septa
- Nodular lung diseases are characterized by the distribution of the nodules within the secondary pulmonary lobule
- Distribution types of pulmonary nodules are centrilobular, random, or perilymphatic

Linear and reticular pattern

F. Molinari; Tourcoing/FR

Body: The reticular pattern is one of the imaging findings that may suggest the presence of a diffuse parenchymal lung disease at HRCT. Reticulations are typically formed by a collection of innumerable small linear opacities that by summation produce an appearance resembling a „net". Lines may vary from smooth to nodular and irregular. The resulting „net" may alter the normal HRCT appearance of the lung and become suspected for an underling lung disease. Chest radiologists typically use a structured approach to interpret this finding and eventually to propose a diagnosis. The radiologic approach consists in identifying the dominant types of lines, in establishing what portion of the lung interstitium is predominantly involved, and in correctly classifying the type of reticulation (namely inter-lobular, peri-lobular, intra-lobular). When all the radiologic features are correctly interpreted, the radiologist can differentiate reticulations that represent an acute disease from those that indicate a chronic inflammatory or fibrotic change in the lung. In addition, by integrating clinical and laboratory data, it is possible to significantly narrow the final differential diagnosis.

Take Home Points:
The correct interpretation of the linear and reticular patterns on HRCT helps narrowing the differential diagnosis especially in the context of diffuse parenchymal lung disease.

GGO opacities and consolidation

M. Silva; Parma/IT

Body: High-resolution computed tomography (HRCT) has an established reference role in the imaging of the chest. The detailed assessment of anatomical pulmonary involvement allows for differentiation of pulmonary findings and their integration with clinical diagnosis.
Ground-glass opacity (GGO) is a common finding in HRCT, which is reported in the vast majority of lung diseases, as well as within the normal range of parenchymal appearance. Such kaleidoscopic etiology confers to GGO the fame of "unspecific finding", however it is of great importance in clinical practice for the diagnosis and prognostication of lung diseases.
Consolidation appears as a homogeneous increase in pulmonary parenchymal attenuation that obscures the margins of vessels and airway walls, air bronchogram may be present . The attenuation characteristics of consolidated lung are only rarely helpful in differential diagnosis, contrast enhanced images can narrow the differential, awarenes of clincial indication and drug administration is especially helpful to drive the clincial reasoning beyond such simple and common HRCT finding.

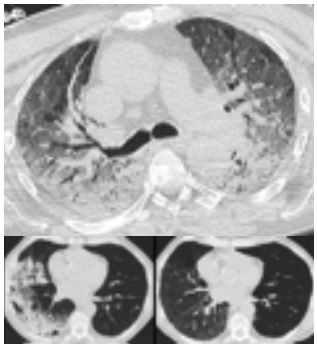

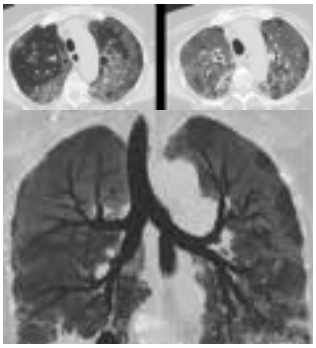

Take Home Points:
Patterns of disease presentation can be recognized and drive the mainstream of clinical differential in diseases that involve airspaces. Clinical intergation is manadatory for the appropriate interpretation of HRCT patterns. HRCT can depict the heterogeneity of the disease with several pattern coexisting, yet a dominant pattern can be recognized to drive the clincial interpretation.

Approach to cystic lung diseases

A. Oikonomou; Toronto, ON/CA

Body: The predominant patterns of cystic lung disease are seen in pulmonary Langerhans cell histiocytosis (PLCH) and in lymphangioleiomyomatosis (LAM).
PLCH is a rare type of histiocytosis occurring in smokers, characterized by infiltration of tissues with dendritic Langerhans cells. PLCH may exclusively involve lungs or rarely be part of multisystem disease. HRCT findings include nodules, combination of nodules and cysts or only cysts with upper lobe distribution and sparing of lung bases. Coexistence of cysts with GGO is common. Cysts are bizarre-shaped, thin or thick-walled and variable in number and size. Nodules with or without cavitation have a centrilobular location. Pneumothorax may be the initial manifestation.
Lymphangioleiomyomatosis (LAM) is a rare cystic lung disease caused by infiltration of the lungs with smooth muscle cells. It occurs in patients with tuberous sclerosis (TSC-LAM) and in a "sporadic" form (S-LAM), exclusively seen in women of reproductive age.
Parenchymal lesions in LAM mainly include cysts, which are thin-walled, well-defined, rounded, may reach large numbers and have no zonal predominance. Nodules are extremely rare in S-LAM and are more commonly seen in TSC-LAM. They may either be solid or ground-glass and usually tiny. They represent multifocal micronodular pneumocyte hyperplasia. Pleural manifestations include chylothorax and pneumothorax. Chylous pericardial effusions may be seen. Recent guidelines for the diagnosis of LAM classify LAM as definite, probable and possible.
When both cysts and nodules coexist then PLCH must be differentiated from lymphocytic interstitial pneumonia (LIP), amyloidosis or light-chain disease. When only nodules or only cysts are present then differential diagnosis includes nodular diseases (only for PLCH) such as sarcoidosis, silicosis, tuberculosis, amyloidosis and metastases or cystic lung diseases (both for PLCH and LAM) such as LAM and PLCH respectively, Birt-Hogg-Dubbe (BHD), LIP and amyloidosis. If cysts coexist with GGO then PLCH is differentiated from Pneumocystis jerovecii pneumonia (PJP), desquamative interstitial pneumonia (DIP) and LIP. In LIP the cysts are round and variable in size but usually small and random in distribution surrounded by ground glass opacity. LIP is associated with pericystic soft tissue nodules which may calcify and represent amyloid deposits. In BHD the cysts are elliptical in shape and have a subpleural, lower zone predominance adjacent to vessels. In amyloid the cysts are variable in size but usually large and diffusely distributed.

Nodules are seen in PLCH, amyloid or light chain disease and LIP. Neurofibromatosis may also rarely present with lung cysts. Other diseases may mimick true cystic lung disease such as centrilobular emphysema, cystic bronchiectasis and metastatic disease.

Take Home Points:
Different entities may present with true lung cysts or combination of true cysts and nodules as well as other ancillary pulmonary findings.
Accurate description of the morphology, size, number, distribution and location of the cysts as well as of the other primary or ancillary peuroparenchymal findings coupled with a detailed clinical history of the patient will narrow significantly the differential diagnosis and will finally lead to the correct diagnosis.

Radiological assessment

T. Frauenfelder; Zurich/CH

Body: Lung nodules are common radiological findings in the clinical practice and the majority of them remain indeterminate at imaging. Determination of lung nodule malignancy is pivotal because the early diagnosis of lung cancer could provide a curative intervention. Therefore, the correct interpretation and management of a lung nodule represent relevant issues for radiologists. The probability of nodule malignancy depends from patient risk factors and nodule characteristics (size, morphology, attenuation, growth). In addition, management is substantially influenced by the nodule size, attenuation and growth rate.
Pulmonary nodules, if defined as such, can be classified into three categories: solid nodules, subsolid nodules, and ground-glass nodules. A fourth entity is the perifissural nodes. Although the classification of nodules into the individual classes may seem simple at first glance, different studies show that even experienced radiologists achieve only moderate agreement. The reason for this is on the one hand a lack of clear definition of each nodule type as well as the subtle nuances in particular of small nodules.
If one sees the classification of lung nodule as a continuum with the solid node at one end and the ground-glass node at the other end, it quickly becomes clear that the greatest variance exists in the sub-solute nodes. This is also reflected in various studies. Since the classification is defined primarily by the density, or the proportion of dense areas, e.g. the representation of the solid parts in the soft tissue window is a good indication for a subsolid node, as shown by Revel et al.
Concerning other methods, which would allow a better differentiation, it has been shown that a histogram analysis leads to a better differentiation. Such is also used in many CAD software today. An even better differentiation allows texture analysis, whereby here malignancy as endpoint plays a higher role rather than the actual classification in the three subtypes mentioned. The so-called deep learning maximally reaches the agreement or the safety as experienced radiologists reach. This is in the cause of nature since the systems also shave in self-training on indications of radiologists with the above-mentioned uncertainties.

Nodule classification

Take Home Points:
Lung nodule classification is a challenging task There is no quantitative standard for nodule type classification PSN most challenging while highes variance The use of different window/level settings provides the highest accuracy Texture analysis or deep learning maybe helpful, but the system trained can never be better than the radiologist providing the input.

Characterization

A.R. Larici; Rome/IT

Body: Lung nodules are common findings in the clinical practice The majority of lung nodules remains indeterminate at imaging, excluding those nodules with certain characteristics of benignity. Determination of lung nodule malignancy is pivotal because the early diagnosis of lung cancer could provide a curative intervention. Therefore, the correct interpretation of a lung nodule is a relevant issue for radiologist. Several are the factors associated with an increase probability of nodule malignancy, in terms of patient risk factors (age, smoking history, previous neoplasm) and nodule characteristics (size, morphology, margins, internal characteristics, attenuation). Nodule growth is another relevant determinant increasing the likelihood of malignancy. Diameter assessment is the method commonly used to measure a lung nodule, even though volumetric analysis (calculated by a semiautomated/automated method) has been increasingly reported over the last two decades as an alternative tool with which to assess nodule growth. Volumetry is a more accurate and repeatable method than diameter measurement, and the volume doubling time (VDT) - time period required for a nodule to double in size – is consider a parameter upon which to determine the further management of the nodule. In this context CAD (Computer-aided-diagnosis) systems have been proposed to assist radiologists in the difficult task of interpreting medical images and in decision making. The most advanced systems based on deep learning (DL)

algorithms are CNNs (convolutional neural networks), which automatically classify all nodule types relevant for the workup. CAD-DL variability in classifying nodules is within the range of inter-observer variability among experienced radiologists. This approach can also be integrated with information taken from radiological quantitative image features (radiomics score of malignancy), with further improvement of the model performance.

Take Home Points:
1. To learn about the characteristics of patient and lung nodule associated with an increased likelihood of malignancy.
2. To highlight the role of imaging and volumetric tools in defining an actionable nodule.
3. To understand the performance of current CAD systems in the characterization of lung nodules.

Management guidelines

A. Devaraj; London/UK

Body: This presentation will review some similaries and differences between the Fleischner Society Guidelines and British Thoracic Society Guidelines for lung nodule management.

Take Home Points:
Decisions to follow up or further investigate lung nodules can be based upon a combination of nodule morphology, nodule size and the use of risk prediction models.

A chest radiography reading guide

M-P. Revel; Paris/FR

Body: Chest radiography is the first line imaging test in patients with thoracic symptoms. It is highly accessible, associated with a low radiation dose but has limited sensitivity. Quality criteria are required to optimize the detection of anomalies. The chest radiograph should include both lung apices and both costophrenic angles. There should be equidistant between the spine of vertebra and medial ends of clavicles, 6 anterior ribs should be counted to ensure sufficient inspiration. For adequate penetration the lower thoracic intervertebral discs should be visible through the heart. Scapula should project out of lung fields. A systematic approach when reading chest radiography is required to avoid missing abnormalities: the mediastinal contours should be analyzed, the higher position of the left hilum and right diaphragm should be assessed, together with symetry of lung parenchyma density and visibility of costophrenic angles. The left heart border is adjacent to the lingula , the right heart border is adjacent to the right middle lobe. Loss of these borders, creating a positive silhouette sign, suggests adjacent pathology. Pulmonary consolidation is characterized by an increased attenuation of the lung parenchyma typically with air bronchograms. Trachea must be visible and in midline, it is pushed towards atelectasis and pushed away from pleural effusion or tension pneumothorax. Special attention should be paid to lung apices, because of bone superposition and frequent location of anomalies

Take Home Points:
Quality criteria are required to optimize the detection of anomalies A systematic approach when reading chest radiography is required Special attention should be paid to lung apices and para hilar regions which are more difficult to analyze

Alveolar, interstitial and nodular syndromes: Lots to choose from

M. Schiebler; Madison, WI/US

Body: Outline
1. AP CXR are for the acute evaluation of tubes and lines not for the diagnosis of lung disease
2. All films should be available for review to show time course of the process
3. Age, Sex, Race, Ethnicity, Travel
4. Electronic medical record
   a. Problem list
   b. Medications
   c. Cancer treatment (current and past)
   d. Cardiac function (LVEF, BNP, Fluids In/out)
   e. Immune reactivity (https://www.pneumotox.com/drug/index/) by Philippe Camus
   f. Symptoms and their duration (fever, shortness of breath, feeling well)
   g. Work exposure
   h. Pet exposure
   i. Smoking exposure

j. Organ transplantation
k. HIV status (T cell count)
l. Lab Results of sputum, pleural fluid, biopsies, gram stain, cultures, cell counts, Hgb
m. Patient metabolome (diabetes types I and II, Obstructive sleep apnea. Sarcopenia)
n. Hiatal hernia and esophageal function (silent aspiration)

5. Location
   a. Right upper lobe
   b. Left and right upper lobes
   c. Lower lobes
   d. Perihilar
6. Single or multiple
7. Symptomatic or not
8. Response to diuresis
9. Bronchoalveolar lavage and/or biopsy

Take Home Points:
A. Multimodality imaging and a wide variety of information may be needed for diagnosis
B. Common diseases can have unusual presentations (TB, Sarcoid, drug reactions)
C. The imaging appearances of infection in the immunocompromised host are unpredictable

Patterns of Lobar Atelectasis

A. Leung; Stanford/US

Body: Radiographic recognition of the patterns of lobar atelectasis is a core skill in the education of radiologists. This talk will focus on the radiographic and CT appearances of lobar atelectasis as well as provide an approach to its differential diagnosis.

Take Home Points:
- Learn to recognize lobar patterns of collapse
- Learn differential diagnosis of lobar collapse

Pleural syndrome

A.P. Parkar; Bergen/NO

Body: Chest radiographs are useful to assess the pleura with little radiation and are easy to perform.
The pleura consists of two fibrous layers, the visceral and parietal pleura. Normally it is not visible on radiographs. However, when there is pathology, either thickening or air in between, it becomes visible.
Usually there is about 10ml physiologic pleural fluid. Plerual effusion can occur as exudate, transudate, empyema or hematothorax. The differention between these is only possible on CT. Pleura effusion is first visible on lateral radiographs when it is more than 75-100ml, on the front radiograph when beyond 175-500ml, on supine images beyond 300ml.
Normally the pleural effusion has a lateral concave shape, compressive pleural effusion has a convex configuration. Sometimes pleural effusion is localised within a fissure and illudes an opacity.
Discrete pleural thickening is easiest to appreciate when there is calcification. Early pleural thickening may be missed on radiographs.
Pneumothorax can be spontaneous (either primary or secondary) or iatrogenic. It is important to recognise the "do-not-miss" state of tension pneumothorax, which can be fatal if left untreated.
Pneumothorax is commonly seen as an area of hyperlucency with lack of vessels in the apical and lateral areas on the radiograph performed standing or sitting. A pneumothorax in the supine position is best seen as the deep sulcus sign as the air moves anteromedially and subpulmonic.
The volume of air within the pleural space has to be at least 50ml on front images. On supine images the volume is minimum 500ml when visible. On lateral decubitus as little as 5ml is visible in the non-dependant areas. Expiration images do not improve detection
A partial pneumothorax is seen when part of the lung is still adherent to the chest wall. To differentiate this from bullous lung disease, it is important to remember that pneumothoraces cause straight or convex lines (from the centre out), wheras bulla cause concave lines.
Pneumothorax when there is also pleural fluid causes an air-fluid level, when the negative pressure between the parietal and visceral pleura is disrupted.

Take Home Points:
Pleural fluid is first seen on lateral view, later on frontal views.
The minimum air-volume needed to produce a visible pneumothorax on radiographs is 5ml in the lateral decubitus and 50ml on the frontal view.
Basal air-fluid level on radiographs is a good indicator of a pneumothorax.

Mediastinal syndromes: What Else Besides Cancer?

L.R. Goodman; Milwaukee, WI/US

Body: There are many acute and chronic conditions of the mediastinum that are seldom discussed because of the imaging emphasis on tumors. Many of these conditions are acute and require rapid and specise workup so that appropriate intervention can be instituted to minimize morbidity/mortality.

Acute conditions to be included:
Acute Mediatinitis (primary, Lemierre's Syndrome)
Post surgical complications
Post radiation complications
Trauma (blunt, penetrating, foreign body)

Subacute/chronic conditions to be included:
Granulomatous infection
Fibrosing mediatinitis
Sarcoidosis
Post radiation complications

Lemierre's Syndrome- Phlebothrombosis, mediatinitis, pulmonary emboli

Boerhaave's Syndrome- esophogeal perforation, mediastinitis

Fibrosing Mediastinitis- bronchial and vascular compromise

Mediastinal varicies simulating a tumor

Take Home Points:
Many non malignant conditions effect the mediatinum. Many require prompt treatment. Awareness of imaging finding required for appropriate management, especially in acute diseases.

The new TNM system: Changes and limitations

A.R. Larici; Rome/IT

Body: Lung cancer is a leading cause of cancer related mortality worldwide. A correct staging is the prerequisite for an adequate management of patients with lung cancer. Recently the 8th edition of the TNM classification introduced relevant changes of the descriptors T and M. Regarding T, it has been demonstrated by survival analyses that from 1 to 5 cm of diameter every centimeter counts, and therefore additional cut points have been added respect to the previous classification. Moreover tumors larger than 5 cm have been better aligned with either T3 (tumor size of more than 5 to 7 cm) or T4 (tumor size of more than 7 cm). This finding further confirms the common intuition that the larger the tumor, the worse the prognosis. Regarding M, the category of extrathoracic lesions has been distinguished in M1b and M1c to indicate respectively one (oligometastatic disease) and more than one lesion. In this context it is advisable that radiologists report the number of lesions if only one organ is involved and the number of organs if many. This approach has a relevant clinical impact because oligometastatic disease nowadays is managed and treated differently respect to an extensive M stage disease. These changes led to an expansion of the number of subcategories for

T and M descriptors and to more stages for a better prognostic stratification of patients. Several limitations still remain, such as categorization of lymphangitic carcinomatosis as an independent descriptor or single tumor involving two lobes across a fissure, and evaluation of multiple lung lesions. Certainties and controversies on the topic will be argued in this session, taking into account that cancer staging should be always considered a multidisciplinary process.

Take Home Points:
- The new TNM staging system added further size cut points and placed additional emphasis on tumor size.
- Single or multiple metastatic foci have different prognostic value.
- More stages have been generated for a more accurate individual patient's prognosis.
- Unsolved issues still remain that should be discussed and further revised.

Immunotherapy: How can imaging help to evaluate the response?

C. Caramella; Villejuif/FR

Body: In the last few years, immunotherapy have rapidly and dramatically been transforming the standard of care in metastatic non small cell lung cancer patients.
Patients under immunotherapy can experience an initial progression followed by a stabilization or response. This phenomon named „pseudoprogression" is described in around 5 % in NSCLC but precise data are still lacking.
Currently, it is recommended, in clinical trials, to continue treatment for all patients exhibiting progression on imaging as long as their clinical status is not deteriorating :new criteria, adapted from RECIST 1.1 and named iRECIST have been proposed in 2017.
More and more patients are nevertheless treated outside clinical trial and it is important for radiologists and clinicians to understand the iRECIST guidelines and philosophy for the radiological follow-up during immunotherapy.
The objectives of this lecture are to explain iRECIST principles, to illustrate pseudoprogression and other atypical patterns of response (dissociated responses, hyperprogresssive disease) that can be experienced during immunotherapy and to give practical tools in order thoroughly identify and report these kind of events.

Take Home Points:
- Regarding the dynamic of recent approvals for immunotherapy (alone or in combination) especially in lung cancer patients, radiologists and clinicians will often be faced to atypical patterns of responses on imaging.
- iRECIST guidelines can help for the management of pseudoprogression
- However, other types of atypical patterns of responses such as dissociated responses and hyperprogressive disease are still challenging

Sarcopenia in Oncology: Consequences for patient outcome and therapeutic consequences

F. Goldwasser; Paris/FR

Body: Reduced muscle mass measured by CT-scan is to date the favored definition of sarcopenia as it is obtained using a reproducible method. The prevalence of sarcopenia varied from 55 % in localized breast cancer to 95 % in metastatic prostate cancer. Sarcopenia has emerged in oncology as a prognostic factor. Its prognostic value is independent of the tumor stage and also independent of the cancer type. Recently, the critical role of the cellular energetic metabolism has been pointed as a major feature of the cancer cells. Weight loss, inflammation and sarcopenia are part of the precachexia syndrom. Early multimodal interventions including physical exercising, prehabilitation or posthabilitation, and protein and caloric intake, are essential to manage to improve outcome and cancer-related morbidity and death. Moreover, sarcopenia is also a predictive parameter for increased treatment-related morbidity, especially following anticancer agents, either cytotoxic agents, targeted therapies or immunotherapy. Altered body composition, especially reduced lean body mass, is associated with modifications of the pharmacokinetics of many anticancer agents, overexposure, resulting in excessive and limiting acute toxicity. As a result, the measurement of muscle mass using CT-scan, by the radiologist, becomes a major parameter to assess from the beginning and all along the disease, and is as important as the measurement of tumor dimensions over time.

Take Home Points:
In cancer patients, sarcopenia is very common.
For any cancer type, sarcopenia has a prognostic value.
The prognostic value of sarcopenia is found at any stage of the disease, including localized tumors.
Sarcopenia is associated with over exposure to many anticancer agents resulting in excessive and limiting acute toxicity. It is a public health issue considering the frequency of sarcopenia in elderly patients.

Functional imaging in COPD

J.B. Seo; Seoul/KR

Body: Despite extensive researches and efforts in past decades, the improvement of therapies that modify chronic obstructive pulmonary disease (COPD) progression or mortality has been slow. This is largely due to limited understanding of the heterogeneous nature of COPD. Even though recent studies have shown that the quantitative CT assessment may be helpful in phenotyping of patients based on morphologic characteristics, there are still limitations to connect these characteristics directly to pathophysiologic and functional aspects of complicated disease. The primary function of the lung is the exchange of oxygen and carbon dioxide between inhaled air and circulating blood at the lung periphery. For efficient gas exchange in the lung, adequate ventilation, perfusion and the matching of ventilation-perfusion are necessary. Morphologic or reflex changes in the lung of COPD affect ventilation and/or perfusion status, and the ventilation-perfusion relationship. Dual-energy CT has opened a new filed of direct visualization of pulmonary perfusion and ventilation with matched high-resolution morphologic images. Perfusion or blood volume imaging, which is based on the ability of extraction of iodine content from contrast enhanced CT images can be used as a surrogate to the real dynamic perfusion function. Xe gas can be used as an inhaled contrast material to directly visualize regional ventilation. Furthermore, by combining perfusion and ventilation imaging, assessment of the whole or regional V-Q mismatch can be assessed in COPD, which can be used to assess the responsiveness of various therapies. Perfusion and ventilation in COPD can be assessed also with MRI without radiation exposure. Dynamic perfusion MRI, with use of GD-based contrast material, can provide detailed assessment of perfusion components of the lung parenchyma, including regional blood flow, regional blood volume and mean transit time. Direct visualization of regional ventilation is also possible with use of various contrast materials such as hyperpolarized noble gases, oxygen or fluorinated gases. Combined assessment of perfusion and ventilation is possible with use of Fourier decomposition technique without contrast material. The unique and complementary ability of both DECT and MRI to measure disease morphological and functional consequences and explore mechanisms of disease pathophysiology of COPD will enhance our understanding of COPD and promote development of optimal therapy of COPD in the future.

Take Home Points:
- Assessment of regional perfusion and ventilation in combination morphology is important to understand heterogeneous pathophysiologic nature of COPD, which will promote the optimal phenotyping of COPD and development of new therapy.
- Functional imaging with various CT and MRI techniques are now available for research and clinical practice in selected situations.

Evaluating the CF patient

M.O. Wielpütz; Heidelberg/DE

Body: Cystic fibrosis (CF) is the most frequent early lethal inherited disease in whites. Highly viscous airway secretions lead to chronic and recurrent infections and inflammation with progressive descruction of the airways and lung parenchyma. As a monogenetic channelopathy, efforts on modulating the function of the causative defect in the cystic fibrosis transmembrance conductance regulator-protein have given rise to a novel class of drugs. Together with the onset of newborn screening programs, the clinical treatment of CF patients has changes dramatically into a preventive strategy in order to conserve normal lung function as long as possible. In this era, imaging plays a key role in assessing disease activity repetitively, when traditional lung function testing lost its power for prognostication and outcome assessment. Traditionally, x-ray and CT have been used to assess lung structure in CF, and more recently MRI has evolved into a robust modality for imaging the CF lung's structural and functional deficits. Apart from the typical imaging finding of irreversible bronchiectasis, assessing lung function with imaging in CF is especially important because airway obstruction is linked to hypoxic vasoconstriction, which is a physiological response to local alveolar hypoxia. By this connection, it is possible to study the functional deficit of the CF lung with perfusion MRI, which is currently the gold standard using proton MRI. In this talk, the imaging modalities x-ray, CT and MRI are discussed in view of the most recent developments in CF therapy, with a focus on a functional assessment of the CF lung.

Take Home Points:
Cystic fibrosis lung disease comprises irreversible and potentially reversible manifestations. Mosaicism, trapped-air, ventilation and perfusion abnormalities are closely linked radiological findings assessing functional changes in the cystic fibrosis lung. Image data is assessed by semi-quantitative scoring and objective quantitative computational post-processing. Screening and novel therapy regimes increase life expectancy and conserve normal lung function for a longer period of time. Imaging will play a key role in assessing disease modifying therapy in patients with normal lung function.

Best technical imaging standards in CT lung cancer screening

A. Snoeckx; Edegem/BE

Body: Large randomized trials have shown that lung cancer screening with low-dose CT in high-risk (ex-)smokers can save lives. Radiation exposure is one of the harms associated with lung cancer screening. Through the use of low-dose CT, radiation dose to screening participants can be minimized in order to decrease the risk of radiation induced cancer. While the large screening trials were initiated more than 15 years ago, technology has advanced. Modern multidetector scanners are able to provide high resolution images with low noise and can be set to yield an effective dose of 1.0 mSv for a standard-sized patient. Dose should be decreased for smaller-sized patients and increased for larger-sized patients. Thin-section images of 1 mm or less are required and low-dose CT-protocols should ensure a sufficient diagnostic quality for accurate volumetric nodule assessment. To improve radiologist performance, computer-aided detection (CAD) software is valuable for nodule detection and to act as second reader. Collaboration with a medical physicist, dose monitoring, timely review and updating of scan protocols and a CT quality assurance program are mandatory. Dose optimisation is furthermore required for all work-up studies in case of a possible malignancy, including diagnostic CT-scans, CT-guided biopsy and/or nuclear imaging studies.

Take Home Points:
Low-dose protocols should be optimized to allow accurate volumetric nodule evaluation Thin-section images of 1mm or less are required Continuous quality assurance and dose monitoring are essential in any lung cancer screening program Dose optimization is mandatory both for low-dose screening CT's as well as for imaging studies during further workup of nodules

Risk models and biomarkers: Do they improve screening?

M. Silva; Parma/IT

Body: Pre-test risk models are available for selection of high-risk individuals in lung cancer screening (LCS). The efficacy of risk models was first tested by retrospective analysis, and recently implemented in prospective trials as well as in population based screening programs. The main prospective trials took place in Canada (PanCan) and United Kingdom (UKLS) and showed impressive detection rate at baseline low-dose CT (prevalent LC 2.1% and 1.7 %, respectively), hogher than the NLSt and NELSON trials with simple age and smoking history threshold. Population based evidence recently followed, the Manchester experience reported exceptionally high detection rate both at baseline (3%) and incidence round (1.6 %), therefore including incident LC. This latter experience also included biennial rounds for those at lower risk after baseline low-dose CT.
The low-dose CT result (e.g. nodule density and volumetry) is the strongest predictor of lung cancer, nonetheless post-test risk models can improve the efficacy of LCS. The PanCan model first included a post-test algorithm for managament of nodules, which blended pre-test descriptors and post-test findings. Similar approach was supported also by large consensus documents in UK (BTS guidleines) and Europe (EuPS). Positron emission tomography is also considered for further risk stratification of lung nodules in the British model.

Molecular biomarkers for implementation in LCS can improve both:
- pre-test selection: the utility of a biomarker for eligibility to LCS is warranted by reduced rate of lung cancer deaths without increased risks and costs, or by maintaining an equal rate of lung cancer deaths while assuring reduction of risks and costs (e.g. subjective estimate of risk even in case of no-eligibility by age/smoking threshold or risk models).
- post-test specificity: the utility of a biomarker for lung nodule management is reflected either by earlier diagnosis with comparable number of procedures(e.g. stratification of risk in indeterminate lung nodules), or reduction of procedures whilst not delaying diagnosis of lung cancer (e.g. biennial or longer inerval between LDCT rounds). Composite LCS algorithm based on low-dose CT and circulating biomarkers with 3-year or 1-year round is being prospectively tested (NCT02247453).

Take Home Points:
Risk models can increase the uptake of subjects at higher risk for lung cancer, with higher detection rate as comapred with more simple selection criteria (e.g. age/smoking threshold). Risk model with pre-test descriptors can blend with post-test findings for optimal management of screenees, based on refined personalized risk profile (e.g. subsolid nodules, emphysema, etc.) Molecular biomarkers could be considered within risk models for pre-test selection of subjects for LCS. Molecular biomarkers can add to LCS algorithms, with the aim of improving efficiency: selection of population at extremely high risk, conversely low intensity screening in those at lower risk of aggressive LC.

Psychosocial consequences of medical screening

J. Brodersen; Copenhagen/DK

Background: Medical screening can lead to intended benefits and will inevitably lead to unintended harms. One of the most frequent unintended harms is false positives, while a more rare but also more severe harm is overdiagnosis. Both of these harms can lead to psychosocial consequences by respectively being put under suspicion of a disease or being unnecessarily labelled with a disease. If it is considered to implement a medical screening programme nationally, it is a necessity to provide high-quality robust evidence about all potential benefits and all potential harms. Otherwise it is not possible to weigh the balance between the benefits and harms of a suggested screening programme. In the scientific literature there is an under-investigation or an under-reporting of the harms of cancer screening, especially the harms related to psychosocial consequences. Therefore, the aim of this presentation is to provide scientifically methodological insight in how psychosocial harms of medical screening can be investigated in a strict scientific sufficient and adequate way.

Methods: Clinical experiences and previously research has revealed that those screening participant experiencing the most severe psychosocial consequences of their screening participation are those getting false positives or being overdiagnosed. These psychosocial experiences can be either qualitatively explored or investigated quantitatively via questionnaires in surveys. In qualitative studies single and focus group interviews can be used. The results from these interviews can qualitatively be analysed using content and theory driven analyses. Moreover, the content from the interviews can be used to assess the content validity of existing questionnaires. If lack of content validity is revealed in existing questionnaires, the content revealed in the interviews can also be used to develop new condition-specific questionnaires that comprehensively measure psychosocial consequences of medical screening. Such condition-specific questionnaires with high content validity for measurement of psychosocial consequences in medical screening should finally also be statistically psychometrically validated. If such condition-specific questionnaires encompass one or more scales item response theory Rasch models are suggested to be used to provide robust evidence about unidimensionality of the scales plus invariant measurement (no differential item functioning) across relevant sub-groups of interest.

Results: Several qualitatively and mixed-method studies have been conducted in different screening settings. These studies reveal that medical screening will inevitably lead to substantial negative psychosocial consequences of false positives and overdiagnosis. Condition-specific questionnaires comprehensively measuring psychosocial consequences in breast, lung and cervical cancer screening have been established with a common core-questionnaire encompassing 49 items: in 10 scales and two single items. Furthermore, each condition-specific questionnaire have to have added single items and scales especially relevant for the different screening programmes. Moreover, the core-questionnaire has also been found relevant in a setting of abdominal aortic aneurysm screening. All these four condition-specific questionnaires have been psychometrically validated with Rasch models and adequate measurement properties of the measures have been confirmed. In addition, several of these condition-specific measures have been used in longitudinal surveys showing that false positives and overdiagnosis have long lasting substantial negative psychosocial consequences. Finally, projects are taking place to develop and validate questionnaires in settings of colorectal cancer screening and prostate cancer screening.

Conclusion: It is feasible to reveal, describe and quantify psychosocial consequences of medical screening in a comprehensive and valid way. Qualitative studies can give an insight in the complexity of severity of the psychosocial consequences of screening. Surveys, using condition-specific questionnaires with high content validity and adequate measurement properties, can reveal the degree and the duration of the psychosocial consequences of medical screening.

Take Home Points:
It is feasible to reveal, describe and quantify psychosocial consequences of medical screening in a comprehensive and valid way.
Qualitative studies can give an insight in the complexity of severity of the psychosocial consequences of screening.
Surveys, using condition-specific questionnaires with high content validity and adequate measurement properties, can reveal the degree and the duration of the psychosocial consequences of medical screening.

Current trends in COPD epidemiology and smoking epidemic

S. Raoof; New York/US

Content

1. Problems with data collection/analysis
2. Prevalence of COPD
3. Burden of COPD globally
4. Trends
5. Mortality associated with COPD
6. Health costs
7. Smoking trends

Problems with collection of COPD data

- 30 % patients with COPD are never smokers
- Other causes:
- Secondary and Tertiary smoking
- Biomass fuels (indoor exposure)
- Airways predominant phenotype
- Less emphysema; more air trapping
- 60 hours-year
- Occupational exposures (dusts, noxious fumes and vapors)
- Drs. do not usually look for COPD unless pts are smokers

COPD: Diagnosis

- 64 % diagnosed by a PCP and 28 % diagnosed by a specialist
- 7 % diagnosed by other HCP
- 31 %-43 % receive spirometry-confirmed diagnosis2
- 12 million patients remain undiagnosed3
- <50 % of PCPs are aware of the existence of GOLD guidelines and even fewer have read them

MMWR Morb Mortal Wkly Rep. 2012;61(46):937-943. 2. National Committee for Quality Assurance. http://www. ncqa.org/ReportCards/HealthPlans/ StateofHealthCareQuality.aspx. 3. National Institutes of Health. https://www. nhlbi.nih.gov/research/ reports/2012-mortality-chart-book. 4.Perez X, et al. Respir Med. 2012;106(3):374-381.

Problems with collection of COPD data

- Definition of case of COPD
- Fixed FEV-1/FVC ratio or lower limit of normal.
- Pre or post BD spirometry
- NHANES survey 2007-2010
- Prevalence of COPD changed from-
- 10.2 % with post BD LLN criteria
- 20.9 % with pre-bronchodilator FEV-1/FVC fixed ratio
- Detection of COPD requires diagnosis requires that this entity should be considered in any patient with:
- Dyspnea
- Chronic cough
- Sputum production
- H/O exposure to risk factors for the disease, usually tobacco smoke
- Most studies report prevalence of irreversible airflow obstruction rather than COPD

Estimates of COPD

- ESTIMATED PREVALENCE OF COPD IS 328 million people worldwide
- 168 million men
- 160 million women

Burden of COPD

(WHO Statistics)

- 65 million people have moderate to severe chronic obstructive pulmonary disease (COPD)
- More than 3 million people died of COPD in 2005 (5% of all deaths globally)
- Most of the information available on COPD prevalence, morbidity and mortality comes from high-income countries
- Even in those countries, accurate epidemiologic data on COPD are difficult and expensive to collect.

- It is known that almost 90% of COPD deaths occur in low- and middle-income countries.
- At one time, COPD was more common in men
- Due to increased tobacco use among women in high-income countries + higher risk of exposure to indoor air pollution (such as biomass fuel used for cooking and heating) in low-income countries, the disease now affects men and women almost equally.

Trends in COPD incidence
- Due to decreasing tobacco use, prevalence of airflow obstruction:
- Has halved from 1997 (9.1%) to 2007 (4.5%)
- Prevalence of chronic bronchitis decreased
from:
- 1982
- 19% men
- 13% women
- 2007
- 13% men
- 11% women

Prevalence surveys of COPD over time
- Mortality of COPD
- Decreasing smoking rates
- Improvements in sanitation
- Improved economy
- Improved life conditions
- Newly available respiratory medications
- YET GLOBAL STATISTICS FOR COPD DEATH RATES will increase

Burden of COPD
(WHO Statistics)
- In 2002 COPD was the fifth leading cause of death
- Total deaths from COPD are projected to increase by more than 30% in the next 10 years
- Imperative that measures be taken to reduce the risk factors-especially smoking
- Estimates show that COPD becomes the third leading cause of death worldwide in 2030

Why the paradox?
- Age standardized death rates from COPD are highest in low-income regions of the world, especially South Asia/India and Sub-Saharan Africa
- COPD mortality closely related to low FVC, which in turn, is associated with poverty.
- Health care costs
- Predominant health care costs emanate from COPD exacerbations
- $18 billion in direct costs annually in US
- 1 year mortality 21%
- 5 year mortality is 55%
- Respiratory burden of disease in Europe (EUR 47.3 billion)
- COPD EUR 38.7
- Asthma EUR 17.7
- Pneumonia EUR 10.1
- TB EUR 2.1
- Epidemiology and Impact

Socioeconomic Trends in Adolescent Smoking in Finland 2000-2015
- Study design: Population based biennial survey in 14-16 year old Finns
- Data collected: frequency of smoking, never smokers, low parental education, parental unemployment over last 1 year, not living with both parents

Socioeconomic Trends in Adolescent Smoking in Finland 2000-2015: RESULTS
- Overall prevalence of frequent smoking 22% boys; 20% girls
- Never smokers 54%--boys and girls individually
- ODDS RATIO for both BOYS AND GIRLS decreased over the study period

- Frequent smoking more common amongst boys and girls:
  · not living with both parents
  · If both parents had only basic education vs if even one parent had higher than basic education
  · With parental unemployment in the last one year
  · Non smoking was also associated with socioeconomic adversities
  · Overall proportion of frequent smoking decreased over 15 years, this decrease was not seen in those with socioeconomic diversity

SMOKING PREVALENCE and attributable disease burden in 195 countries and territories from 1990-2015: GLOBAL BURDEN OF DISEASE
- Study design:
- Synthesis of 2818 data sources
- Spatiotemporal Gaussian process regression
- Analysis of 38 risk outcome pairs

- Data generated:
• Disease burden from smoking
• Smoking attributable mortality
• Disability adjusted life years DALY)

SMOKING PREVALENCE and attributable disease burden in 195 countries and territories from 1990-2015: GLOBAL BURDEN OF DISEASE
- Results
- Worldwide, prevalence of daily smoking was 25 % for men; 5.4 % for women
- Over 25 yrs of study period, this represents-
- 28.4 % reduction in men
- 34.4 % reduction in women
- In 2015, 11.5 % global deaths (6.4 million) were attributable to smoking worldwide
- 52.2 % took place in China, India, USA and Russia

Summary
1. Problems with data collection/analysis
2. Prevalence of COPD
3. Burden of COPD globally
4. Trends
5. Mortality associated with COPD
6. Health costs
7. Smoking trends

Smoking-related interstitial lung disease

J.R. Galvin; Silver Spring/US

Body: The Range of Cigarette Smoke Related Lung Injury: Rad-Path Correlation
Symptomatic cigarette smokers are a common source of referral for diagnostic imaging. Radiologists are regularly confronted with an array of findings on plain radiography and computed tomography that mirror varying combinations of emphysema, airway inflammation, airway fibrosis, alveolar wall fibrosis and the changes of pulmonary Langerhans' cell histiocytosis.
Lung tissue responds to injury with a combination of destruction, remodeling, and repair that is manifest by airspace enlargement and laying down of collagen and elastin. The process of remodeling and repair has been well documented as a response to the inflammation and destruction from cigarette smoke that involves all compartments of the respiratory system from the conducing airways to the alveolar walls. The inflammation, destruction, remodeling, and repair from inhaled cigarette smoke are reflected radiologically and histologically as a variety of airway and parenchymal alterations. These alterations have been described over decades as separate diseases, including emphysema, respiratory bronchiolitis, respiratory bronchiolitis–interstitial lung disease, desquamative interstitial pneumonia, and pulmonary Langerhans' cell histiocytosis. Small-airway injury, including submucosal and adventitial fibrosis, remodeling evidenced by distortion, and increased bronchus-associated lymphoid tissue, along with thickening of walls of small arteries and arterioles, are well-recognized histologic findings in cigarette smokers.
In addition, there is growing acceptance of a link between cigarette smoke and alveolar wall fibrosis. There is consistent evidence that smokers who have combined emphysema and fibrosis can be extremely dyspneic and may present with normal flow rates on spirometry, normal total lung capacity and strikingly low diffusion capacity. Some patients meet the criteria for usual interstitial pneumonia, which is not unexpected as smoking is considered a risk factor for idiopathic pulmonary fibrosis.

These injuries are best understood through correlation of the imaging with pathology and physiology. Below you will find representative images from individual responses to cigarette smoke. It is important to recognize that these changes on histology and radiology and often combined and are best described as "smoking-related" diffuse lung disease". The dominant components can then be included as part of a more complete explanation.

Bibiolography
Auerbach, O., Garfinkel, L., & Hammond, E. (1974). Relation of smoking and age to findings in lung parenchyma: a microscopic study. Chest, 65(1), 29–35.
Cottin, V., & Cordier, J.-F. (2009). The syndrome of combined pulmonary fibrosis and emphysema. Chest, 136(1), 1–2. http://doi.org/10.1378/chest.09-0538
Franks, T. J., & Galvin, J. R. (2014). Smoking-Related "Interstitial" Lung Disease.Archives of Pathology & Laboratory Medicine, 141201162107003. http://doi.org/10.5858/arpa.2013-0384-RA
Galvin, J. R., & Franks, T. J. (2009). Smoking-related lung disease. J Thorac Imaging, 24(4), 274–284. http://doi.org/10.1097/RTI.0b013e3181c1abb7
Kligerman, S., Franks, T. J., & Galvin, J. R. (2016). Clinical-Radiologic-Pathologic Correlation of Smoking-Related Diffuse Parenchymal Lung Disease. Radiologic Clinics of North America, 54(6), 1047–1063. http://doi.org/10.1016/j.rcl.2016.05.010
Niewoehner, D. (1982). Lung fibrosis and emphysema: divergent responses to a common injury?Science.
Niewoehner, D., Kleinerman, J., & Rice, D. (1974). Pathologic changes in the peripheral airways of young cigarette smokers. The New England Journal of Medicine,291(15), 755–758. http://doi.org/10.1056/NEJM197410102911503
Wells, A. U., Nicholson, A. G., Hansell, D. M., & Bois, du, R. M. (2003). Respiratory bronchiolitis-associated interstitial lung disease. Seminars in Respiratory and Critical Care Medicine, 24(5), 585–594. http://doi.org/10.1055/s-2004-815606

The histologic responses to cigarette smoke are often seen in combination and best thought of as cigarette smoke related diffuse lung disease. Varying components may dominate but they rarely occur in isolation

There are two forms of lung fibrosis associated with cigarette smoke exposure. 1. Alveolar wall fibrosis that is related to the intensity and duration of exposure and (2) UIP in which there is a strong association, however the mechanism is unclear.

Take Home Points:
Cigarette smoke related diffuse lung disease is usually a combination of inflammatory cells, emphysema and fibrosis

Hypersensitivity pneumonitis: An update

A. Devaraj; London/UK

Body: This presentation will review the typical and atypical CT features of subacute and chronic hypersensitivity pneumonitis, including distinguishing between fibrotic and non-fibrotic forms and from other fibrotic interstitial lung diseases.
Integration of clinical aspects will be discussed, covering aspects relating to exposure history and bronchoalveolar lavage.
Recent updates on classification will be reviewed, with discussion of the role of expiratory CT also.

Take Home Points:
1. CT appearances of hypersensitivity pneumonitis may be classical and diagnostic, but in many instances there is overlap with other fibrotic lung diseases, commonly UIP
2. Integration of clinical radiological and pathological findings can be helpful in establishing an MDT diagnosis of hypersensitivity pneumonitis

Aspiration: Imaging manifestations

J. Ryu; Rochester/US

Body: Aspiration of foreign matter into the airways and lungs can cause a wide spectrum of pulmonary disorders with varying presentations. The type of syndrome resulting from aspiration depends on the quantity and nature of the aspirated material, chronicity, and host responses. Risk factors for aspiration include decreased level of consciousness, compromised airway defense mechanisms, dysphagia, gastroesophageal reflux, and recurrent vomiting. Commonly recognized aspiration-related syndromes include aspiration pneumonia (typically defined as infection caused by aspirated microorganisms), aspiration pneumonitis (acute chemical lung injury from aspiration of acidic gastric contents), and large airway obstruction with a foreign body. However, there are less well-recognized aspiration-related syndromes: other airway disorders including vocal cord dysfunction, bronchiectasis, bronchoconstriction, and diffuse aspiration bronchiolitis; and parenchymal disorder of exogenous lipoid pneumonia. Aspiration has been implicated in disease progression and acute exacerbation seen in idiopathic pulmonary fibrosis. Aspiration may increase the risk of bronchiolitis obliterans syndrome in patients with lung transplants. Accumulating evidence suggests that a causative role for aspiration is often unsuspected in patients presenting with aspiration-related pulmonary diseases; thus, many cases go undiagnosed. In this talk, I will discuss the broadening spectrum of these aspiration-related pulmonary syndromes with a focus on imaging features.


Aspiration pneumonitis and pneumonia

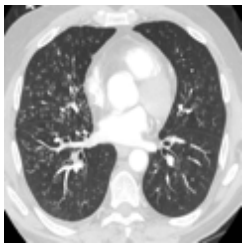
Diffuse aspiration bronchiolitis


Mass-like lesion from aspiration

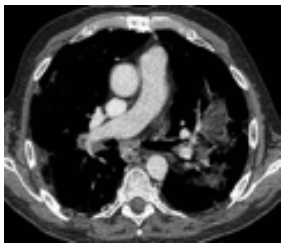
Exogenous lipoid pneumonia

Take Home Points:
Commonly recognized aspiration-related syndromes include aspiration pneumonia, aspiration pneumonitis, and large airway obstruction with a foreign body. Less commonly recognized aspiration-related syndromes include other airway disorders such as vocal cord dysfunction, bronchiectasis, bronchoconstriction, and diffuse aspiration bronchiolitis, and parenchymal disorder of exogenous lipoid pneumonia. Aspiration-related syndromes can present a wide array of imaging features including patchy consolidative/ground-glass opacities, diffuse interstitial opacities, mass-like lesions, diffuse bronchiolitis, bronchiectasis, and fat-attenuation containing opacities.

How do I evaluate CT radiation dose

D. Tack; Baudour/BE

Body: As there is no direct method to measure the radiation dose delivered by CT, a standardized method has been used since the early 1980ies, using a plastic (PMMA) phantom. Two main metrics are derived from this strategy. First, the computed tomography dose index volume (CTDIvol), estimating the dose absorbed by the phantom for a single axial slice, and second, the dose-length product (DLP) representing the dose absorbed during an helical acquisition.
Both metrics are generated by all CT scanner devices around the world and can be collected in order to compare them between devices, through surveys performed in the EU.
Limitations and uncertainties of both local dose estimations and national dose surveys will be discussed. In particular, the need for large sample sizes to estimate de dose delivered by a CT scanner will be commented.
Attention will also be paid in the presentation to pitfalls when estimating the real patient absorbed dose and subsequent cancer risks from CTDIvol and DLP. The concept of size specific dose estimate (SSDE) will be introduced to better approach the real absorbed dose by patients.
Comparisons of local doses with the national survey data are needed on order to determine the objectives for dose optimization. As a general rule, the diagnostic reference levels (DRLs or P75) do not represent objectives for dose optimization but only limits that should not be reached. The 25th percentiles of dose distribution (P25) represent better objectives, whereas the ultimate goal could be the first percentile of dose distribution.

Take Home Points:
CTDIvol and DLP are useful to compare the dose delivered by a CT scanner to those delivered by other devices in the country SSDE take into account patient size for estimating the absorbed dose. Large samples of data (either CTDIvol or DLP) are needed to avoid over- or underestimation of the dose delivered by a CT scanner. P25 is a better objective for dose optimization than P50 or the DRL (P75).

Ultra-low dose CT protocols: Clinical indications

G.R. Ferretti, M. Ludwig, A. Cole, E. Reymond, A. Jankowski; Grenoble/FR

Body: Advance CT technology with iterative reconstruction allows for acquisition with ULD (Ultra low dose) protocols with a DLP<10mGy.cm. ULD CT is particularly suitable for exploring the lung parenchyma due to spontaneous high contrast. We present a review of the literature regarding current applications in clinical practice of ULD CT, as well as advantages and drawbacks of these acquisitions.

Take Home Points:
- ULD CT is possible for imaging lung parenchyma
- Indications should be carefully selected

Imaging the lung with no dose: Current role of MRI

J. Biederer; Heidelberg/DE

Body: The traditional workhorses for thoracic imaging in diagnostic radiology are Chest X-ray, computed tomography (CT) and in some cases lung ultrasound (US). Only more recently MRI has joined the "zoo" of available lung imaging modalities, not only as a radiation-free alternative to the established methods, but also coming with additional options for tissue characterization (exclusion of malignancy) and functional imaging capacities (perfusion, ventilation, respiratory motion). Depending on the indication, MRI may serve well as the modality of first choice or as a valuable adjunct to the other modalities.
For patients who should not be exposed to ionizing radiation (children and young subjects, pregnant patients), MRI at the present state of art may be chosen as a radiation-free first choice modality, e.g. in patients with cystic fibrosis. In young patients, it may well be used for the long term follow-up of malignancy (e.g. seminoma) or inflammatory disease (e.g. GPA/Wegener's disease) (Fig. 1). As an adjunct or alternative to other modalities, MRI can be helpful in lung cancer staging and follow-up (differentiation of atelectasis and lung cancer, Fig. 2) or the characterization of lung nodules („actionable nodules" with contrast uptake, high NPV in nodules with no or low contrast uptake, fatty content in hamartoma). This even qualifies MRI as a potential tool for early detection of lung cancer, either as screening tool or for the further diagnostic work-up of detected lesions. Furthermore, lung MRI can be applied as an adjunct to other modalities for comprehensive lung imaging in COPD. In some cases of interstitial lung diseases it may provide valuable additional information, for example in confirming mediastinal lymphadenopathy related to sarcoidosis (dark lymph node sign).
Since many radiologists are still reluctant to use Lung MRI being not familiar with its application and diagnostic scope, straightforward, standardized protocols have been set up to facilitate implementation of this new modality in clinical practice. Customized lung imaging protocols with suitable pre-sets may be already available with the MR equipment or are easy to implement.
The basic protocol approach uses T2-weighted fast spin echo (FSE) for infiltrates/soft lesions (1), T2-weighted FSE with fat suppression for lymph nodes/bone lesions (2), Steady state free precession sequences (SSFP) for respiratory motion/lung vasculature (3) and T1-weighted 3D gradient echo (3D-GRE) for nodules/masses and airways (4, Fig. 3). Optional sequences comprise MR angiography, dynamic contrast enhancement (DCE) for lung/tumor perfusion and diffusion weighted imaging (DWI) for lymph nodes/lesion characterization (Fig. 4). Examination times range from 15 minutes (standard) to 25 minutes (all options). With these standardized protocols, the sensitivity of MRI for infiltrates is at least similar to X-ray and CT, lung nodule detection is superior to X-ray and slightly inferior to CT.

Imaging inflammatory disease in children (suspected TB, respiratory triggered T2-weighted sequences)

Differentiation of mediastinal masses

Available sequences (choice for routine protocol)

Protocol options

Take Home Points:
- Depending on the indication, MRI may well serve as potential first choice modality for imaging and follow up of pulmonary disease in young or pregnant patients …
  … or be used as an alternative or adjunct to other modalities, e.g. in COPD or interstitial lung diseases.
- Standardized Protocols are available for an easy implementation of lung MRI with any state of the art equipment.

Hemoptysis: KSTR guidelines

J.-H. Kim; Daejeon/KR

Body: Radiation exposure from diagnostic medical imaging has increased. Justification of a radiologic examination and optimization of protection are the two basic principles of medical radiation protection for patients who may need to undergo such a procedure. Justification in the field of radiology refers to the appropriate use of radiologic imaging modalities, i.e., the net benefit must outweigh possible detriment. Upon clinically justifying a diagnostic examination, to ensure a radiation dosage that is as low as reasonably achievable (ALARA), the imaging process must be optimized to obtain the necessary diagnostic information. Evidence-based clinical guidelines act to support a clinician's decision for optimal clinical practice and to reduce patient's radiation exposure. The clinical imaging referral guidelines could be applicable globally, keeping local and regional variations in mind.

In 2014, the American College of Radiology (ACR) established clinical guidelines for the appropriate diagnostic approach and treatment of patients according to the severity of hemoptysis and risk of lung cancer. The ACR emphasized the importance of undiagnosed lung cancer in hemoptysis patients. However, application of the ACR guidelines in Korea may not be appropriate because the main etiology of hemoptysis in Korea is respiratory infection or bronchiectasis. South Korea has the highest incidence rate of tuberculosis among members of the Organization for Economic Cooperation and Development. Thus, the Korean Society of Radiology and the Korean Society of Thoracic Radiology have proposed new guidelines tailored for Korean medical circumstances. The Korean guidelines are based on a guideline adaptation methodology process suggested by the development committee. These new guidelines were developed through the consensus of a development committee, a working party, and an advisory committee. The guidelines are summarized below.

Summary of Guidelines
Recommendation 1-1. Chest radiography is suggested for initial evaluation in all adult patients with hemoptysis. (Recommendation Grade A, Evidence level II)
Recommendation 1-2. Contrast-enhanced chest CT is recommended to diagnose the cause of hemoptysis in all adult patients with hemoptysis and who have two risk factors for lung cancer (>40 years old and >30-pack-year smoking history). (Recommendation Grade A, Evidence level II)
Recommendation 1-3. Contrast-enhanced chest CT is recommended to diagnose the cause of hemoptysis in all adults patients with moderate hemoptysis (>30 mL/24 hours) or recurrent hemoptysis. (Recommendation Grade A, Evidence level II)
Recommendation 1-4. Contrast-enhanced chest CT should also be considered for adult patients with massive hemoptysis (>400 mL/ 24 hours) and preserved cardiopulmonary function. (Recommendation Grade A, Evidence level III)
References Malone J, Guleria R, Craven C, Horton P, Jarvinen H, Mayo J, et al. Justification of diagnostic medical exposures: some practical issues. Report of an International Atomic Energy Agency Consultation. The British Journal of Radiology. 2012;85:523-538. Steinberg E, Greenfield S, Mancher M, Wolman DM, Graham R. Clinical practice guidelines we can trust: National Academies Press; 2011. Ketai LH, Mohammed TL, Kirsch J, Kanne JP, Chung JH, Donnelly EF, et al. ACR appropriateness criteria® hemoptysis. J Thorac Imaging. 2014 May; 29(3):W19-22. Choi SJ, Jeong WK, Jo AJ, Choi JA, Kim MJ, Lee M, et al. Methodology for Developing Evidence-Based Clinical Imaging Guidelines: Joint Recommendations by Korean Society of Radiology and National Evidence-Based Healthcare Collaborating Agency. Korean J Radiol 2017;18(1):208-216 Kang MJ, Kim, JH, Kim YK, Lee HJ, Shin KM, Kim JI et al. 2018 Korean Clinical Imaging Guideline for Hemoptysis. Korean J Radiol 2018;19(5):866-871 Khalil A, Fartoukh M, Parrot A, Bazelly B, Marsault C, Carette M-F. Impact of MDCT angiography on the management of patients with hemoptysis. AJR Am J Roentgenol 2010;195(3):772-778 Abdulmalak C, Cottenet J, Beltramo G, Georges M, Camus P, Bonniaud P, et al. Haemoptysis in adults: a 5-year study using the French nationwide hospital administrative database. Eur Respir J. 2015 Aug; 46(2):503-511.

Take Home Points:
Hemoptysis is challenging because of the variety of etiologies and clinical presentations ranging from a nonalarming bloody expectoration to a life-threatening condition. The Korean Society of Radiology and the Korean Society of Thoracic Radiology have proposed new imaging guidelines for hemoptysis based on a guideline adaptation methodology process. The recommendations are acceptable and applicable to the situation in Korea. This is the first evidence based guideline for hemoptysis in Korea. Regular updating is necessary to provide a sustainable and available diagnostic pathway according to justification and optimization; therefore, nationwide, multicentre studies conducted to define the epidemiology of hemoptysis will contribute to improve the evidence-based guidelines.

Fleischner Society guidelines for management of solid and subsolid nodules

H. MacMahon; Chicago/US

Body: The Fleischner Society Guidelines for management of solid nodules were published in 2005, and additional guidelines for subsolid nodules were issued in 2013. Since then, new information has become available, and the guidelines have been revised to reflect current thinking on nodule management. The revised guidelines incorporate several changes that reflect current thinking on the management of small nodules. The minimum threshold size for routine follow-up has been increased, and recommended follow-up intervals are now given as a range rather than as a precise time period to give radiologists, clinicians, and patients greater discretion to accommodate individual risk factors and preferences. The guidelines for solid and subsolid nodules have now been combined in one simplified table, and specific recommendations have been included for multiple nodules. The current guidelines emphasize the importance of contiguous thin section technique, for accurate characterization of small solid and subsolid nodules. Correct CT measurement methods will also be addressed, as both guidelines and lung cancer staging depend upon accurate dimensional measurements, and automated approaches, which will have an increasing role to play during the coming decade, will be briefly discussed.

Take Home Points:
The Fleischner Nodule Management Guidelines apply only to newly detected incidental nodules in adult patients, and should not be used for lung cancer screening, for patients with potential metastatic disease, or who are immunocompromised. Correct scanning technique with contiguous thin sections is important to allow accurate measurement and characterization of small nodules. Automated measurement techniques will play an increasingly important role, but standardization and validation remain important for consistent results.

ATS/STR Clinical Practice Guidelines for Evaluation of Suspected PE During Pregnancy

A. Leung; Stanford/US

Body: Pulmonary embolism (PE) is the leading cause of maternal mortality in the developed world. This talk will focus on guidelines for the diagnostic work-up of suspected PE in pregnancy developed by a multidisciplnary panel of major medical stakeholders using Grades of Recommendation, Assessment, Development and Evaluation (GRADE) methodology.

Take Home Points:
Given the overall low quality of direct evidence pertaining to diagnostic test accuracy and patient important outcomes in the pregnant population, the choice of diagnostic studies rests squarely within the purview of the treating physician who also needs to consider individual patient characteristics and preferences as well as the availability of local resources.

Guidelines for lung cancer screening: European and US perspectives

A. Bankier; Boston, MA/US

Body: This presentation will highlight the European and the US American approaches to CT Lung Cancer Screening. The presentation will summarize the historical background and the regulator groundwork that has been put in place in both worlds. Finally, the presentation will discuss the perspectives on lung cancer screening, as determined by these different frameworks, and intend to anticipate future developments in the field.

Take Home Points:
What does it take to establish a CT lung cancer screening program?
How does the European and the US American approach differ?
What future developments can be anticipated?

Multidisciplinary conferences: Where is and how do we quantify „added value“

J.A.J.J. Verschakelen, W. de Wever, J. Coolen, A. Dubbeldam; Leuven/BE

Body: Nowadays multidisciplinary conferences (MDC's) form part of the daily work in most hospitals caring for cancer patients and are also considered central to the diagnosis and treatment planning of patients with fibrotic diffuse lung disease. Although these MDC's are a mandatory part of cancer care in many countries and are an obligatory step in the diagnosis of idiopathic pulmonary fibrosis, their impact on patient outcome and in particular on the survival of patients is not entirely clear. Designing studies that can assess the effectiveness of an MDC has proven difficult and while some studies have found a positive effect on patient care and survival, others have found no difference in diagnosis pre- and post-MDC. There are several reasons for this, such as the fact that MDC's are made up of health care providers introducing human factors that can influence their working in a positive or negative way and also the fact that treatment, technology and services evolve continuously often making the study of patient outcome difficult. Despite this there is an increasing amount of literature suggesting that multidisciplinary care improves several aspects of lung cancer care and allows a better diagnostic and prognostic discrimination among fibrotic diffuse lung diseases.
It is obvious, however, that an MDC can only have a positive effect on clinical discussion making when it works optimally.
In this presentation the advantages but also the potential pitfalls of a multidisciplinary conference will be discussed. Also characteristics of an effective multidisciplinary team will be covered.

Take Home Points:
1. The evidence of the impact of MDC's on patient outcomes and patient survival is mixed and not entirely clear.
2. Despite this there is an increasing amount of literature suggesting that multidisciplinary care improves several aspects of lung cancer care and allows a better diagnostic and prognostic discrimination among fibrotic diffuse lung diseases.
3. In order to have an optimally functioning MDC it is important to know the factors that make the team successful and to recognize the barriers to successful multidisciplinary care.

Small vessel vasculitis

A.-L. Brun; Paris/FR

Body: The pulmonary vasculitides are a rare group of heterogeneous disorders sharing a common histopathologic finding of inflammation and destruction of the blood vessel wall. According to the revised Chapel Hill Consensus Conference Nomenclatures of Vasculitides, small vessel vasculitides can be divided into ANCA-associated vasculitis (AAV) and immune complex vasculitis, depending on the presence of specific autoantibodies, and importance of immune deposits on the vessel walls.
AAV include microscopic polyangiitis (MPA), granulomatosis with polyangiitis (GPA, formerly Wegener's disease), and eosinophilic granulomatosis with polyangiitis (EGPA, formerly Churg-Strauss syndrome). The lung is a frequent target in this group, with various pulmonary manifestations including diffuse pulmonary hemorrhage, parenchymal infiltrates, nodules, cavitating lesions and airway involvement. Pulmonary fibrosis is a rare but therapeutically challenging manifestation observed in patients with AAV, particularly those associated with MPO-ANCA.
Idiopathic pauci-immune pulmonary capillaritis (IPIPC) is a small vessel vasculitis isolated to the lungs and sometimes considered to behave as a "lung-limited" MPA.
Anti-glomerular basement membrane (anti GMB) disease (formerly Goodpasture syndrome) is part of the immune complex-mediated group and a type of pulmonary-renal syndrome. The main thoracic manifestation is diffuse pulmonary hemorrhage, resulting from damage to the alveolar basement membranes by a cytotoxic antibody.
As most clinical symptoms and imaging patterns are nonspecific, the diagnosis of small vessel vasculitis can be challenging. The radiologist plays a central role in the diagnosis and should be familiar with the cardinal features of each vasculitis to avoid delays in diagnostic and treatment of these potentially life-threatening diseases.

Take Home Points:
- Diffuse pulmonary hemorrhage can reveal a small vessel vasculitis, and is the main radiological feature in anti-GMB disease and MPA.
- Sub-glottic tracheal stenosis and cavitating nodules are two particular features associated with GPA.
- Pulmonary fibrosis is a rare manifestation of AAV, particularly those associated with MPO antibodies.

Radiomics: How does it work?

L. Fournier, A. Bouchouicha, L. Duron, D. Balvay, J. Deidier, A.-L. Gaultier, A. Lecler, B. Rance; Paris/FR

Body: Radiomics is a new ‚data-driven' approach for extracting large sets of complex descriptors from routine (or not) clinical images. Advanced methods of image processing are applied to images to extract a large number of descriptors analysed using bio-informatics and bio-statistics methods to select the parameters most predictive of outcomes or biological markers. Seven steps are identified in the radiomics process.

1/ Acquisition
Radiomics can be performed on any imaging technique, and can combine imaging-derived parameters to non-imaging parameters.
2/ Segmentation
Radiomics is often applied to a region of interest, delineated manually, semi-automatically, or automatically. Several delineations are often performed to allow for estimation of intra- and inter-observer variability.

3/ Pre-processing
This step will allow harmonisation of signal intensity (i.e. grey level) range, signal-to-noise ratio, pixel size among images, particularly important if images are acquired with different acquisition parameters, on different devices or in different centres. It will also allow resampling of pixel size, and discretisation of grey levels to allow calculation of texture parameters. It is a very important step which strongly impacts results obtained.

4/ Feature extraction
A large number of features are generated describing shape, signal distribution derived from histograms and spatial organisation (or texture) derived from matrices such as the co-occurrence matrix, after applying various pre-processing methods. They can be augmented by semantic descriptors and non-imaging parameters.

5/ Feature selection
This step allows the selection of a subset of the most-promising parameters, to reduce the number of candidate biomarkers to a more statistically acceptable number. Features may be selected according to their robustness to observer delineation, their capacity to bring independent information, etc...

6/ Correlation to the parameter of interest
Features are then correlated to outcomes, such as treatment response or survival, or underlying biology such as gene expression profiles (called radiogenomics), molecular profiles, expression of receptors, microenvironment such as immune cell infiltration or angiogenesis. Unsupervised or supervised techniques may be used, and cross-validation is often applied to compensate the insufficient number of patients. The most promising features define a ‚radiomics signature'.

7/ Validation

The discovery of possibly predictive or prognostic radiomics signature must then be validated in an independent population to demonstrate its performance.
In conclusion, radiomics is a high-throughput technique developed to effectively mine images for information not visible to the radiologists' eye, and allow discovery of new potential biomarkers.

Take Home Points:
Radiomics is a big data technique extracting large numbers of a parameters from images.
The purpose is to improve biomarker discovery efficacy by simultaneously analysing this large number of parameters.
Shape, histogram-derived and texture features are extracted.
Signatures can be discovered that reflect prognosis or predict treatment response, gene expression, molecular profiles, etc...
The radiomics process allows discovery but signatures must be validated in independent populations.

Deep learning: How does it work?

M. Vakalopoulou; Paris/FR

Body: Artificial intelligence and machine learning are some of the most popular topics today for a variety of applications and communities with special focus on deep learning since in the last ten years deep learning based methods have defined the state-of-the-art in a large variety of tasks. In this talk, we will make an introduction to deep learning, discussing the essentials of it. Moreover, we will discuss the basic components that are needed to create algorithms that can benefit from all the capabilities of deep learning. Finally, we will explore the application of deep learning approaches in medical imaging, presenting different success and failure cases to provide practical experience.

Take Home Points:
Machine learning and deep learning will play a significant role in the near future of healthcare and medical imaging and it is of utmost importance to know its limitations and capabilities.

Radiomics: Characterization or prognosis tool in lung cancer?

J.M. Goo; Seoul/KR

Body: Radiomics is defined as high-throughput extraction, analysis, and interpretation of quantitative features from medical images. Radiomics have been applied various aspect of lung cancer imaging: differentiation benign from malignant nodules, histologic correlation in terms of tumor grade, prediction of mutation status, prognosis, clinical outcomes, and treatment response. Many studies have suggested that more heterogeneous tumors are more aggressive and associated with poorer prognosis/survival and tumors that become more homogeneous during treatment seem to be responding to therapy. Although radiomics showed many potentials, there are still challenges and limitation. Because of the nonstandardized protocols and relative lack of multicenter studies, the results are still hard to be generalized. Standardized data collection, establishment of evaluation criteria, and reporting guidelines are required.

Take Home Points:
Radiomics have been applied and showed potential in various aspect of lung cancer imaging. Despite potential, current results are still hard to be generalized in lung cancer management. Standardization of protocols and validation through multicenter studies are required for clinical acceptance.

Deep learning for classification and quantification of lung fibrosis

G. Chassagnon; Paris/FR

Body: Machine learning approaches have been used for evaluating interstitial lung diseases (ILD) on computed tomography (CT) images, in order to quantify ILD extent or for pattern classification. ILD segmentation allows quantifying disease extent and several studies have shown the superiority of deep learning over classic machine learning algorithms for this task. The patch-based approach is the most commonly used approach for ILD segmentation. However, this method suffers from several limitations, especially a difficulty to classify voxels located at the periphery of the lung. The aim of this lecture is to provide a comprehensive review of deep learning applied to the evaluation of ILD.

Take Home Points:
Deep learning can be used for ILD quantification and classification Deep learning usually outperforms classic machine learning methods for disease segmentation

Deep learning for detection and characterization of lung nodules

B. van Ginneken, C. Jacobs; Nijmegen/NL

Body: The success of deep learning, the implementation of lung cancer screening, and recent public challenges have created a revived interest for research of automatic nodule detection and characterization algorithms. In this talk, I will give an overview of deep learning for nodule detection and characterization. Public challenges, such as the LUNA16 challenge and the Kaggle Data Science Bowl 2017 challenge, and publicly available databases have been drivers for development of novel deep learning algorithms and the performance of these novel algorithms is very promising. However, there are remaining challenges that need to be solved. Almost all approaches still rely on only one scan, while a radiologist typically looks at all available scans and the clinical history of the patient. Next to this, integration of these algorithms into clinical practice is still not easy, and validation of algorithms on larger datasets and real-world data are needed to further validate these algorithms.

Take Home Points:
- LUNA16 and Kaggle Data Science Bowl 2017 have shown the potential for deep learning for nodule detection and deep learning.
- Integration of these algorithms into clinical practice is still suboptimal.
- Validation of these algorithms on larger and modern datasets is needed to further validate these algorithms.

Acute and chronic pulmonary embolism: Diagnostic imaging strategies

S. Tan[1], L. Haramati[2]; [1]Montreal/CA, [2]Bronx/US

Body: Pulmonary embolism (PE) is considered a serious diagnosis with potentially morbid or mortal complications. Unfortunately, PE often presents with nonspecific symptoms. Therefore, it is the imagers' role to guide clinicians toward an appropriate diagnostic evaluation and to interpret the imaging findings in the context of the patient's clinical presentation. This talk will discuss imaging strategies for PE in the acute and chronic setting. In acute PE, several risk assessment tools have been described, each with their own limitations and particular characteristics to consider. The decision to image and choice of imaging modalities for PE diagnosis should be customized to the patient and according to institutional resources and expertise. Particular attention should be paid to radiosensitive patients, such as pregnant women. Overdiagnosis is an unfortunate byproduct of technological advances, nuancing the significance of a PE diagnosis nowadays in contrast to classic teachings. In chronic PE, a less common disease, the V/Q scan has been a mainstay, particularly for ruling out the diagnosis. The interpretation of CTPA requires careful attention and specialized knowledge to enhance the detection of the varied manifestations of chronic PE. An algorithm for pulmonary hypertension workup has recently been proposed, highlighting the role of imaging in identifying chronic thromboembolic pulmonary hypertension (CTEPH).

Take Home Points:
In acute PE, selecting a risk stratification method and imaging modality that are adapted to the patient population, and understanding their limitations are necessary for appropriate care. Evaluation for chronic PE, a less common disease, requires heightened awareness of the diagnosis and its varied imaging manifestations. CTEPH is a complication of chronic PE, with sometimes subtle diagnostic findings.

Different risk assessment tools are available to determine the likelihood of acute pulmonary embolism. (a) Geneva Score. (b) PERC Rule. (c) Well's criteria. (source: MDcalc.com)

Complicated acute pulmonary embolism (PE) in a 43-year-old man with history of bladder cancer. (a) The scout image shows an opacity in the right lower lobe (white arrow), corresponding to a pulmonary infarct on CTPA (b, white arrow).

Chronic thromboembolic pulmonary hypertension (CTEPH) with multimodality findings in a 58-year-old woman.

The role of CT for risk stratification in acute PE

G. Aviram; Tel-Aviv/IL

Body: Pathophysiological studies suggest that in acute pulmonary embolism (PE), severe obstruction of the pulmonary arteries by the emboli leads to abrupt increase in the afterload on the right ventricle (RV). RV dilatation occurs as a compensatory function, with interventricular septal shifting toward the left ventricle (LV). This may eventually lead to marked reduction in LV filling and of the cardiac output, resulting in systemic hypotension and hemodynamic collapse, leading to mortality.
Management of patients diagnosed with acute PE varies between immediate rescue reperfusion therapy to those in shock, and on the other side, early or immediate discharge for home treatment in case of a low risk patient. Decisions should be based on clinical, laboratory and imaging evaluation. According to the 2014 European Society of Cardiology guidelines, imaging plays a major role among intermediate risk patients (those who are normotensive, with a simplified PE severity index (sPESI) >0. These patients should be further classified into intermediate-high risk and thus, be very closely monitored, if they have both imaging signs of right ventricular dysfunction as well as elevated cardiac biomarkers.
The diagnostic CT pulmonary angiography (CTPA) scan can contribute to immediate risk stratification by showing the pathophysiological cardiac response to the PE event. Various CT parameters were reported to be associated with adverse outcome in acute PE. The most validated and widely used is the increased right to left ventricular diameter ratio≥1, which has been shown in most but not all studies, to have a predictive value for mortality in 30-days. Severe reflux of contrast to the IVC and the hepatic veins and reduced left atrial volume were also reported in association with adverse outcome. In addition, two systems of CT pulmonary angiographic scoring of the clot burden are available, but have not consistently correlated with mortality, and are rarely used in clinical practice. Dual energy CT, which enable both anatomic clot detection as well as functional iodine perfusion-like map creation, may also be contributive, since increased perfusion defect volume was reported to be associated with increased risk of death.

Take Home Points:
- Mortality in acute PE is a result of under filling of the left heart due to the vascular obstruction by the emboli and to the compression by the dilated dysfunctioning right heart.
- Management decisions should be based first on clinical status using the simplified PE severity index (sPESI), and then, in intermediate risk patients, using laboratory and imaging evaluation for evidence of right ventricular dysfunction.
- The diagnostic CTPA data can contribute to immediate risk stratification by revealing findings which are consistent with right ventricular dysfunction, with increased right to left ventricular diameter ratio≥1 being the most accepted parameter. Additional CT findings include reflux of contrast to the IVC, reduced left atrial volume, and increased volume of the perfusion defects on dual energy CT.

New MR sequences: Current performance and remaining limitations in acute PE

B. Ghaye; Brussels/BE

Body: Up to twenty-five % of patients suspected of PE may present with contraindication to iodinated CM which indicates a potential role for MR. Recent MR technical refinements have been substantial in this field with faster sequences, larger coverage, lung perfusion imaging and high-resolution pulmonary MR angiography (MRA). Basic sequences for PE include unenhanced SSFP and 3D GRE pulmonary MRA. Technically inadequate examinations were reported in 25-30 %, mainly due to poor vascular opacification and artifacts in two large studies. MR direct signs of acute PE are similar to those of CT, including partially occluding endoluminal filling defects and complete arterial obstruction showing a meniscus termination outlining the clot. Reported sensitivity and specificity of MRA in large series were around 80 % and 95-100 %, respectively. Sensitivity decreases from central to lobar level (close to 100 %), segmental level (70-90 %) and subsegmental level (30 %). Unenhanced MRA has 65-82 % sensitivity and 90-99 % specificity in the 48-62 % interpretable examinations, showing a similar decrease of sensitivity from proximal to distal level. Perfusion lung MR also showed a 75-79 % sensitivity and 85-90 % specificity in the 50-58 % interpretable examinations. The timely acquisition of CE bolus-triggered pulmonary MRA may be difficult and the addition of an ultrafast GE in the recirculation phase may counterbalance any unoptimal first MRA. Similar to CT, MR can provide alternative diagnoses or ancillary findings altering the management of the patient. A comprehensive assessment of the venous thromboembolic disease may be achieved by the addition of a MR venous phase without further injection of Gadolinium CM. The sensitivity of the combined test may however be increased at the expense of a higher rate of technically inadequate examinations. It is expected that newer 3D MR angiography sequences will increase yield of this technique in the field of venous thromboembolism.

Take Home Points:
1. Basic sequences for PE detection include unenhanced SSFP, 3D GRE pulmonary MRA and CE-recirculation phase ultrafast GE.
2. MR has a high specificity for PE diagnosis and a high sensitivity for proximal PE.
3. Main limitations remain a lower sensitivity for distal PE detection and possibly a remaining center- or vendor-dependent accuracy.

Evaluating PE with dual layer CT

E. Coche; Brussels/BE

Body: Dual-layer spectral detector CT enabling the retrospective on-demand spectral CT analysis, including ea virtual monochromatic imaging, Z effective cartography and iodine mapping represents a significant step forward for various thoracic disorders work-up. The goal of this presentation is to share our experience with this this unique mode of spectral CT data acquisition in the field of acute pulmonary embolism and highlight the various advantages of this technique.

TECHNICAL ASPECTS

Current clinical Spectral CT scanners enable the discrimination between different materials based on the differential X-ray attenuation properties in two "energy bands" of the spectrum instead of averaging the entire polychromatic X-ray beam like conventional CT does. In other words, the spectral dependencies of the net X-ray attenuation can be imaged and analyzed as a material characteristic and can be used to discriminate tissues beyond the Hounsfield Unit paradigm. The „dual energy" information can be obtained using various acquisition methods, each being characterized by its respective advantages and disadvantages: 1) Single X-ray source, Dual kVp Spin (Philips-Canon), 2) Single X-ray source, Dual kVp Switch (General Electric), 3) Dual X-ray source (Siemens) and 4) Single X-ray source, Dual-Layer Detector (Philips), SingleX-ray source and X-ray beam prefiltration (Siemens) [1, 2]. The dual-layer spectral-detector CT (IQON, Philips Healthcare, Best, The Netherlands) is always operating in a dual-energy mode. The main advantage of the IQon Spectral CT is the retrospective dual-energy analysis with no additional radiation dose. This instrument acquires both conventional images and dual-energy images by measuring the low-energy regions of the emitted spectrum from the upper layer of the detector and high-energy regions from the deeper layer of the detector, allowing for the measurement of iodine density as well as clear visualization of thromboembolism.
In our practice, study, chest CT scans are obtained with a routine protocol using 120 kVp without modifying the imaging protocol or patient selection process to obtain spectral information. If the patient is obese, 140 kVp is preferred and the mAs adjusted to keep the dose neutral. In dual-layer detector spectral CT, SBI images (spectral based images) are captured during each CT examination. The SBI images data set are loaded into the ISP (Intelli Space Portal, Philips Healthcare, Best, The Netherlands) workstation and inspected using different reconstruction algorithms. Analysing the images using a dynamic approach is preffered. Virtual monoenergetic images can be extracted and extrapolated at wide energy levels, ranging from 40 to 200 keV, by simply sliding the cursor to the desired energy level on a dedicated workstation or using the "magic glass" in the PACS. The images are optimized using the concept of « spectral surfing" giving the opportunity to adjust on line the contrast of the image and the noise with potential reduction of artifacts. In our daily routine, the use of iodine, iodine no water and Zeff atomic number maps is the first display used for the detection of small perfusion defects caused by peripheral pulmonary clots, followed by anatomical inspection of the corresponding suspicious feeding artery using the « related slice function ». The iodine distribution within the lung parenchyma is displayed on a gray-scale or in color with different optional colors scales depending on user preference. This simplified process for image acquisition and post-processing in dual-layer detector spectral CT may widen practical uses of spectral information in daily practice such as for the evaluation of incidental findings or improvement of suboptimal studies.

ADDED VALUE OF SPECTRAL CT IN THE DIAGNOSIS OF PE

The diagnostic value of spectral CT for detecting pulmonary embolism has been demonstrated in the international literature. The capability of dual-energy layer CT to use diagnostic information available from both low and high energy levels optimizes the contrast-to-noise ratio within pulmonary vessels and facilitates detection of peripheral endoluminal clots compared with images acquired at fixed energy alone (120 or 140 kVp). The low-energy acquisition allows generation of images with increased vascular enhancement. This property is particulary interesting in daily routine because there are many potential causes affecting the pulmonary vascular enhancement in chest CT such as technical errors, extravasation, transient interruption of contrast material due to Valsalva manoeuvers, or increased circulatory volume in pregnant women. This suboptimal opacification is rarely known in advance and the use of virtual monoenergetic imaging in retrospect can improve vascular opacification at low energy levels (Figure 1A, 1B). The performance of virtual monoenergetic imaging for pulmonary CT angiography (CTA) with a reduced iodine dose has been studied by various groups. In our daily routine, we have reduced the contrast volume by approximately 30% compared to our injection protocol used with conventional CT. Bae and colleagues [3] have determined whether virtual monoenergetic images of good quality obtained from dual-layer detector spectral CT can yield additional diagnostic information. They compared the diagnostic performance for detecting PE of virtual monochromatic imaging at 40 keV and conventional 120-kVp images in patients with a suboptimally enhanced pulmonary artery. They showed that 40-keV virtual monoenergetic images showed higher diagnostic accuracy in the detection of PE than conventional 120-kVp images. In our daily practice, images reconstructed at 50 keV are systematically reconstructed and sent to the PACS for better vessel content analysis.
In addition to monochromatic images, produced at a lower energy if necessary, Iodine no water or iodine maps can improve the diagnostic accuracy of pulmonary embolism also, as mentioned before. The use of virtual monochromatic dual-layer spectral CT imaging at high energy level results in a significant reduction of streak artefacts produced by beam-hardening [4] (Figure 1C). This technical possibility can be useful when high density contrast is present in the subclavian vein or in the superior vena cava during a pulmonary CT angiography performed at high rate of injection or with dense contrast material.
The spectral CT lung blood volume quantification may predict outcomes in patients with pulmonary embolism, but additional validation is needed [5].

ADDITIONAL ADVANTAGES

Many incidental findings localized in the chest wall, breasts, adrenal and thyroid gland discovered during angio CT examination of the pulmonary arteries would benefit of this technique. Some authors have demonstrated that incidental adrenal nodules discovered during a contrast-enhanced spectral CT examination of the abdomen may avoid additional imaging studies for further adrenal nodule characterization [6].

REFERENCES

Fornaro J, Leschka S, Hibbeln D, Butler A, Anderson N, Pache G et al., Dual- and multi-energy CT: approach to functional imaging, Insights Imaging (2011), 2:149-159. Vlassenbroek A, Dual Layer CT, in „Dual Energy CT in Clinical Practice"; Medical Radiology, DOI: 10 10.1007/978-3-642-01740-7, Springer-Verlag Berlin Heidelberg (2011). Bae K, Jeon KN, Cho SB, et al. Improved Opacification of a Suboptimally Enhanced Pulmonary Artery in Chest CT: Experience Using a Dual-Layer Detector Spectral CT. Am J Roentgenol (2018);201:734-741 Wellenberg RH, Boomsma MF, van Osch JA, et al. Quantifying metal artefact reduction using virtual monochromatic dual-layer detector spectralCT imaging in unilateral and bilateral total hip prostheses. Eur Radiol (2017) ;88 :61-70 Apfaltrer P, Bachmann V, Meyer M, Henzler T, Barraza JM, Gruettner J, Walter T, Schoepf UJ, Schoenberg SO, Fink C. Prognostic value of perfusion defect volume at dual energy CTA in patients with pulmonary embolsim : correlation with CTA obstruction scores, CT parameters of right ventricular dysfunction and adverse clinical outcome. Eur J Radiol. (2012);81(11):3592-7 Glazer D, Maturen K, Kaza R, Francis I, Keshavarzi N, Parker R, et al. Adrenal incidentaloma triage with single-source CT. AJR (2014);203:329-335

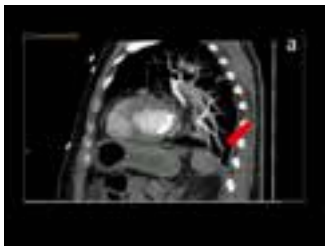

A patient referred to CT for suspicion of pulmonary embolism. (a) A Valsalva maneuver during breathold results in a poor enhancement of the pulmonary arteries on the conventional CT images.

From right to left: Zeff map showing a perfusion deficit of the lung parenchyma (white arrow); - monoE 70 keV; -monoE 55 keV and –monoE 40 keV. When decreasing the energy, the thrombus appears obvious (colored arrows) in a subsegmental artery

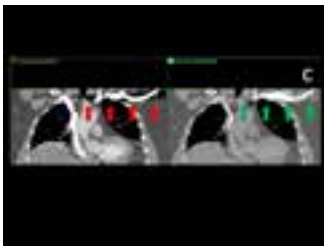

MonoE 200 keV reduces beam hardening from dense contrast medium compared to conventional CT images.

Take Home Points:

1. Dual-layer spectral detector CT improves the diagnostic accuracy and diagnostic confidence in PE detection especially for peripheral clots.
2. This technology enables the reduction of contrast medium dose and increase the vascular contrast enhancement with a significant quality improvement in missed injections and suboptimal studies.
3. Iodine quantification within the pulmonary vascular bed using iodine mapping may represent a new way to evaluate severity and patient outcome in PE but future research is needed to demonstrate its real usefulness
4. Incidental chest and upper abdominal findings will benefit from this retrospective spectral CT analysis but its impact on patient care and clinical management has to be further investigated.

Acute exacerbation: Current definition, differentials and imaging features

N. Sverzellati; Parma/IT

Body: Acute exacerbation is increasingly recognised as an important and relatively common complication of idiopathic pulmonary fibrosis (IPF). The most recent diagnostic criteria for acute exacerbation require a previous or concurrent diagnosis of IPF, an acute worsening or development of dyspnoea typically less than 1 month in duration, evidence on computed tomography (CT) of new bilateral ground-glassopacity and/or consolidation superimposed on a background imaging pattern of usual interstitial pneumonia (UIP) not fully explained by cardiac failure or fluid overload. However, acute exacerbation of IPF characteristically manifests as acute or organizing diffuse alveolar damage and three corresponding CT patterns have been described: peripheral, multifocal, and diffuse parenchymal opacification (predominantly ground-glass opacity but sometimes consolidation), all occurring against a background of preexisting fibrotic change typical of UIP. It was shown that patients with the diffuse pattern of parenchymal opacification at CT had a higher risk of death than those with the multifocal or peripheral pattern. However, in the results of another study, other investigators showed that both the pathologic findings and the CT score were more predictive in terms of prognosis than the CT pattern itself.

Take Home Points:

Many important and potentially treatable acute complications of IPF may be recognisable on CT.
The differential diagnosis of new ground glass opacity on the background of fibrotic changes may be challenging.
In suspected acute exacerbation, CT scans comparison may be crucial and should account for potential confounding factors.

TB: The role of imaging in the worldwide battle

R.R. Gill; Lexington, MA/US

Body: Tuberculosis is a common worldwide infection and a grave medical and social problem causing high mortality and mobidity, especially in developing countries. The traditional imaging concept of primary and reactivation TB has recently been challenged, and it has been proposed that imaging features depend on the level of host immunity rather than elapsed time after infection. The presentation will illustarte the imaging spectrum of Tuberculosis in both typical and atypical TB with an emaphsis on primary and post primary Tuberculosis and multi-drug resistance.

Spectrum of Tuberculosis

Take Home Points:

1. Imaging plays a vital role in diagnosis, monitoring response and guiding management in Tuberculosis.
2. Immune reconstitution syndrome and sarcoidosis can mimic tuberculosis on imaging.
3. Emerging multi-drug resistance to Tuberculosis needs a multidisciplinary approach to help limit the spread of TB and ensure complete treatment.
4. Familiarity with imaging features and reactivation in immune compromised host will help early detection and timely treatment.

Emerging infections: What can imaging tell us?

T. Franquet; Barcelona/ES

Body:

Emerging infections: What can imaging tell us?

Respiratory infections are the commonest illnesses occurring in humans and pneumonia is the leading cause of death due to infectious disease. The spectrum of causative pathogens of pneumonia in humans includes gram-positive bacteria (Streptococcus pneumoniae, Staphylococcus aureus), gram-negative bacteria (Haemophilus influenzae, Escherichia coli, Klebsiella pneumoniae), atypical bacteria (Mycoplasma pneumoniae, Chlamydia pneumoniae, Legionella pneumophilia), oral anaerobes and viral agents, fungi, protozoa and parasites.

Emerging infectious diseases are those that are newly discovered, recently have increased in prevalence, or are expected to increase in prevalence in the future. Causes of emerging infections are environmental changes, rapid population growth, and migration of populations. These infections have rapidly spread around the globe during the modern air-travel era, contributing to the rapidity of communicable disease transfer across international borders.

Several newly discovered viruses with epidemic potential have threatened global health security. New emerging pathogens include among, others community-acquired methicillin-resistant Staphylococcus aureus (MRSA), human metapneumovirus (HMPv), avian influenza A viruses (H5N1), coronavirus associated with severe acute respiratory syndrome (SARS), swine flu (H1N1) (Fig 1) and Middle East Respiratory Syndrome Coronavirus (MERS-CoV) (Fig 2) (Courtesy of Kyung S. Lee)

The clinical evaluation of these patients faces a diagnostic challenge because of the majority of processes presenting with similar signs and symptoms.

Although the imaging findings do not provide a specific etiological diagnosis, the most useful imaging techniques for the evaluation of pulmonary infections are chest radiography and computed tomography. Furthermore, radiographic manifestations of a given infectious process may be variable, depending on the immunologic status of the patient as well as the pre- or coexisting lung disease.

Significant progress has been made over the last several years in dissecting out the molecular biology and pathogenesis of the many emerging and re-emerging pathogens.

Immune reconstitution inflammatory syndrome (IRIS) in HIV-infected patients with mycobacterial infections starting highly active antiretroviral therapy is defined as an exacerbation of symptoms, signs, or radiological manifestations of a pathogenic antigen, which are not due to relapse or recurrence. Patients affected with IRIS undergo deterioration in their clinical status at a time when viral replication appears to be under control and CD4 counts are rising, known as a paradoxical response. These paradoxical reactions have been reported to occur in patients with both infectious and non-infectious antigens.

The most common imaging features of IRIS consist of mediastinal lymph node enlargement, with central low attenuation, diffuse and bilateral pulmonary nodules, organizing pneumonia and small pleural effusions.

H1N1 influenza infection. PA chest radiograph shows multiple bilateral ill-defined opacities (arrows)

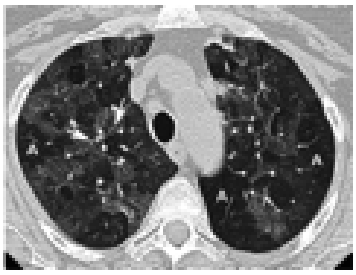

H1N1 influenza infection. b) Axial CT image shows a pattern of „mosaic perfussion" secondary to air-trapping (A) and bronchial wall thickening (arrows)

MERS infection. PA chest radiograph shows a lobar consolidation in the RUL (arrow)

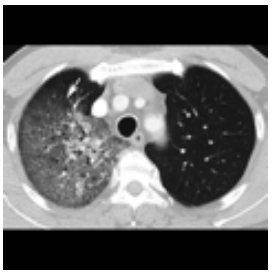

MERS infection. Axial CT image shows extensive ground-glass opacities with superimposed lines („crazy-paving" pattern) in the RUL (arrow).

Take Home Points:
Emerging infections are commonly around the globe during the modern air-travel era Travel and residence history are important in the diagnosis Radiographic manifestations may be variable and may mimic non-infectious processes

The many faces of pulmonary aspergillosis: A memoir

W. Gefter; Philadelphia/US, Penn Medicine, University of Pennsylvania

Body:
Aspergillus is an intriguing pathogen, given the wide variety of lung disorders which this fungal species can cause. These disorders fall along a spectrum depending upon the host immune status and underlying lung structure. This presentation will provide an update on this spectrum of pulmonary aspergillosis, told in the context of a personal narrative.

Background
Aspergillus is a ubiquitous, spore-forming fungus found worldwide, primarily in soil and decaying biomass. The spores (conidia), dispersed by wind in the atmosphere, are easily aerosolized and inhaled. In the normal host, innate immune responses and inflammatory processes limit fungal growth and prevent disease. With immune dysfunction or underlying pulmonary pathology, however, the spores may geminate into hyphae in the respiratory mucosa, leading to disease.
Aspergillus was named in 1729 by Pier Antonio Micheli, an Italian priest and biologist, who noted that the spore-forming conidiophore resembles an aspergillum, the religious instrument used to sprinkle holy water. [1]
Of significance to this ESTI meeting, the first reported case of Aspergillus infection (sinus) occurred in Paris in 1789 during the French revolution [1] and the first radiological description of an aspergilloma was also made in France in 1938.

Semi-invasive and Other Forms of Chronic Pulmonary Aspergillosis
Nearly forty years ago Gefter and colleagues reported cases of intermediate pathogenicity between classic aspergilloma and frankly invasive disease. [2] These cases did not fit into earlier classifications of allergic, saprophytic or invasive forms. They were associated with mild immunosuppression and/or underlying non-cavitary lung disease. Called "semi-invasive", it was observed in patients with sarcoid, chronic debilitating illness, diabetes, malnutrition, alcoholism, advanced age, prior radiation therapy, and COPD.
Radiographic manifestations included chronic consolidation, unilateral or bilateral and most commonly in the upper lobes, usually with associated pleural thickening, and progressive cavity formation (thick walled), with or without mycetoma.
Clinically, the patients may have marked constitutional symptoms, chronic productive cough, fever, malaise, weight loss and hemoptysis. The histology demonstrates tissue necrosis and granulomatous inflammation (similar to reactivation TB)
As noted in the paper, these cases suggested a spectrum related to underlying immune status, rather than the discrete forms indicated in many prior classifications. This is illustrated below in Figure 1 from the original paper. [2]

A follow-up paper by Gefter elaborated further upon this spectrum, as shown in Figure 2 from that paper. [3]
Furthermore, it was predicted that other intermediate chronic forms of aspergillus along this continuum would be observed. [3]
There was initial skepticism among pulmonologists and pathologists about the concept of "semi-invasive" aspergillosis. However, shortly thereafter another paper was published demonstrating similar cases, which the authors called "chronic necrotizing aspergillosis". [4] Over the ensuing years many more papers were published describing chronic forms of pulmonary aspergillosis. These went under a large, bewildering array of names, including the following:
- Simple and complex aspergilloma
- Semi-invasive pulmonary aspergillosis
- Subacute invasive pulmonary aspergillosis (SAIA)
- Chronic necrotizing pulmonary aspergillosis (CNA)
- Chronic cavitary pulmonary aspergillosis (CCPA)
- Chronic fibrosing pulmonary aspergillosis (CFA)

There are more and less aggressive chronic forms of pulmonary aspergillosis, ranging from simple aspergilloma, aspergillus nodule(s), chronic cavitary and fibrosing disease, to more subacute semi-invasive/chronic necrotizing infection, consistent with the spectrum paradigm. [5] CFA is a late stage of CCA. While there are no preexisting cavities in CNA, underlying cavities predate the development of CCPA. Subacute invasive pulmonary aspergillosis (SAIA), which includes the former semi-invasive and CNA types, shows a more rapidly progressive infection (1- 3 months) than that of CCA/CFA, and occurs in more moderately immunosuppressed patients. Pathology in SAIA shows parenchymal invasion by the fungus, and thus the therapy is similar to IPA.
However, the clinical, histopathologic and radiographic manifestations of these chronic forms of pulmonary aspergillosis show considerable overlap. Moreover, one form may evolve into another over time. It may be impossible to differentiate these in the absence of pathology and/or data on temporal progression. Therefore, more recently it has been proposed that these all be classified under the more inclusive and practical general term "chronic pulmonary aspergillosis" [6] or "chronic progressive pulmonary aspergillosis". [7]
Aspergillus Nodule is a less common manifestation of CPA. The nodules may be single or multiple, of variable size, and may have low attenuation or cavitation and spiculated edges.
Thus "semi-invasive PA" became CNA, then SAIA and finally CPA!
Thus the current spectrum can be represented as shown in Figure 3.

Incidence:
In stark contrast to the initial skepticism regarding the existence of "semi-invasive pulmonary aspergillosis", these chronic forms of aspergillosis are now widely recognized. In fact, CPA is estimated to affect 3 million people worldwide (1.74 million following TB, and nearly double that figure given other underlying diseases predisposing to CPA). [8] Given the variable disease forms, the associated respiratory co-morbidity, limited therapeutic options and need for prolonged treatment, CPA is challenging for both patients and care providers. [8] Now recognized as a major global health problem with significant morbidity and mortality, February 1sthas been declared annual "World Aspergillosis Day".

CPA:
As noted above, the symptoms of CPA include weight loss, productive cough, possible hemoptysis, dyspnea and low grade fever, with a duration greater than 3 months. It is almost indistinguishable from TB ("smear-negative TB"). Mistaken for TB and other lung diseases, the diagnosis of CPA is often missed for years.
Predisposing factors include conditions with mild forms of immunocompromise, including COPD, diabetes, CF, corticosteroid therapy, connective tissue disease, alcoholism, debilitation, and cancer.
Co-existing lung diseases include: mycobacterial infection (TB and nontuberculous mycobacterial infection (NTM), which may precede, follow or occur concurrently with CPA), COPD, bronchiectasis, sarcoid, previously treated cancer, ABPA, ankylosing spondylitis, and silicosis.
Diagnostic blood/serological findings include elevated Aspergillus-specific IgG or precipitins (elevated in over 90 % of patients), and total and Aspergillus-specific IgE. Galactomannan aspergillus antigen in BAL (not serum) is also useful.
Positive aspergillus cultures and strong PCR signals in respiratory fluids are supportive of the diagnosis. Biopsy of the cavities demonstrate the fungal hyphae.
Imaging findings include a combination of those due to the CPA as well as the underlying disease. These include: unilateral or bilateral consolidation, usually in the upper lobes, with single or multiple new or pre-existing enlarging cavities of variable wall thickness, with or without an intracavitary fungus ball, peri-cavitary infiltrates, adjacent bronchiectasis, pleural thickening and progressive volume loss. [9] As noted above, the findings may mimic mycobacterial infection.
The diagnosis of CPA is based upon the following criteria [9]:
1. Consistent appearance on thoracic imaging
2. Direct evidence of aspergillus infection or immunological response to Aspergillus species
3. Exclusion of alternative diagnoses
4. Duration greater than 3 months (although SAIA forms may be less than 3 months)

The therapy of CPA is primarily that of long-term antifungal medications (itraconazole for minimum of 6 months). This results in control of symptoms and progression in about 60 % of patients. Unfortunately, many drug (azole)-resistant forms are now being seen and this is of increasing concern.
Small series suggest the benefit of percutaneous intracavitary amphotericin for refractory hemoptysis. [10]
This presentation will also provide more brief updates on important features of the other two major forms of pulmonary aspergillosis along the spectrum, namely IPA and ABPA.

IPA
The "Air Crescent Sign"
During the period of skepticism about semi-invasive aspergillosis, the author and colleagues turned their attention to IPA, and in particular to the "air crescent" ("Monod") sign seen in angioinvasive IPA in patients with acute leukemia and chemotherapy-induced neutropenia. [11,12]. Specifically, the observation was made that the air crescent appears during the recovery phase of infection, coincident with recovery from neutropenia. Radiographic signs of improving consolidation are consistently observed within 2-3 days before cavitation. WBC had recovered to at least 1,000/mm^3 in all patients at the time of cavitation, and the air crescent was associated with better survival. The rounded intracavitary mass outlined by the air crescent is often mistaken for an

"aspergilloma" due to its resemblance to a standard fungus ball, but is actually a sequestrum of infarcted lung due to the vascular invasion by the fungus. There can be life-threatening hemoptysis during this phase of IPA. As illustrated in Figure 4, one of the original figures from [3], when an intracavitary mass is present, the radiographic appearances of IPA, SA, and CPA may appear somewhat similar, but are generally quite different in terms of their clinical settings, temporal evolution, and underlying pathology.
The incidence of IPA has quadrupled in last 13 years. The number of hospitalizations in the U.S. from 2000-2013 has increased 3 % per year. [13] This is a consequence of intensive chemotherapy regimens for solid tumors and others, increased solid organ transplantation, stem cell transplants, and immunosuppression of patients with autoimmune disease.
IPA includes both angioinvasive and airway invasive forms. The mortality rate continues to be very high, greater than 50% in neutropenic patients and greater than 90% in stem cell transplant recipients.
As early neutrophil recruitment inhibits germination of conidia into hyphae, prolonged neutropenia is the major risk factor. [9] However, as shown below, increasingly IPA is occurring in non-neutropenic patients (T cell dysfunction important risk factor) and non-traditional patient groups. Even modest degrees of immunosuppression increase risk, depending on host factors. For example, IPA can occur in patients with COPD exposed to oral or inhaled corticosteroids and in critically ill patients [10]

Risk Factors: [9]
Classic:
- Prolonged, profound neutropenia
- Neutrophil dysfunction
- Hematological malignancy (acute leukemia)
- Hematological stem-cell transplant
- Glucocorticoid therapy
- Immunosuppressive therapy

Emerging risk factors:
- Critically ill (ICU) patients [14]
- ICU patients with influenza [15]
- COPD (especially with oral or inhaled steroids)
- Solid organ transplants
- HIV infection
- CMV infection or reactivation
- Chronic granulomatous disease
- Liver disease
- Diabetes mellitus

The diagnosis of IPA is challenging and often delayed. A high index of suspicion is required.
Tissue biopsy and histopathology demonstration of tissue invasion by fungal hyphae is the gold standard, but is often not feasible due to poor respiratory status and bleeding tendency. BAL with washings for culture and cytology can be attempted. [9]
Aspergillus from sputum has a high PPV for IPA in patients with leukemia and post stem cell transplantation.
Aspergillus antigen detection in serum or BAL with Galactomannan testing (approx. 50 % PPV, 90 % NPV) or Aspergillus polymerase chain reaction (PCR) assay in BAL have high diagnostic value and are increasingly used. [9]
CT imaging provides earlier diagnosis and better prognosis. The most common initial manifestations are solid nodule(s) with a perinodular rim of ground glass opacity, the so-called "halo sign" due to hemorrhage. The halo sign is associated with a significantly better response to therapy and greater survival. [9] However, the halo sign may be missed if CT is not performed early in the course of the disease. Continued neutropenia may result in progressive consolidation, and in some cases the opacities may have a peripheral infarct pattern.
Airway Invasive Aspergillosis: In this form of IPA, the Aspergillus hyphae invade deep to airway basement membrane. Clinical manifestations include acute tracheobronchitis, bronchiolitis and bronchopneumonia. Imaging may show tracheal and bronchial wall thickening, centrilobular nodules, "tree-in-bud" opacities, and peribronchial consolidation. [16] In lung transplants ulcerative, pseudomembranous and obstructive variants can occur.
The principal therapy for IPA is the anti-fungal agent voriconazole, along with an attempt to decrease the immunocompromised state when possible.

Allergic Pulmonary Aspergillosis
In 1981, the author turned attention to the opposite, hypersensitivity end of the immune spectrum, namely that of ABPA. [17]
Spores can be trapped in viscid sputum and colonize airways in susceptible asthmatics. The conidia may germinate within airways and form hyphae, leading to an inflammatory response. Strong humeral and cellular immunological responses involving heightened T-helper cell (Th2 CD4 T-cell response) lead to aspergillus sensitization. [18]
Resulting disorders of the airways due to aspergillus sensitization include the following:
- ABPA
- Aspergillus-induced asthma (AIA)
- Severe asthma with fungal sensitization (SAFS) (recently described)
- Hypersensitivity pneumonitis
- (Allergic aspergillus sinusitis)

ABPA:
ABPA occurs in approximately 2.5 % of asthmatics, and in 8 % of patients with cystic fibrosis. [9] In high TB prevalent areas, ABPA, like CPA, is frequently misdiagnosed as TB.
Clinically, in addition to asthmatic symptoms, patients may expectorate golden-brown plugs.
Chest radiographic findings include transient, migratory opacities, consolidation, "toothpaste" and "finger-in-glove" branching tubular opacities (mucus plugs), atelectasis, and findings of bronchiectasis. Pulmonary fibrosis with contracted upper lobes occurs in late-stage disease.
CT demonstration of central bronchiectasis is classic for ABPA, but peripheral bronchiectasis is also common. [9] Bronchiectasis may be absent early in the course of the disease. [10] Cases without bronchiectasis are referred to as "serological ABPA". There is associated bronchial wall thickening. High-attenuation mucus plugs (HAM) (greater than 70 HU) are present in up to 20 % of patients and considered pathognomonic for ABPA. [9] Other findings include consolidation and/or non-homogeneous opacities, segmental or lobar atelectasis, and cavitation.

Diagnostic criteria for ABPA: [9]
1. Predisposing condition: asthma or CF
2. Obligatory criteria: positive Aspergillus skin test or elevated IgE against A. fumigatus
3. Total IgE greater than 1,000 IU/ml

Supportive criteria (2/3):
1. Serum precipitins or IgG against A. fumigatus
2. Radiographic features consistent with ABPA
3. Recent blood eosinophil count greater than 500 cells/L in corticosteroid naïve patients

Oral corticosteroids are the mainstay of ABPA treatment. This may be supplemented with anti-fungal agents (itraconazole). Omalizumab (a monoclonal antibody against IgE) is promising.

Common chronic lung diseases predisposing to pulmonary aspergillosis:
In light of the above, it is evident that many common, chronic lung diseases may be complicated by aspergillus. Examples are the following:
- Asthma and CF: ABPA, CPA
- COPD: CPA, IPA
- Post-TB: CPA
- Nontuberculous mycobacteria (NTM): CPA
- Sarcoid: CPA

Transformations between types:
One form of pulmonary aspergillosis may transform into another, examples including:
ABPA (bronchiectasis) to aspergilloma
Aspergilloma (hypersensitivity) to ABPA
Aspergilloma (with immunosuppression) to IPA or CPA

Bringing the personal story to a close
A recent 10-year retrospective study comparing mortality in CPA vs IPA vs simple aspergilloma (SA) has demonstrated that the survival of patients with "semi-invasive" features of pulmonary aspergillosis is intermediate between those with simple aspergilloma (SA) and those with IPA (although considerably closer to SA). [19] This is in keeping with the original concept that the manifestations of pulmonary aspergillosis fall along a clinically relevant spectrum.

References
1. Lee J. www.antimicrobe.org
2. Gefter WB et al. Semi-invasive pulmonary aspergillosis: a new look at the spectrum of Aspergillus infections of the lung. Radiology 1981; 140: 313-321]
3. Gefter WB. The spectrum of pulmonary aspergillosis. J Thorac Imaging 1992; 7:56-74]
4. Binder RE et al. Chronic necrotizing pulmonary aspergillosis: a discrete clinical entity. Medicine 1982; 61:109
5. Denning et al. Eur Respir J 2016; 47: 45-68
6. Desai et al. Chronic aspergillosis of the lungs: unravelling the terminology and radiology. Eur Radiol 2015]
7. Izumikawa K et al. J Infect Chemother 2014; 20: 208-12
8. Hayes GE, Novak-Frazer L. Chronic pulmonary aspergillosis–Where are we? And Where are we going? J Fungi 2016; 2:18]
9. Kanj A. The spectrum of pulmonary aspergillosis. Respir Med 2018; 141: 121-131
10. Patterson KC, Strek ME. Diagnosis and treatment of pulmonary aspergillosis syndrome. Chest 2014: 146:1358-1368
11. Albelda SM et al. Pulmonary cavitation and massive hemoptysis in invasive pulmonary aspergillosis. Am Rev Respir Dis 1985; 131: 115-120
12. Gefter WB et al. Invasive pulmonary aspergillosis and acute leukemia. Limitations in the diagnostic utility of the air crescent sign. Radiology 157; 605-610
13. CDC-Fungal Diseases. https://ww.cdc.gov/fungal/diseases/aspergillosis/statistics.html
14. Taccone FS et al. Critical Care 2015; 19:7]
15. Schauwvlieghe A et al. Lancet Respir Med 2018; 6: 782-7920
16. Franquet T et al. Spectrum of pulmonary aspergillosis: histologic, clinical and radiologic findings. RadioGraphics 2001; 21: 825-833
17. Gefter WB et al. Allergic bronchopulmonary aspergillosis. Less common patterns. Radiology 1981; 140: 307-312
18. Shah A, Panjabi C. Allergic aspergillosis of the respiratory tract. Eur Respir Rev 2014; 23: 8-29].
19. Chan JFW et al. Emerging microbes and infections 2016; 5, e37

Figure 1

Figure 2

Figure 3

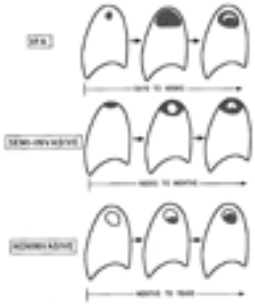

Figure 4

Take Home Points:
The concept that the varying forms of pulmonary aspergillosis form a spectrum largely dependent upon the patient's immune status together with underlying lung pathology, originally introduced in 1981 [2], has been validated over subsequent years.
Chronic forms of pulmonary aspergillosis, occurring along this continuum between saprophytic aspergillomas and frankly invasive IPA, beginning with the observation of "semi-invasive" aspergillosis [2], have been described and labelled with a wide variety of names. However, given their substantial overlapping clinical, histopathologic and imaging features, they can be grouped under the more practical and general term "chronic pulmonary aspergillosis" [6].
Pulmonary aspergillosis can complicate many common chronic lung diseases, including CPA occurring in patients with COPD, post-TB, and nontuberculous mycobacteria NTM; and ABPA complicating patients with asthma and cystic fibrosis.
Pulmonary aspergillosis is increasing in incidence. Stem cell and solid organ transplants, and aggressive chemotherapy and immunosuppressive regimens have resulted in an increased occurrence of IPA. The latter is also emerging in non-traditional patient populations such as those with COPD on steroids, critically ill patients in the ICU, and recently observed complicating severe influenza.
Taken together, all of these forms of pulmonary aspergillosis constitute a growing global health burden.

Evaluating the pulmonary veins before and after ablation

M. Das; Duisburg/DE

Body: Atrial fibrillation (AF) is a serious socioeconomic health problem. The prevalence has increased over the recent years. The prevalence currently is about 2%. A significant increase of AF in the general population has been estimated – probably due to more sensitive detection and treatment options. If proper screening would be applied prevalence could be as high as 3%. AF is frequently associated with cardiac disease especially coronary artery disease (CAD), valvular heart disease and cardiomyopathy. Patients with AF have an 2-5 fold increased risk of stroke and death, which makes sufficient treatment essential. It is estimated that 14-17 million people will suffer from AF in 2030. Risk modification and antithrombotic treatment are among the basic treatment options, while cardioversion to restore sinus rhythm should be attempted as next step. In patients with symptomatic paroxysmal AF or patients refractory to antiarrhythmic medication should be treated with catheter ablation. Prior to catheter ablation imaging of the left atrium (LA) is beneficial for ablation planning as LA anatomy varies greatly and ablation success depends on the appropriate sizing of the catheters. Furthermore, LA radiofrequency ablation is associated with several potential complications, such as air embolism, atrial-esophageal fistula and cardiac tamponade and perforation. Traditionally transesophageal ultrasound was the method of choice, but since cardiac CT can be performed at a low radiation dose level, with high spatial resolution – CT has become more and more important. Furthermore, dedicated post processing software can facilitate thin section CT for guiding the procedure. Usually a prospective triggered CT scan, similar to dedicated coronary CTA protocols can be used – depending on the heart rate of the patient. But contrary to the imaging of the coronary arteries movement is not a critical issue. Using dedicate post processing software the LA can be assessed and especially the origin of the pulmonary veins should be described and measured. Using appropriate imaging technique and precise measurement decreases procedure time, accuracy and reduces the risk for complications.

Take Home Points:
- Learn about the etiology of atrial fibrillation
- Learn about different treatment option of atrial fibrillation
- Understand how different imaging techniques help in treatment planning and how the benefit treatment success

Coronary calcium scoring on ungated CT: As useful as dedicated scoring on gated CT?

R. Vliegenthart; Groningen/NL

Body: The coronary calcium score (CCS) based on non-contrast, ECG-synchronized cardiac CT is a reliable and reproducible non-invasive measure of coronary atherosclerosis. The CCS has emerged as the strongest predictor of coronary events in asymptomatic individuals. While elevated CCS is related to a high risk of coronary events, a CCS of 0 makes the risk of coronary events negligible for the next 5-10 years. In particular in individuals at intermediate risk based on cardiovascular risk factors, the CCS results in better risk stratification for primary prevention.
Coronary calcium can also be detected on routine chest CT, including low-dose CT for lung cancer screening. Calcium scoring or ordinal assessment of coronary calcium on non-ECG-synchronized chest CT correlates well with results from cardiac CT. However, CCS derived from chest CT usually underestimates the amount of coronary calcium compared to dedicated cardiac CT. Thus a CCS of 0 on chest CT does not reliably exclude the presence of coronary calcium. Even so, an estimate of the amount of coronary calcium based on chest CT has value. A number of studies has described the relationship between extent of coronary calcium on chest CT and cardiovascular risk as well as mortality. Reporting coronary calcium on chest CT provides an opportunity for identifying individuals at elevated risk of coronary events, and may potentially help to increase the efficiency of lung cancer screening.

Take Home Points:
1. The CCS is the strongest non-invasive predictor of coronary events.
2. ECG-synchronized cardiac CT with newer CT systems results in the most robust CCS.
3. Chest CT offers the opportunity to derive an estimate of the amount of coronary calcium with relation to the risk of coronary events.

Cardiac calcifications: What do they tell us?

F. Pontana; Lille/FR

Body: Population ageing and other risk factors are not only associated with calcification of coronary arteries but are also likely to induce changes in the cardiac structure. These changes can be evaluated on a standard chest CT without cardiac synchronisation. Calcifications of the cardiac valves may be a sign of valvulopathy. Aortic valve calcium scoring by CT is useful to estimate aortic stenosis severity when echocardiography is not feasible or not conclusive. Previous myocardial infarction can also be identified on non-gated CT with features including mural thinning, calcifications in a coronary artery territory and calcified thrombus. Myocardial calcification may be due to abnormalities of calcium homeostasis or more rarely to calcium accumulation in necrotised cardiac myocytes in the context of septic shock. Pericardial calcification is a sign of constrictive pericarditis.

Take Home Points:
- Calcification is a common finding on non-gated Chest CT
- The four main locations of calcifications are the coronary arteries, the myocardium, the pericardium and the heart valves
- Every radiologist should report pathological aspects such as CAD, healed MI and constrictive pericarditis

Imaging-guided bronchoscopic biopsy: New indications and strategies

J.B. Stern, T. Vieira, L. Perrot, R. Caliandro; Paris/FR

Body: The discovery of pulmonary nodule(s) on chest CT is a frequent situation in pulmonary medicine. Obtaining a pathologic diagnosis on peripheral pulmonary nodules (PPN) may be challenging. The choice between transthoracic CT/US approach, standard bronchoscopy or more recent endoscopic techniques, such as imaging-guided bronchoscopy, depends on the location and size of the nodule(s), the presence or absence of a bronchus in contact with the PPN (“bronchus sign”), but also on the patient’s condition such as the presence of emphysema or a risk of bleeding.
We review the different imaging-guided endoscopy techniques allowing biopsies of PPNs, including virtual bronchoscopy, radial endobronchial ultrasonography, and electromagnetic navigated bronchoscopy (ENB).
We discuss the respective place of these techniques, their diagnostic yield and the future directions.

Figure 1: Presence of an 11 mm right upper lobe pulmonary nodule in a 72 years old woman who had a breast cancer in 2007, and a colon cancer in 2012.

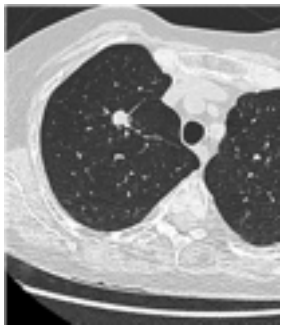

Figure 2: electromagnetic navigated bronchoscopy (ENB) showing the position of the probe in contact with the nodule.

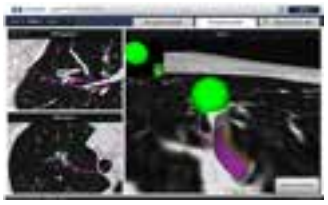

Figure 3: Distal biopsies; final diagnosis: pulmonary metastasis of colon cancer.

Take Home Points:
In addition to standard bronchoscopy, or CT/US guided pulmonary biopsies, new imaging guided bronchoscopic techniques have emerged for the pathological diagnosis of peripheral pulmonary nodules, including virtual bronchoscopy, radial endobronchial ultrasonography, and electromagnetic navigated bronchoscopy (ENB), with efficient diagnostic yields.

Percutaneous ablation of lung malignancies

J. Klein; Burlington/US

Body: Advances in the detection of lung cancer and pulmonary metastases along with parallel development of percutaneous needle ablation systems positioned under imaging guidance has led to the development of minimally-invasive techniques that can be employed in the treatment of localized thoracic malignancy. These procedures can be performed under conscious sedation or general anesthesia with precise placement of probes that induce infarction of lung tumors with minimal damage to lung and surrounding structures. This presentation will review the various modalities employed in percutaneous ablation of lung tumors with a focus on patient selection, choice of ablation modality and technical aspects of the procedures, and the published data supporting use of these systems with illustrative examples.

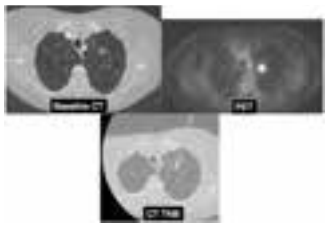

CT-guided biopsy of FDG-avid left upper lobe lung cancer

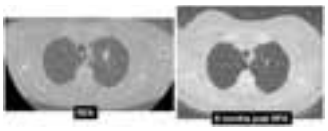

CT-guided radiofrequency ablation of left upper lung tumor shows reduction in tumor size at 6 months

Take Home Points:
1. The three main modalities employed in percutaneous image-guided ablation of lung tumors are radiofrequency ablation, cryoablation, and microwave ablation.
2. Patient and lesion selection are crucial to safe and effective use of percutaneous lung ablation.
3. Each modality has benefits and shortcomings that must be taken into account when choosing the appropriate modality to employ.
4. There is strong data supporting the benefit of these techniques in the selective treatment of lung tumors, particularly in patients with oligometastatic disease.

Pleural interventions

F. Gleeson; Oxford/UK

Body: This presentation will focus on when interventions should be performed. The anatomy of the pleura and chest wall will be explained, and the benefits of using US or CT as the image guidance technique will be discussed.
The imaging differentiation of infected and non-infected pleural effusions will be discussed, and the differentiation of pulmonary abscesses from pleural infection explained.
The use of PET-CT to identify areas for biopsy in patients with malignant pleural thickening will also be illustrated

Take Home Points:
1. It is important to understand the position of the intercostal arteries when performing pleural intervention
2. CT is able to differentiate transudative from exudative pleural effusions
3. CT can differentiate a pulmonary abscess from an empyema
4. US is the imaging technique of choice for insertion of chest drains, but has limitations
5. CT is the imaging technique of choice for most pleural biopsies

Closed chest limited anatomical pulmonary resections: The role of new imaging modalities

D. Gossot; Paris/FR

Body:
Dominique Gossot and Agathe Seguin-Givelet
Thoracic Department,
Curie-Montsouris Thoracic Institute, Institut Mutualiste Montsouris, Paris, France

Disclosure: None

Thoracic surgery has been impacted by 2 major trends in recent years: 1) closed chest techniques, known as VATS (video-assisted thoracic surgery), be they thoracoscopic or robotically assisted and 2) the notion of parenchymal savings (1). Several studies have demonstrated that sublobar resections for NCSCS have a survival equivalent to that of lobectomies while having a lower morbidity (2). This reduction in morbidity is optimal when the procedure is performed via closed chest surgery. But performing an anatomical sublobar resection by thoracoscopy is a real technical challenge, mainly because the surgeon cannot manipulate the parenchyma and expose all anatomical structures as he/she would through an open chest surgery.
The purpose of our presentation is to present the new imaging modalities that assist the surgeon.

Electromagnetic endobronchial navigation (ENB)
More and more patients are now being referred to the surgeon with a suspicion of pT1a NSCLC or with GGOs. One of the features of these newly encountered lesions is the difficult detection because of their size and their inconsistency at palpation, particularly for ground glass opacities. Different criteria have been reported for preoperative localization: preoperative injection of dyes (methylene blue, lipiodol, colored collagen etc.), metallic markers placement within the lesion (coils, fiduciaries) or hooks, transthoracic or thoracoscopic ultrasound with all their advantages and limitations. Particularly noteworthy are the risks of pneumothorax for CT-guided procedures, the migration of hooks or coils, logistical difficulties related to the transfer of the patient from the radiology room to the operating theatre. These potential complications could be reduced by performing these techniques immediately before surgery in the operating room thanks to hybrid rooms equipped with C-arm CT. We are progressively replacing preoperative marking under CT scan by ENB (Fig.1) that is done immediately before surgery on a patient under general anesthesia (3). Technical principles of ENB will be described in another presentation.

3-D modelization
The bronchovascular anatomy of the pulmonary segments is complex and includes multiple variations (4,5). It can even be asserted there is no standard segmental anatomy. The concern related to the thoracoscopic approach is the difficulty to properly expose anatomical structures and the lack of global vision of the lung. The distribution and direction of arteries and veins is therefore often difficult to apprehend. For example, the opening of the fissure and extensive dissection of the vessels only allows them to be exposed over a limited length, so it is often problematic to state that a particular vessel is intended for a particular segment. This is why it is essential backing on mapping during the procedure but also beforehand to study anatomical variations in the preoperative period. This mapping is based on a three-dimensional (3D) reconstruction from an injected CT-scanner (CT) (Fig.2). Several software programs allow navigation through the anatomy, layer by layer and superimposing elements, for example bronchi and arteries or bronchi and veins. In our department, we have found that when the surgeon has a cartography, it is used during surgery in more than 75% of cases, even if he/she has studied the reconstruction before the operation.

Several teams have demonstrated the study of preoperative computed tomography three-dimensional reconstruction helps asserting the number and direction of arteries with good correlation. Oizumi et al. reported a correlation rate between 3D model and intraoperative findings of 98% (6). Eguchi et al. demonstrated in 14 consecutive patients the usefulness of manipulating the 3D CT navigation using a tablet interactively during the thoracoscopic procedure, helping them to perform the procedure safely and offering a valuable learning with regard to pulmonary vessel anatomy (7).
With the vascular pattern in mind the surgeon can perform a safer dissection of the pulmonary artery branches, especially when the fissure is fused and/or when lymph nodes are present. The 3D model can be used via a planning software and manipulated from any direction, either on a laptop, on a tablet or smartphone. All members of the surgical team have a direct access to the images on their own phone or tablet so that strategy and technical issues can be discussed within the group at any time. The software not only allows studying the main anatomical landmarks, in total or separately, but provides the following helpful functions:1) Display of virtual segmentectomy by clicking on a selected bronchus, 2) Calculation of the volume of the resected segment, 3) Calculation and simulation of a safety margin (8,9). This helps visualizing if the planned segmentectomy will have a safe margin, or if a more extended resection must be chosen for carcinological safety (Fig.3).
Although 3D modeling is an insight, it is not yet the ideal tool and does not solve all orientation and comprehension problems during the procedure. The perfect system would be the use of augmented reality with overlaying on the screen of real and virtual anatomy. Unfortunately, it seems we have to wait several years for such a system. The technological challenge is indeed major because of the movements of the anatomical structures related to heartbeats and especially the fact that the models are made from a CT on a ventilated lung while the surgeon operates on a non-ventilated lung.

Near-infrared imaging
Inadequate determination and division of the intersegmental plane (ISP) can determinate unsatisfactory oncological and surgical results, being the main cause of locoregional recurrence and impaired long-term survival following segmentectomy.
The conventional and most common maneuver used for delineation of the ISP consists of inflating the whole lung after occlusion of the target segmental bronchus inducing collapse of the segment to be resected and inflation of the remaining lung. However, because of the collateral ventilation and because the inflated segments limits working space during thoracoscopic procedures, this method is unreliable. Near-infrared imaging with indocyanine green (ICG) systemic injection after the division of the segmental vessels and bronchi is a major improvement (10). The fluorescence covered all structures except the isolated segment to be resected. The reported success rate ranges from 85 % to 100 %. We are using systemic injection of ICG routinely in all our segmentectomy cases for 2 years and in our experience, the success rate is closer to 90 % (Fig.4). It seems that poor vascularization of the parenchyma, as observed in patients presenting with COPD, can be a cause of failure.

References:
Cao C, Tian DH, Wang D, Chung C, Gossot D, Bott M. Sublobar resections—current evidence and future challenges. J Thorac Dis. 2017;9:4853-5. Lutz J, Seguin-Givelet A, Grigoroiu M, Brian E, Girard P, Gossot D. Oncological results of full thoracoscopic major pulmonary resections for clinical Stage I non-small-cell lung cancer. Eur J Cardiothor Surg. 2019;55:263-70. Seguin-Givelet A, Grigoroiu M, Brian E, Gossot D. Planning and marking for thoracoscopic anatomical segmentectomies. J Thorac Dis. 2018;10:S1187-S94 Gossot D, Seguin-Givelet A. Anatomical variations and pitfalls to know during thoracoscopic segmentectomies. J Thorac Dis. 2018;10:S1134-S44. Nomori H, Okada M. Illustrated anatomical Segmentectomy for Lung Cancer. Springer-Verlag; 2012. Oizumi H, Kanauchi N, Kato H, Endoh M, Suzuki J, Fukaya K, et al. Anatomic thoracoscopic pulmonary segmentectomy under 3-dimensional multidetector computed tomography simulation: a report of 52 consecutive cases. J Thorac Cardiovasc Surg. 2011;141(3):678-82. Eguchi T, Takasuna K, Kitazawa A, Fukuzawa Y, Sakaue Y, Yoshida K, et al. Three-dimensional imaging navigation during a lung segmentectomy using an iPad European journal of cardio-thoracic surgery : Eur J Cardiothor Surg. 2012;41:893-7. Iwano S, Yokoi K, Taniguchi T, Kawaguchi K, Fukui T, Naganawa S. Planning of segmentectomy using three-dimensional computed tomography angiography with a virtual safety margin: technique and initial experience. Lung Cancer. 2013;81:410-5. Gossot D, Lutz JA, Grigoroiu M, Brian E, Seguin-Givelet A. Unplanned Procedures During Thoracoscopic Segmentectomies. Ann Thorac Surg. 2017;104:1710-7. Abdelsattar Z, Blackmon S. Using novel technology to augment complex video-assisted thoracoscopic single basilar segmentectomy. J Thorac Dis. 2018;10:S1168-S78.

Fig.1: Immediate preoperative localization of a ground glass opacity under electromagnetic endobronchial navigation.

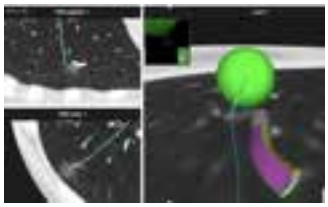

Fig.2: 3D modelisation of arteries in a patient who will undergo a sublobar resection for a cT1a adenocarcinoma.

Fig.3: 3D modelisation with determination of the safety margin (nodule in green, margin in pale yellow) The nodule is located in right S10segment. The addition of a safety margin shows resection must be extended to S9 segment.

Fig.4: Delineation of the intersegmental plane between segment S6 and the basilar segments by systemic injection of indocyanine green under near-infrared imaging.

Take Home Points:

1) New sophisticated imaging systems are almost indispensable for safe and oncologically valid sublobar resections
2) Three-dimensional reconstructions help the surgeon detecting anatomical variations and studying mapping before and during thoracoscopic anatomical segmentectomies.
4) Several imaging systems help determining the intersegmental plane. Near-infrared imaging with indocyanine green systemic injection after the division of the segmental vessels and bronchi seems is currently the most accurate method.

ORAL ABSTRACTS

Low-dose computed tomography (LDCT) screening reduces lung cancer mortality beyond 5 years

M. Silva[1], F. Sabia[2], S. Sestini[2], M. Boeri[2], G. Sozzi[2], A. Marchianò[2], N. Sverzellati[1], U. Pastorino[2]; [1]Parma/IT, [2]Milan/IT

Purpose/Objectives: To assess the long-term benefit of lung cancer screening (LCS) by low-dose computed tomography (LDCT), notably the overall and lung cancer (LC) specific mortality beyond 5 years and until 10 years.

Methods and Materials: The Multicenter Italian Lung Detection (MILD) trial prospectively enrolled 4,099 participants, randomized to either LDCT arm (n=2,376) or control arm (n=1,723); 39,293 person-years of follow-up were accumulated between 2005 and June 2018. The primary outcomes were 10-year overall and LC specific mortality. A landmark analysis was used to test the specific long-term effect of LCS beyond 5 years, notably by selective exclusion of events that occurred < 5 years. Cumulative mortality was evaluated using Kaplan-Meier estimator and differences among groups were tested using Log-rank test, adjusted for sex, age and pack-years. The prognostic value of assigned arm in predicting mortality was investigated by Cox's proportional-hazard's regression adjusted for the above variables.

Results: In the whole 10-year LCS, LDCT arm showed a protective non-statistically significant trend for reduction of overall mortality (HR: 0.80, 95 % CI 0.62 to 1.03) and a significant 39% reduced risk of LC mortality (HR 0.61, 95 % CI 0.39 to 0.95), compared to the control arm. The landmark analysis beyond the 5thyear of screening showed significant reduction of mortality in the LDCT arm: 32 % reduction of overall mortality (HR: 0.68, 95 % CI 0.49 to 0.94), 58 % reduced risk of LC mortality (HR 0.42, 95 % CI 0.22 to 0.79).

Conclusion: LDCT screening reduces lung cancer mortality and overall mortality, especially in the long-term range between 5 and 10 years.

Lung cancer risk after baseline round of screening: Only 20% of NLST eligibles require annual round

M. Silva[1], G. Milanese[1], F. Sabia[2], C. Jacobs[3], B. van Ginneken[3], M.M. Prokop[3], C.M.M. Schaefer-Prokop[4], A. Marchianò[2], N. Sverzellati[1], U. Pastorino[2]; [1]Parma/IT, [2]Milan/IT, [3]Nijmegen/NL, [4]Amersfoort/NL

Purpose/Objectives: To calculate the risk of lung cancer (LC) in 1 year and 3 years after baseline low-dose computed tomography (LDCT) in high-risk subjects selected by the National Lung Cancer Screening Trial (NLST) criteria.

Methods and Materials: Subjects from the Multicentric Italian Lung Detection (MILD) trial were selected according to NLST criteria: age ≥55 years and pack-years ≥30. Baseline characteristics were: smoking status (former/current), gender, percent of predicted forced expiratory volume in first second (FEV 1% pred, 90 % threshold), Tiffeneau ratio (70 % threshold), nodules at baseline LDCT. The risk of LC in 1 and 3 years was calculated by multivariate models.

Results: In 1,248 NLST eligible screenees, LC frequency was 1.2 % at 1year, 2.6 % at 3 years. At 1 year, nodule volume on LDCT was the only predictor of LC risk (volume >250 mm^3, odds ratio (OR) 34.25, p=0.0009). At 3 years, the risk of LC was predicted by: nodule volume 113-250 mm^3 (OR9.52 p=0.01), nodule volume >250 mm^3 (OR29.07, p<0.001), Tiffeneau ≤70 % (OR2.08 p=0.0195). A simulation of triennial screening rounds, with selective annual round only for nodule volume ≥113 mm^3 (19,9 % in our population) showed 40 % reduction of LDTC through 3 years, and 80 % LDCT saving at each annual round.

Conclusion: Annual round is worthwhile for nodule ≥113mm^3 (about 20 % in our population). Screening every 3 years can safely reduce the LDCT burden for nodule <113mm^3 (about 80 % in our population).

Lung Cancer Screening with Ultralow Dose Chest CT: Potential Pitfalls of Pulmonary Findings in Different Readers with Various Experience Levels

K. Martini[1], T. Ottilinger[2], B. Serralach[2], S. Markart[2], N. Glaser-Gallion[2], C. Blüthgen[1], S. Leschka[2], R.W. Bauer[3], S. Wildermuth[2], M. Messerli[1]; [1]Zurich/CH, [2]St. Gallen/CH, [3]Wiesbaden/DE

Purpose/Objectives: To assess the interreader variability of ultralow dose CT for lung cancer screening in radiologists with various experience levels.

Methods and Materials: Six radiologists with different degrees of clinical experience in radiology (range, 1-15 years), rated 100 ultralow dose CT chest studies as either negative screening finding (no nodules, benign nodules, nodules <5 mm), indeterminae finding (nodules 5-10 mm), positive finding (nodules >10mm) (Figure 1). Each radiologist interpreted the scans randomly ordered and reading time for each scan was recorded. Interobserver agreement was assessed with a k statistic. Nodule size agreement was calculated using the interclass correlation coefficient. Reasons for differences in nodule classification were analysed on a case-by-case basis. Reading time was correlated with reader experience using Pearson correlation (r).

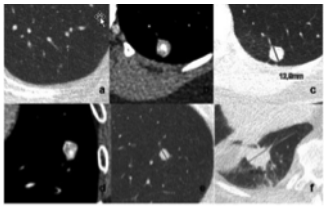

a) benign nodule measuring ✣4 mm (N3), b) and c) partially calcified benign nodule (N2/C), d) benign nodule with fat content (N2/F),e) indeterminate nodule (I) measuring 5-10mm and f) positive nodule measuring >10mm (P).

Results: The overall interobserver agreement between all readers was moderate (k = 0.454; p<0.001). In 57 patients, all radiologists agreed on the differentiation of negative (no further action required) and indeterminate/positive finding (further work-up needed). In 64 cases disagreement between readers led to different nodule classification. In 43 of these cases disagreement led to different management: in 35 cases some readers rated the nodule as benign (N1-N3), while other rated the finding as indeterminate (I) – in other 8 cases some readers rated the nodule as benign, whereas others scored the case as positive (P) (Figure 1). Overall, disagreement in nodule classification was mostly due to failure in identification of target lesion (n = 40), lesion measurement (n = 44) or missed calcium/fat-content (n = 26). Mean overall reading time per scan was of 2 min 2 s (range: 7 s - 7 min 45 s) and correlated with reader-experience (r = -0.824) (Firgure 3).

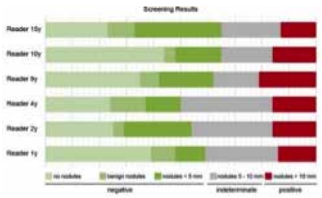

Frequency distribution of different nodule classification among the six readers.

Correlation of reading time and reader experience.

Conclusion: Our study showed substantial interobserver variability in nodule detection and classification in ultralow dose CT for lung cancer screening. This highlights the importance for standardisation of screening programs harmonizing reading results in different radiologists and institutions. We identified and report the most frequent pitfalls in pulmonary nodule detection in ultralow dose CT for lung cancer screening.

Regional polish lung cancer screening program - CT results and lung cancer detection rate

M. Jelitto-Gorska, W. Rzyman, K. Dziadziuszko, M. Magnus, A. Durawa, E. Szurowska; Gdansk/PL

Purpose/Objectives: Low dose computed tomography (LDCT) screening is proved to reduce lung cancer mortality due to detection of early stages of this malignancy. Apart from detected lung cancers in such programs many incidental nodules are found. The goal of the study is to summarize the results of regional polish lung cancer screening program with lung cancer detection rate.

Methods and Materials: In the northern region of Poland, between April 2016 to May 2018, 6640 healthy volunteers aged 50-79 years with at least 30 pack-years history of cigarette smoking, were enrolled into lung cancer screening study with LDCT. Both Computed Aided Diagnosis (CAD) software and visual assessment by experienced radiologist were applied in LDCT reading. Nodule volumetry was the base for results categorization. Changes in tumor size were assessed by volume doubling time (VDT) and progression was diagnosed when VDT was between 20-400 days. The negative result was set when no nodule or nodule below 0,049 ml was detected and no further follow-up was recommended. All nodules larger than >0,049 ml were treated as positive results and further recommendations were applied according to tumor size, but the final decision was made by an experienced radiologist. Participants with nodules 0,05-0,5 ml were sent to control LDCT after 6 months. Tumors at least >0,5 ml or with progression after follow-up was sent to multidisciplinary tumor board. Patients with suspicious nodules were sent to thoracic surgery department for diagnostic work-up and surgery when needed.

Results: The negative result was described in 4115 (62 %) and positive result in 2525 (38 %) cases. In positive group lesions between 0,05-0,5 ml were noticed in 2001 (79 %) cases but only 1560 nodules were recommended to follow-up after 6 months. Up to May 2018, 1201 control LDCT were performed. In follow-up 624 (52 %) lesions regressed, 438 (36 %) lesions were stable in size, 127 (11 %) progressed. In 12 cases new lesions appeared. Multidisciplinary tumor board was recommended in 462 cases, 335 after baseline LDCT and 127 after follow-up. 228 patients were admitted to department od thoracic surgery for diagnostic work-up. On the base of diagnostic procedures and surgery 127 primary lung cancers were proved with 85% cases in early stage I or II which were radically treated. Overall lung cancer detection rate was 1,9 %.

Conclusion: Lung cancer screening program with LDCT has potential to detect many incidental nodules, but also early stages of lung cancer, which could be treated radically.

Lung cancer screening in an oncologic patient population. Results of our 7 year experience

E. O'Dwyer, D. Halpenny, M.S. Ginsberg; New York/US

Purpose/Objectives: The aim of this study was to describe the clinical characteristics and radiological findings in patients presenting to Computed Tomography (CT) lung cancer screening program performed within a Cancer Center, whose screening population predominantly contains patients with prior history of malignancy.

Methods and Materials: All patients referred for CT screening for lung cancer between May 2, 2011 to November 28, 2018, including patients with previous history of malignancy and a life expectancy of a least 5 years. Patients with prior history of lung cancer were included as per current National Comprehensive Cancer Network (NCCN) guidelines.
Demographics regarding risk factors including smoking history, family history and prior radiotherapy to thorax were collected. CT scan features assessed nodule size, morphologic features and number. The Lung-CT Reporting and Data System scoring system was retrospectively applied to studies performed before October 2014 and prospectively applied to remainder of studies. Institutional review board approved this study and data was collected in HIPAA compliant manner.

Results: Preliminary results show a total of 1072 individuals were studied (mean age of 65 years; 57.9 % female, 42.1 % male; median smoking history of 50 pack year). 930 (86.8 %) of these patients had a previous history of cancer, most commonly breast cancer. Patients with previous cancers with strong association with smoking were evaluated: 14.1 % had a previous lung cancer, 11.2 % had a previous head and neck carcinoma and 0.9 % had a previous bladder carcinoma.
Overall 44 (4.1 %) lung cancers were detected in our population: 34 (3.7 %) lung cancers in patients with prior history of malignancy and 10 (7 %) lung cancers in patients without prior history of malignancy. Five additional patients with suspicious findings (LUNG-RAD 4B) on screening CT during study period are awaiting tissue sampling.

Conclusion: The rate of diagnosis of lung cancer in our population, predominantly those with a previous history of malignancy, is higher than in several previously published studies. Patients with a smoking history and a previous malignancy, especially a smoking related one, may be at an increased risk of lung cancer and benefit for inclusion in screening program.

Characterization of mediastinal anterior masses with magnetic resonance imaging using diffusion-weighted imaging and prediction of World Health Organization classification

M. Gavrel[1], E. Auclin[2], E. Fadel[3], M.-R. Ghihna[4], V. Thomas de Montpréville[3], P.-Y. Brillet[5], C.S. Balleyguier[1], B. Besse[1], C. Caramella[1]; [1]Villejuif/FR, [2]Paris/FR, [3]Le Plessis Robinson/FR, [4]Le Plessis-Robinson/FR, [5]Bobigny/FR

Purpose/Objectives: To assess the effectiveness of magnetic resonance imaging (MRI) using chemical-shift sequence and diffusion-weighted imaging (DWI) to characterize mediastinal anterior masses (MAM) and thymic epithelial tumors (TET).

Methods and Materials: A retrospective analysis was performed of 88 patients referred for a MAM between 2000 and 2017. Patients were classified as benign (rebounds, lipoma, normal thymus) or 'non-typically benign' (lesions needing further investigation or malignant) MAM. TET were classified as low-risk (type A, AB, B1), high-risk thymomas (type B2, B3) and thymic carcinomas. Qualitative analysis of morphologic criteria and pattern of enhancement and quantitative analysis of the chemical-shift ratio (CSR) and apparent diffusion coefficient (ADC) were performed. The discrimination capacity of CSR and ADC was evaluated with ROC curves and optimal cutoff points were determined according to the Youden index. The relationship between diagnosis and MRI findings were evaluated with logistic regression models.

Results: Sixty-four patients were eligible, 20 with benign MAM (9 males, 11 females, mean age 30.7 years) and 44 with non-typically benign MAM (25 males, 19 females, mean age 56.7 years). CSR and ADC significantly differed between groups (P<0.01). The CSR optimal cutoff point was 0.885 (sensitivity 93.5 %, specificity 88.9 %). The ADC optimal cutoff point was 1.3 10-3 mm^2/sec (sensitivity 73.3 %, specificity 87.5 %). MAM tumor probability increased with higher CSR (P=0.02) and lower ADC (P=0.04). A small (P=0.02) homogeneous mass (P=0.02) with homogeneous enhancement (P<0.01) and high ADC value (P=0.03) suggested low-risk thymomas.

Conclusion: CSR and ADC are independent factors which can be used to characterize MAM.

Automated CT quantification of interstitial lung disease: Comparison between convolutional neural network and ground truth

Y.-W. Kim[1], S. Tarando[1], C. Fetita[1], H. Cho[1], C. de Margerie-Mellon[1], M.-P. Debray[1], S. Boussouar[1], M.-L. Chabi[1], P.A. Grenier[1], P.-Y. Brillet[2]; [1]Paris/FR, [2]Bobigny/FR

Purpose/Objectives: The goal of the study was to evaluate a convolutional neural network (CNN) optimized for computerised tomography (CT) quantification of interstitial lung disease (ILD).

Methods and Materials: The study population included of 130 patients addressed for fibrotic idiopathic interstitial pneumonia work-up to 4 pulmonology departments (Assistance publique – Hôpitaux de Paris).
After image quality control, 10 axial CT images/patient were selected to build up the ground truths. Two readers, including one radiologist expert in ILD, segmented the images into three different classes ("normal", "ILD/fibrosis" and "hypoattenuation").
A CNN composed of 7 convolutional layers and 3 fully-connected layers was implemented, with 3 possible outcomes, corresponding to the 3 classes considered for the ground truths (fig. 1). The CNN has been trained on 110 patients and was tested on 20 patients.
We first evaluated the results provided by the CNN, both qualitatively and quantitatively (in comparison to the ground truths).
Secondly, we calculated the correlation between "ILD" extent, as given by the CNN, and lung function tests.

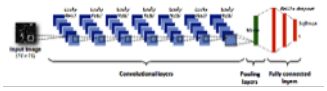

Fig. 1. Convolutional neural network architecture.

Results: On qualitative evaluation, we noted a good inter-slice robustness for a given patient, but a slight overestimation of „ILD/fibrosis" in a few patients (n=3, including one obese patient) (fig. 2).
On quantitative evaluation, the accuracy was good (78.9 %, 82.6 % and 93.4 % for the classes "normal", "ILD/fibrosis" and "hypoattenuation", respectively) (fig. 3).
Clinically, the fibrosis extent predicted by the CNN was correlated with lung function tests (r=-0.49 and p=0.04 for diffusing capacity of the lung for carbon monoxide; r=-0.50 and p=0.03 for forced vital capacity).

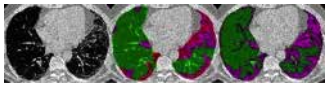

Fig. 2. Example of CNN classification. Original image on the left; ground truth in the middle; CNN prediction on the right. Green: normal; pink/red: ILD/fibrosis.

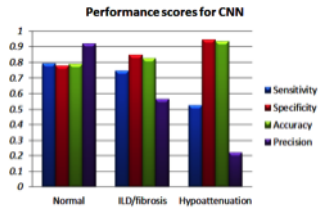

Fig. 3. Performance scores of CNN.

Conclusion: The results from the CNN were good and robust for fibrosis quantification with a trend to overestimation in a few patients.

Deep Muti-Atlas Driven Elastic Nets For segmentation of scleroderma-related ILD on chest CT

G. Chassagnon, M. Vakalopoulou, N. Paragios, M.-P. Revel; Paris/FR

Purpose/Objectives: To develop a deep learning-based model for segmentation of scleroderma-related interstitial lung disease (ILD) on chest computed tomography (CT).

Methods and Materials: This single-center, retrospective study was approved by an institutional ethics committee and the need for patient consent was waived. A total of 217 scleroderma patients who had undergone unenhanced chest CT between January 2009 and October 2017 were evaluated. The training cohort included 17 CT scans either normal or showing ILD, whereas the test and validation cohort were respectively based on 25 and 175 CT scans with ILD, respectively. Inclusion criterion for the validation cohort was the availability of diffusing capacity of the lung carbon monoxide (DLCO), total lung capacity (TLC) or forced vital capacity (FVC) measurement within three months before or after the CT examination. The CT exams in the training cohort were fully annotated by 1 radiologist, whereas the CT exams in the test cohort were partially annotated by 3 radiologists. The deep learning-based model was composed by a fully convolutional neural network and a deformable registration to project each subject to different atlases and was trained on the fully annotated images. The model was then applied to the test and validation cohorts, allowing calculating the percentage of diseased lung for each subject. The model was evaluated 1/in the test cohort by calculating dice scores between radiologists' and model's segmentations, and 2/ in the validation cohort by calculating Spearman correlation coefficients between the percentage of diseased lung and DLCO, TLC and FVC.

Results: Dice scores for lung segmentation ranged from 0.66 to 0.68 between radiologists, and from 0.69 to 0.71 between radiologists and the model. The percentage of diseased lung on CT calculated with the proposed segmentation model correlated well with DLCO, TLC and FVC (R=-0.78, -0.72 and -0.64, respectively; $p<0.001$).

Conclusion: The developed deep learning-based model performed as well as radiologists for segmentation of scleroderma-related ILD on chest CT. Percentage of disease extent correlated well with pulmonary function.

Deep iodine: Artificial intelligence-based normalized subtraction CT iodine maps for improved detection of pulmonary embolism

D. Grob, M.M. Engels, L.J. Oostveen, M.M. Prokop, M. Brink, I. Sechopoulos, J. Teuwen; Nijmegen/NL

Purpose/Objectives: To develop a deep learning-based method to normalize lung iodine maps derived from subtraction computed tomography (SCT) for improved detection of pulmonary perfusion defects (PDs) such as those caused by pulmonary embolism (PE).

Methods and Materials: 2515 patients underwent clinical CTPA with subtraction imaging on two 320-multidetector row CT scanners (Aquilion ONE VISION and GENESIS, Canon Medical Systems, Japan) between January 2013 and August 2017 for suspicion of PE. Iodine maps were obtained by subtracting the pre contrast from the contrast-enhanced scan after non-rigid registration. After examination of patient records and images, 74 patients (2.9 %) without any apparent pulmonary or systemic pathology were selected. An adapted pix2pix convolution neural network, a conditional generative adversarial network, was used to predict the normalized contrast-enhanced scan from the registered pre-contrast scan of these normal patients. To train the network, it compared the predicted contrast-enhanced scan to the clinical contrast-enhanced CT scan. The iodine maps were created by subtracting the pre-contrast from the contrast-enhanced scan, after which we removed the large vessels and applied an anisotropic diffusion filter. The resulting network predicts the normalized iodine map based on the pre-contrast scans as if they do not actually have any pulmonary PD. Therefore, the difference between the predicted normalized map and the real iodine map reflects the PD. The network was initially tested by comparing the difference in mean and standard deviation between the predicted and the real iodine maps in the 74 normal patients and on the maps of two patients with PDs caused by PE.

Results: Using deep learning methods we were able to predict what a contrast-enhanced CT scan would look like for patients without any PDs, based on pre-contrast scans. As a result of predicting the "normal" iodine map, differences between it and the real one highlight the presence of PDs. The mean difference in the iodine map of normal patients was 4.43±30.1 HU, while for the PE patients it was +8.88±27.4 HU.

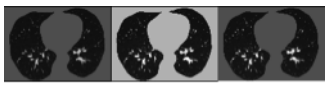

(left) Real pre-contrast, and (middle) contrast-enhanced CT images of the lungs, and (right) deep learning-predicted contrast-enhanced (ww/wl: 1600/-600) CT images.

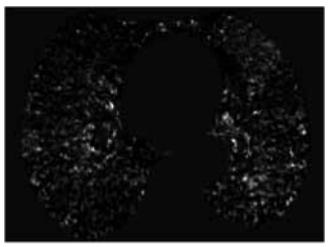

Difference between the real iodine map and the predicted iodine map of a patient with pulmonary embolism (ww/wl: 120/50). The mean enhancement inside the triangular region-of-interest, which reflects the location of the perfusion defect, was 15.8±16.1 HU

Conclusion: The enhancement of the pulmonary parenchyma on subtraction CT imaging in patients without any pulmonary pathology varies widely. However, with a deep learning network it appears possible to normalize these maps across patients so as to isolate and highlight actual PDs. This method could be the first step in accurately quantifying enhancement in iodine maps, giving additional diagnostic information on pulmonary perfusion.

Performance of an AI-powered lung nodule detection and segmentation algorithm in a patient cohort with histologically confirmed lung tumors

T.J. Weikert[1], J. Sperl[2], P. Durlak[2], L. Noordtzij[1], T. Akinci D'antonoli[1], B. Stieltjes[1], G. Sommer[1], J. Bremerich[1], A.W. Sauter[1]; [1]Basel/CH, [2]Forchheim/DE

Purpose/Objectives: Manual segmentation and annotation of pathological findings on cross-sectional images is time-consuming and therefore cost-intensive. However, this task is essential for the secondary utilization of radiological imaging data, e.g. for the training of AI-algorithms and radiomics. The purpose of this study was to assess the performance of an AI-powered lung nodule algorithm for the automatic detection and 3D segmentation of lung tumors.

Methods and Materials: 75 FDG-PET/CTs for non-small-cell lung cancer (NSCLC) staging were preselected from our RIS/PACS archive (confirmed by histology, solid and peripheral T1/T2 stages). First, the pulmonary lesions were manually segmented by a radiologist on the CT component of the PET/CT slice-by-slice using a modified software 3D slicer version. Lesion volumes were calculated. The same series were fed into interlinked deep convolutional neural networks (DCNNs; Siemens Healthineers, Germany) for automated analysis. The time required for both procedures was recorded. The intraclass correlation coefficient (ICC) for the detected volumes as measure of interrater reliability between manual and automatic analysis was calculated.

Results: The DCNNs detected 75 of 75 lesions and attributed them to the correct location in the respective lung lobe. ICC was 0.956 (95% confidence interval from 0.931 to 0.972). Mean process time of the algorithm was 64 seconds compared to 342 seconds needed for manual segmentation.

Conclusion: The evaluated algorithm allows a fast and reliable detection and 3D segmentation of solid peripheral pulmonary T1 and T2 tumors. Further evaluation will focus on advanced (T3/T4) and subsolid tumors.

CT 3D texture analysis: Differentiation of thymoma from thymic cyst by enhanced CT imaging

S. Lim, S. M. Lee; Seoul/KR

Purpose/Objectives: To investigate the differentiation performance of texture analysis in diagnosing thymoma and thymic cyst on enhanced CT image.

Methods and Materials: This retrospective study had obtained the institutional review board approval. From 2001 to 2014, we selected patient who underwent surgical resection for anterior mediastinal lesion. thin section image was obtained. Texture analysis was performed with enhanced thin section image. After manual segmentation of the lesion, several 3D texture features were extracted by in-house analysis program. Two independent observers evaluated anterior mediastial lesion to dignose whether thymic cyst or thymoma with five-scale, respectively. The predictive model for texture analysis was developed using multivariate logistic regression. The performance of the predictive model was assessed by c-statics. ROC analysis was used for evaluating the performance of two observers. Subsequently the performances of predictive model and two observers were compared.

Results: There were 50 thymomas and 34 thymic cysts. On univariate analysis for texture analysis, several histographic features including mean attenuation value, standard deviation, entropy and several percentile CT numbers were significant. On multivariate analysis, mean attenuation value, standard deviation and entropy were revealed as independent predictors for thymoma. The AUC was 0.905. The sensitivity and specificity was 84 and 91, respectively. The AUC of two observers were 0.886 and 0.917. The sensitivity and specificity was 90.0, 79.4 and 78.0, 91.2, respectively. There were no significant differences in performance between the predictive model and two observers (predictive model versus observer 1, P=0.71; predictive model versus observer 2, P=0.70; and observer 1 versus observer 2, P=0.49).

Conclusion: The differentiating performance of the predictive model using texture analysis was feasible on enhanced CT image and comparable to the visual assessment of radiologists.

Predicting overall survival of lung cancer patients using Radiomics CT features

J. R Ferreira Jr, M. K. Santos, C. Vb Machado, M. C Faleiros, D. T Wada, F. Eg Cipriano, A. T Fabro, P. M Azevedo-Marques; Ribeirao Preto/BR

Purpose/Objectives: To perform an overall survival analysis using Radiomics-based quantitative computed tomography (CT) features in patients with lung cancer.

Methods and Materials: This was a retrospective stud with a cohort of 101 patients with lung cancer diagnosed and treated at our institution during 2010-2017 with definitive pathological diagnosis and clinical staging. Pre-treatment contrast-enhanced CT images were semi-automatically segmented using a volumetric region growing algorithm from the medical image analysis tool 3DSlicer v4.3.1. Tumors were characterized by 2465 quantitative features extracted from segmented images, including gray-level intensity, histogram, cooccurrence matrix, run-length matrix, neighborhood intensity-difference matrix, Tamura texture, Laplacian of Gaussian filters, Gabor filters, Fourier transform, Haar wavelet, fractal dimension, and shape. The tools Ibex v1.0, Lire-JFeatureLib v1.6.3, and ImageJ v1.50i were used for features extraction. Prognosis assessment was based on Kaplan-Meier analysis with the calculation of time to death from any cause. Risk groups of patients were divided according to the median value of the quantitative feature. Statistical differences on Kaplan-Meier curves were assessed by the log-rank Test. Identification of most prognostic Radiomics features was performed by the package survival from the programming language R v3.3.3.

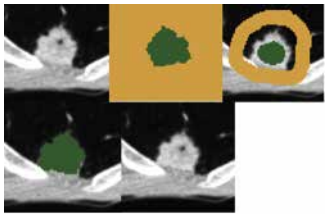

Example of semi-automatic segmentation of a nodule representing a pulmonary adenocarcinoma.

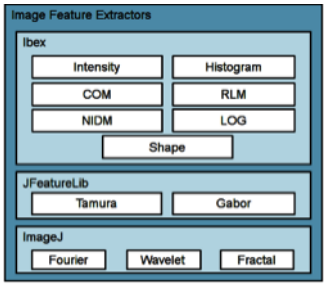

Feature extractors used in this work for images Radiomics analysis.

Results: 38 patients died during the study (16 caused by lung cancer), and 73 were censored. Mean overall survival time was 1819.4 days (95% confidence interval – CI: 1481.2-2157.5). One quantitative Radiomics feature presented statistically significant difference in Kaplan-Meier curves (p-value < 0.05): mean from Fourier. A high-risk group of patients was identified by high values of mean from Fourier, presenting 18 events, 33 censored cases, mean survival of 1465.4 days (CI: 985.2-1945.6). Low-risk group of patients was identified by low values of mean from Fourier, presenting 10 events, 40 censored cases, mean survival of 2164.8 days (CI: 1745.4-2584.1), and a hazard ratio of 0.47 (CI: 0.22-0.99).

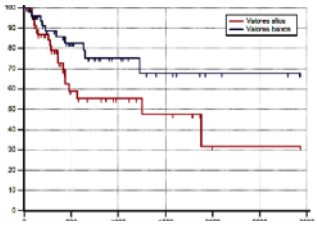

Kaplan-Meier curves of the mean Fourier attribute associated with overall survival. Each dash in the curves represents a censored patient. Red = high values of mean Fourier. Blue = low values of mean Fourier. Time presented in days.

Conclusion: Radiomics has grown as an efficient development tool of quantitative imaging biomarkers to assess prognosis for precision medicine. This study presented a Radiomics-based CT feature as a potential quantitative biomarker for prognostic assessment of patients with lung cancer, independent of the clinical staging or histopathological subtypes.

Which Imaging Characteristics Predict Recurrence In Stage 3A Lung Cancer After Chemotherapy And Radiation Therapy Treatment?

C. Simmers, A.J. Plodkowski, J. Girshman, M. Raj, J. Zheng, A. Rimner, M.S. Ginsberg; New York/US

Purpose/Objectives: To determine CT imaging characteristics of Stage 3A lung cancers that predict increased likelihood of local, nodal or out-of-field failure after definitive combined chemoradiotherapy treatment.

Methods and Materials: For this Institutional Review Board-approved, Health Insurance Portability and Accountability Act-compliant study we retrospectively reviewed CT imaging for patients with Stage 3A lung cancer. Pre-treatment CT scans were reviewed initially for primary tumor and lymph node characteristics. CT features assessed included location, consistency, contour, presence of cavitation, necrosis, and calcification. Presence of pleural effusion and satellite nodules were also recorded. Post-treatment CT scans were reviewed for evidence of local, nodal and out-of-field failure and correlated with the radiotherapy field data. Competing risk regressions were used to examine associations between CT features and local or distant recurrence.

Results: 91 patients (46 males; 45 females) with Stage 3A lung cancer were included. The median age was 64 years (range, 38-84 years). The median follow up of patients was 51.5 months (range 3.2-111.2), with the median overall survival of 25.6 months. At the last follow up, 72 patients had died, 36 experienced local failure, 35 experienced nodal failure and 30 patients had out of field recurrence. The presence of satellite nodules around the primary tumor on the initial staging CT was significantly associated with local failure after chemoradiotherapy (HR 2.58, 95% CI 1.21-5.49, p<0.05). Primary tumors with greater than 50% necrosis were significantly associated with out of field recurrence (HR 0.15, 95% CI 0.02-1.06, p<0.05). Medium/large ipsilateral pleural effusion on the staging CT was significantly associated with local failure (HR 6.78, 95% CI 3.26-14.08, p<0.001), nodal recurrence (HR 6.62, 95% CI 3.01-14.52, p<0.001) and out of field recurrence (HR 8.55, 95% CI 3.88-18.82, p<0.001).

Conclusion: The presence of satellite nodules around the primary tumor; primary tumor necrosis; or moderate/large ipsilateral pleural effusion were all associated with increased likelihood of tumor recurrence in patients with Stage 3A lung cancer after receiving chemoradiotherapy treatment. Identification of these characteristics on the pre-treatment CT scans may help guide management and follow-up of these patients.

Endovascular management of severe hemoptysis in patients with lung transplantation

W. Mohammad, V. Phou, E. Mahdjoub, B. Lortat-Jacob, Y. Castier, O. Brugière, M.-P. Debray, A. Khalil; Paris/FR

Purpose/Objectives: The aim of our study is to report our experience in endovascular management of hemoptysis in patients with lung transplantation and its mechanisms

Methods and Materials: We conducted a retrospective analysis of patients with lung transplantation from a prospective database of patients who underwent endovascular treatment for hemoptysis. We analysed clinical data such as age, gender, primary pulmonary disease, type of transplantation, date of transplantation, possible complications and reviewed both CT-angiography and angiography.
The interpretation of CT-scan was focused on the identification of the bleeding site, the mechanisms of bleeding and the systemic arteries network.

Results: Between September 2015 and December 2018, 129 patients underwent endovascular treatment for severe hemoptysis, 7 of them (4 men, 3 women; median age: 58 years old) had a lung transplantation (3 mono-pulmonary and 4 bi-pulmonary transplantations).
The complications leading to hemoptysis were iatrogenic hemoptysis following a transbronchial biopsy (n=1), ischemic bronchitis with broncho-mediastinal fistula (n=1), angio-invasive pulmonary aspergillosis with parenchymal necrosis and pulmonary artery false aneurysm (n=1), acute lung rejection with Pseudomonas aeruginosa pneumonia (n=1), Pseudomonas aeruginosa pneumonia in the native lung (n=1), hemoptysis in the native lung with pulmonary fibrosis (n=1) and chronic lung rejection for 10 years with bronchial hyper vascularization (n=1).
The delay between the transplantation and the hemoptysis was respectively 9 days, 25 days, 30 days, 48 days, 20 months, 5 years and 10 years.
The patient with iatrogenic hemoptysis had no sign of active bleeding on bronchial artery and pulmonary artery angiographies, therefore he had no embolization and was still alive 19 months after it.
The endovascular treatment could control the hemoptysis in five out of the six other cases.
The patient with pulmonary aspergillosis had recurrent hemoptysis leading to its death 46 days after the first episode despite antifungal and endovascular treatments.
In the five other cases, hemoptysis was controlled but three patients died due to other conditions 3, 15 and 97 days after the first episode and the two other patients were still alive 8 and 16 months after it.

Conclusion: Different mechanisms lead to hemoptysis, they vary according to the delay after the transplantation and the involved lung (transplanted or native).
Furthermore, the only case of hemoptysis in the transplanted lung that was directly linked to the death of the patient was the angio-invasive pulmonary aspergillosis. In the remaining five cases, embolization was able to stop the bleeding.

Hemoptysis requiring bronchial artery embolization in patients with nontuberculous mycobacteria lung disease

S.S. Shim, H. Kwon, Y.J. Ryu, Y. Kim; Seoul/KR

Purpose: Although nontuberculous mycobacteria (NTM) infections are increasing, there are few data about hemoptysis in patients with lung disease caused by NTM. This study investigated the characteristics and prognosis of hemoptysis secondary to NTM infection.

Methods and Materials: Following a retrospective review of cases managed between 2006 and 2016, 183 patients with NTM lung disease were enrolled and analyzed.

Results: Among 183 patients with NTM lung disease, Mycobacterium intracellulare (n=64, 35 %) was the major cause of NTM infection, followed by M. avium (n=59, 32.2 %), and M. abscessus complex (n=40, 21.9 %). Hemoptysis developed in 78 patients (42.6 %), among whom 33 (42.3 %) required bronchial artery embolization (BAE). Between patients with and without hemoptysis, there were no significant differences with respect to sex, radiographic manifestations, distribution over 3, presence of old pulmonary tuberculosis history, antiplatelet or anticoagulation therapy, and species of NTM. However, mean age at diagnosis was significantly lower in the hemoptysis group in univariate and multivariate analysis (65.7±12.8 vs. 59.7±11.8, P=0.002, odds ratio: 0.969, 95 % confidence interval: 0.944-0.996). Among patients with hemoptysis, those requiring medical therapy and those requiring with BAE were not significantly different in terms of demographic characteristics, radiographic manifestations, and distribution over 3 lobes. All patients who received BAE showed immediate clinical improvement, no procedure-related complications or mortality.

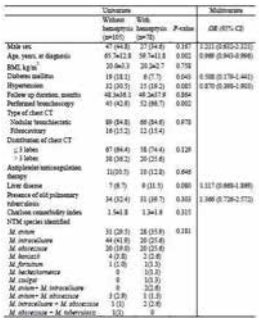

Comparison of groups with and without hemoptysis

Conclusion: NTM lung disease patients commonly experienced hemoptysis without specific risk factors except relatively young age. Although some patients with hemoptysis needed BAE, the success rate of BAE was high, and there were no serious complications associated with BAE.

References: Adjemian J, Frankland TB, Daida YG, et al. Epidemiology of Nontuberculous Mycobacterial Lung Disease and Tuberculosis, Hawaii, USA. Emerging Infectious Diseases. 2017;23(3):439-447. Stout JE, Koh WJ, Yew WW. Update on pulmonary disease due to non-tuberculous mycobacteria. International journal of infectious diseases : IJID : official publication of the International Society for Infectious Diseases. 2016;45:123-134. Johnson MM, Odell JA. Nontuberculous mycobacterial pulmonary infections. Journal of Thoracic Disease. 2014;6(3):210-220. Griffith DE, Aksamit T, Brown-Elliott BA, et al. An official ATS/IDSA statement: diagnosis, treatment, and prevention of nontuberculous mycobacterial diseases. American journal of respiratory and critical care medicine. 2007;175(4):367-416.

Transthoracic rebiopsy for mutation analysis in lung adenocarcinoma: Outcomes and risk factors for non-diagnostic specimen in 199 patients

B. Nam, T.J. Kim, K. Park, M.-J. Ahn, Y.-L. Choi, M.J. Chung, T.S. Kim, K.S. Lee; Seoul/KR

Purpose: To determine the outcomes of transthoracic rebiopsy for epidermal growth factor receptor (EGFR) mutation in patients with lung adenocarcinoma and to explore the clinical and procedure-related risk factors for the acquisition of non-diagnostic rebiopsy specimens.

Methods and Materials: We retrospectively reviewed 367 patients with lung adenocarcinoma who underwent transthoracic core needle biopsy for mutation analysis from September 2011 to October 2016. Of these, 199 patients underwent rebiopsy. Patient characteristics, treatment history, target lesion characteristics, and procedure-related factors were evaluated. The adequacy rate of specimens for mutation analysis was evaluated. Univariable and multivariable analyses were performed to determine the independent predictors of non-diagnostic specimens.

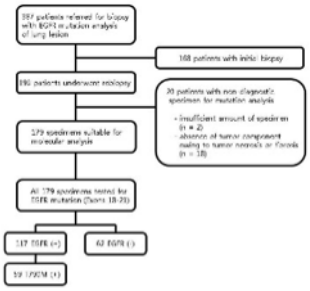

Results: Ninety percent of specimens (179 of 199) were adequate for mutation analysis. The EGFR mutation (exon 18-21) was 65 % (117 of 199) and the EGFR T790M mutation was 33 % (59 of 199) of specimens. In univariable analysis, an internal low-attenuation area in the target lesion P=.001) and pleural contact P=.004) on CT were significant risk factors for non-diagnostic specimens. In multivariable analysis, an internal low-attenuation area in the target lesion (P=.006; odds ratio=7.333, 95 % confidence interval: 1.755-30.633) was an independent predictor for acquisition of non-diagnostic specimens.

Conclusion: Image-guided transthoracic rebiopsy to obtain specimens for mutation analysis in lung adenocarcinoma provides high diagnostic accuracy, with a low rate of non-diagnostic specimens. The presence of internal low-attenuation area in the target lesion on CT was an independent predictor for acquiring non-diagnostic specimens.

References: Rosell R, Carcereny E, Gervais R, et al. Erlotinib versus standard chemotherapy as first-line treatment for European patients with advanced EGFR mutation-positive non-small-cell lung cancer (EURTAC): a multicentre, open-label, randomised phase 3 trial. Lancet Oncol 2012; 13:239-46 Yoon HJ, Lee HY, Lee KS, et al. Repeat biopsy for mutational analysis of non-small cell lung cancers resistant to previous chemotherapy: adequacy and complications. Radiology 2012; 265:939-48 Kuiper JL, Heideman DA, Thunnissen E, et al. Incidence of T790M mutation in (sequential) rebiopsies in EGFR-mutated NSCLC-patients. Lung Cancer 2014; 85:19-24. Nosaki K, Satouchi M, Kurata T, et al. Re-biopsy status among non-small cell lung cancer patients in Japan: A retrospective study. Lung Cancer 2016; 101:1-8. Kim H, Chae KJ, Yoon SH, et al. Repeat biopsy of patients with acquired resistance to EGFR TKIs: implications of biopsy-related factors on T790M mutation detection. Eur Radiol 2017

Diagnostic outcome and safety of CT-guided core needle biopsy for mediastinal mass: A Systematic review and meta-analysis

H.N. Lee; Seoul/KR

Purpose: To systematic review and meta-analyze the diagnostic outcomes (yield and accuracy) and complication rates (total, pneumothorax, hemoptysis, hemothorax) of computed tomography (CT)-guided core needle biopsy (CNB) for mediastinal mass

Methods and Materials: A computerized search of the PubMed and EMBASE databases was performed to identify relevant original articles on the use of CT-guided CNB for mediastinal mass. The pooled proportions of the diagnostic yield and pooled accuracy estimates were assessed using random-effects modeling. We also assessed pooled proportions of the complicate rates as subgroup analyses using random-effects or fixed-effects modeling. Heterogeneity among studies was determined using the inconsistency index (I2). Meta-regression analyses were performed to evaluate the potential sources of heterogeneity for diagnostic outcome and total complication rate.

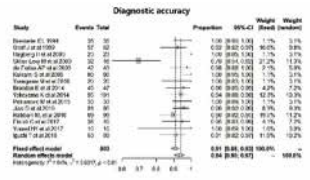

Diagnostic accuracy

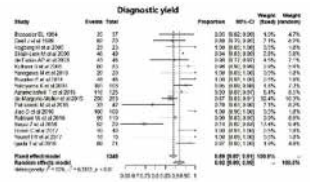

Diagnostic yeild

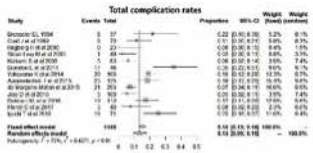

Total complication rates

Results: Eighteen eligible studies, involving 1345 CT-guided CNBs for diagnostic yield, and 803 CT-guided CNBs for diagnostic accuracy, were included. The pooled proportion of the diagnostic yield and accuracy of CT-guided CNB for mediastinal mass were 0.92 (95 % CI, 0.89-0.95) and 0.94 (95 % CI, 0.90-0.97), respectively. In the subgroup analysis, the pooled proportion of the total complication rate, pneumothorax, hemoptysis, and hemothorax were 0.13 (95 % CI, 0.09-0.19), 0.06 (95 % CI, 0.03-0.11), 0.02 (95 % CI, 0.01-0.03), and 0.02 (95 % CI, 0.01-0.03), respectively. In the meta-regression analyses, number of sampling (odd ratio [OR]=3.3, p=0.03), needle approach with CT-fluoroscopy or CT-navigation (OR=2.1, p=0.02), and percentage of lymphoma (OR=2.2, p<0.001) for diagnostic yield, number of sampling (OR=2.0, p=0.02) for diagnostic accuracy, and biopsy needle size (OR=2.5, p=0.002) for total complicate rate were sources of heterogeneity

Conclusion: CT-guided CNB for mediastinal mass demonstrates excellent diagnostic outcome and low complication rate. These findings indicate that CT-guided CNB may be an accurate and safe diagnostic tool for mediastinal mass.

References: Kim H, Park CM, Lee SM, Goo JM. C-Arm Cone-Beam CT Virtual Navigation-Guided Percutaneous Mediastinal Mass Biopsy: Diagnostic Accuracy and Complications. European Radiology 2015;25:3508-3517 De Margerie-Mellon C, De Bazelaire C, Amorim S, Brice P, Tazi A, Brière J, et al. Diagnostic yield and safety of computed tomography-guided mediastinal core needle biopsies. Journal of Thoracic Imaging 2015;30:319-327 Date H. Diagnostic strategies for mediastinal tumors and cysts. Thorac Surg Clin 2009;19:29-35, vi

Diagnostic accuracy of CT-guided core biopsy of thin-walled cavitary pulmonary lesions

K.E. Shin[1], J.S. Park[2], J.W. Lee[3]; [1]Bucheon-si, Gyeonggi-do/KR, [2]Bucheon/KR, [3]Seoul/KR

Purpose: To evaluate the accuracy of CT-guided percutaneous core biopsy of thin-walled cavitary pulmonary lesions.

Methods and Materials: The study included 28 patients (21 men, 7 women; age range 32-84 years) who had thin-walled cavitary pulmonary lesions and underwent CT-guided core needle biopsy. Thin-walled cavitary lesions were defined as having a wall thickness of less than 5 mm based on chest CT. Diagnostic accuracy, sensitivity, and specificity were calculated on the basis of 26, as 2 lesions had indeterminate biopsy results. Each case was reviewed for complications including pneumothorax, thoracostomy tube insertion and hemoptysis.

Results: There were 17 (61 %) malignant and 9 (32 %) benign lesions on final diagnosis. Two (7 %) biopsy results were indeterminate (anthracofibrosis, focal interstitial thickening) and excluded from calculation of sensitivity, specificity, diagnostic accuracy because of loss of follow up. Wall thickness ranged from 1 to 5 mm and cavities ranged from 7 to 27 mm in diameter. The sensitivity, specificity, and diagnostic accuracy of thin-walled cavities were 88 %, 100 %, and 92 %, respectively. Metastasis from colon cancer and pulmonary adenocarcinoma were misdiagnosed as chronic nonspecific inflammation and fragment fibrotic tissue on CT guided core biopsy, respectively. Four (14 %) patients developed a pneumothorax, one (3 %) requiring placement of a thoracotomy tube. Mild hemoptysis occurred in 3 patients (10 %).

Final diagnosis of 28 cavitary lesions

Diagnosis	Number of lesions
Malignant lesions	**17**
Adenocarcinoma	8
Metastatic cancer	6
Squamous cell carcinoma	2
Adenosquamous cell carcinoma	1
Benign lesions	**9**
Organizing pneumonia	4
Tuberculosis	3
Nontuberculous mycobacteria	1
Cryptococcal infection	1
Indeterminate lesions	**2**
Total	**28**

Conclusion: CT guided core biopsy is useful diagnostic technique for cavitary pulmonary lesions with high diagnostic accuracy and has an acceptable complication rate.

References: 1. Florian U, Jesaja K, William R. Lung cancers associated with cystic airspaces: Natural history, pathologic correlation, and mutational analysis. J Thorac Imaging 2017; 32(3); 176-188
2. Tae Jung Kim, Jae-Ho Lee, Choon-Taek Lee. Diagnostic Accuracy of CT-Guided Core Biopsy of Ground-Glass Opacity Pulmonary Lesions. American Journal of Roentgenology. 2008;190: 234-239

Efficacy of advanced knowledge-based iterative reconstruction in coronary CT angiography for plaque quantification: A comparison with intravascular ultrasound

J.Y. Yoo[1], E.J. Chun[2], J.M. Lee[3]; [1]Cheongju-si/KR, [2]Seongnam-Si/KR, [3]Seongnam-Si, Gyeonggi-Do/KR

Purpose/Objectives: To evaluate the efficacy of knowledge-based iterative model reconstruction (IMR) for assessment of plaque burden on coronary computed tomography angiography (CCTA) compared with intravascular ultrasound (IVUS) according to the plaque types.

Methods and Materials: We prospectively enrolled 18 patients with significant coronary artery disease who underwent CCTA and transferred to IVUS. CCTA images were reconstructed with a filtered back projection (FBP), hybrid iterative reconstruction (iDose4) and IMR. Two independent observers assessed plaque types (calcified, mixed, non-calcified) and semi-automatically quantified Plaque burden with commercial software. We compared Plaque burden of CCTA datasets reconstructed with FBP, iDose4, and IMR with those derived from IVUS using Spearman's rank correlation (r) and Bland-Altman analysis. We also evaluated whether the differences in these agreements depend on plaque types.

Results: A total of 56 lesions (27 calcified, 15 mixed and 14 non-calcified plaques) were analyzed. When using IMR, the inter-observer reproducibility and CCTA-IVUS agreement for plaque burden were increased compared to those of FBP or iDose4. According to the plaque types, IMR significantly improves agreement with IVUS for plaque burden in mixed plaques than FBP (r=0.73 vs. 0.31) or iDose4 (r=0.41), and also improves agreement in non-calcified plaques than FBP (r=0.72 vs. 0.56) (all p<0.05). For quantifying calcified plaques, CCTA-IVUS agreement was good across all reconstruction techniques, IMR being the best (IMR vs. iDose4 vs. FBP; r=0.96 vs. 0.90 vs.0.86).

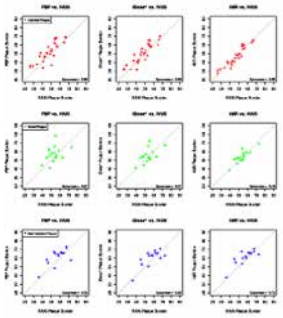

Conclusion: Compared to FBP or iDose4, IMR can significantly improve agreement with IVUS for the assessment of plaque burden in non-calcified and mixed plaques.

Preoperative CT-determined emphysema and postoperative pulmonary complication for non-small cell lung cancer

H.Y. Lee, E.Y. Kim, J.H. Kim; Incheon/KR

Purpose/Objectives: Surgical resection offers the best opportunity for long-term survival and cure in patients with resectable non-small cell lung cancer (NSCLC). Although CT-determined emphysema has been reported as a prognostic indicator for outcome of resected NSCLC, there was no study regarding the predictive value of CT-determined emphysema for postop complications.

Methods and Materials: For a total 266 NSCLC patients (male=161, mean age=63±3 years) that underwent surgery between 2011 and 2016, emphysema was semi-quantitatively scored using baseline chest CT images according to the Goddard scoring system, (range, 0 to 24). Data on clinical characteristics and postop complications were retrospectively collected. Univariable and multivariable logistic analysis was performed to evaluate factors associated with overall postoperative complications.

Results: A total 44 patients (16.5%) had postop pulmonary complication. 91 patients had CT-determined emphysema (CT emphysema score ≥ 2). In univariable analysis, patients with CT-determined emphysema showed a significant OR to determine postop pulmonary complication (p=0.007). In the multivariable model, CT-determined emphysema was a significant independent indicator to predict postop pulmonary complication (OR, 1.94, p=0.067) along with male gender (p=0.001), pack-year smoking (p<0.001), and past history of tuberculosis (p<0.001).

Conclusion: Preoperative CT-determined emphysema could be used to predict postoperative outcome for non-small cell lung cancer.

Imaging of lung transplantation and common postoperative complications

Y. Choi, W.H. Cho, D.H. Kim; Yangsan/KR

Learning objectives: Lung transplantation has been established as a treatment for end-stage pulmonary disease. Complications of lung transplantation may include problems related mechanical factor, airway or vascular anastomosis, variable pulmonary parenchymal or pleural disease that can occur in the early, intermediate and late postoperative period.

Background: Lung transplantation has been established as a treatment for end-stage pulmonary disease. Complications of lung transplantation may include problems related mechanical factor, airway or vascular anastomosis, variable pulmonary parenchymal or pleural disease that can occur in the early, intermediate and late postoperative period.

Imaging findings OR Procedure details: Mechanical problems are related to size mismatch between donor lung and recipient thoracic cage. Collapsed lobe in atypical location, bronchial cutoff, abnormal position of pulmonary vasculature, position change of an opacified lobe on sequential radiographs can be seen. Airway complications include bronchial dehiscence, stenosis and stricture. Bronchial dehiscence can be seen as extraluminal gas, focal bronchial wall defect on CT, and can be suspected indirectly with persistent air leak or pneumothorax. Bronchial stenosis and stricture are mostly related to ischemia and inflammation, due to suboptimal vascular supply, and most commonly seen at bronchus intermedius. Vascular problems include anastomotic site stenosis and thromboembolism. Various pulmonary parenchymal or pleural complications can be seen at different postoperative periods. In the early postoperative period (beween 24 hour-1 week), primary graft dysfunction, acute rejection, pneumothorax, hemothorax, pleural effusios are common problems. In the intermediate postoperative period(8 day-2 months), opportunistic infection by funus or vius, and acute rejection can be seen. In case of late postoperative period (2 months -), bacterial infection, posttransplantation lymphoproliferative disorder, and bronchiolitis obliterans syndrome are common problems.

Conclusion: Radiology plays an important role in the early diagnosis and management of complications of lung transplantation. Radiologists must be able to understand the imaging findings of common surgical techniques and complications of lung transplantation.

References: AJR 2009; 192:S1-S13. Imaging of Lung Transplantation: Review. Yuen Li Ng et al. AJR 2008; 191:1046-1056. Pictorial Essay. MDCT Evaluation of Central Airway and Vascular Complications of LungTransplantation. Ritu R. Gill et al. RadioGraphics 2007; 27:957–974. Postoperative Complications of Lung Transplantation: Radiologic Findings along a Time Continuum. Krishnam MS et al. AJR 2008; 191:1046–1056. MDCT Evaluation of Central Airway and Vascular Complications of Lung Transplantation. Gill RR et al. Radiology 2001; 221:207–212. Acute rejection following lung transplantation: limitations in accuracy of thin-section CT for diagnosis. Gotway MB et al.

Clinicoradiologic significance of Late-Onset Noninfectious Pulmonary Complications (LONIPCs) after allogenic hematopoietic stem cell transplantation (HSCT)

K.E. Shin[1], J.S. Park[2], J.W. Lee[3]; [1]Bucheon-si, Gyeonggi-do/KR, [2]Bucheon/KR, [3]Seoul/KR

Learning objectives: To introduce several clinical and radiological findings of late-onset noninfectious pulmonary complications (LONIPCs) that can occur after allogenic hematopoietic stem cell transplantation (HSCT).

Background: Advancement in prevention, diagnosis, and treatment of infectious complications after allogeneic HSCT has greatly decreased early mortality. With increased survival periods, morbidity and mortality due to LONIPCs have now emerged as a threat to patients undergoing HSCT. LONIPCs can occur in up to 20 % of patients receiving allogenic HSCT. Since LONIPCs are related to immune suppression or drug related toxicity, it can manifest in all parts of the lung, including bronchi, parenchyma, vessel or pleura, with in various ways.

Imaging findings OR Procedure details: There are several noninfectious complications that can occur around 100 day, or three months, after HSCT. The most common LONIPC is chronic graft versus host disease (GVHD), such as bronchiolitis obliterans, organizing pneumonia, or nonclassifiable interstitial pneumonia are also possible. Other complications include pneumothorax, pneumomediastinum due to air-leak syndrome. It can also cause pulmonary vascular diseases which will lead to pulmonary hypertension, thrombotic microangiopathy, or venoocclusive disease. Other rare complications include post-transplant lymphoproliferative disorder or pleuroparenchymal fibroelastosis.

Conclusion: There are several LONIPCs that can occur after HSCT, but several clinical signs and respiratory symptoms may be nonspecific. Therefore, radiologists should be aware of the possible CT findings of LONIPCs to provide patients the most appropriate management.

References:
1. Anne Bergeron. Late-Onset Noninfectious Pulmonary Complications After Allogeneic Hematopoietic Stem Cell Transplantation.Clin Chest Med 2017;38:249–262
2. Elena Peña, Carolina A. Souza, Dante L. Escuissato. Noninfectious Pulmonary Complications after Hematopoietic Stem Cell Transplantation: Practical Approach to Imaging Diagnosis. RadioGraphics 2014; 34:663–683
3. Ayman O. Soubani, Chirag M. Pandya. The spectrum of noninfectious pulmonary complications following hematopoietic stem cell transplantation. Hematol Oncol Stem Cel Ther 2010;3(3):143-157

Chest Magnetic Resonance Imaging: Current Applications and Future Perspectives

Y.J. Jeong, Y. Lee, J.W. Lee, S.M. Park, G. Lee; Busan/KR

Learning objectives:
1. Describe the MR imaging physics principles facilitating chest MR imaging and understand recent technical advances.
2. Describe major clinical indications for chest MR imaging and identify key components of chest MR imaging protocols.
3. Discuss new development and future perspectives of chest MR imaging.

Background: Despite its nonionizing technique and excellent soft tissue characterization, MR imaging of the chest has been considered impractical due to various challenges such as low proton density in the lung, susceptibility artifacts, and physiological motion. However, recent technical advances such as ultrafast sequences and radial k-space data sampling enables to overcome these limitations.

Imaging findings OR Procedure details: In this exhibit, we review recent advances in MR imaging techniques, describe clinical indications for chest MR imaging with proper imaging protocols, and discuss new developments and future perspectives of chest MR imaging.

Conclusion: MR imaging evolves as a modality of choice or alternative to CT in the evaluation of thoracic diseases, offering combined morphological and functional information in a single imaging session. Thoracic radiologists can increase the use of chest MR imaging in daily practice for the benefit of improved decision making in patients' care.

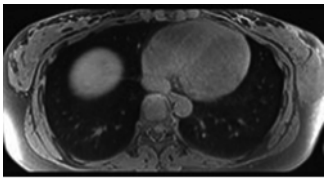

The respiratory triggering radial 3D fat-suppressed T1-weighted gradient echo sequence image with ultra-short echo time (TR 3.20 ms; TE 0.05 ms; flip angle 5°) visualizes lung morphology with excellent image quality.

References: Biederer J, Mirsadraee S, Beer M, et al. MRI of the lung-current applications and future perspectives Insights Imaging 2012; 3:373-386. Raptis CA, McWilliams SR, Ratkowski KL, et al. Mediastinal and pleural MR imaging: practical approach for daily practice. 2018; 38:37-55. Ohno Y, Koyama H, Yoshikawa T, et al. Pulmonary high-resolution ultrashort TE MR imaging: comparison with thin-section standard- and low-dose computed tomography for the assessment of pulmonary parenchymal diseases. J Magn Reson Imaging 2016; 43:512-532. Biederer J, Hintze C, Fabel M. MRI of pulmonary nodules: technique and diagnostic value. Cancer Imaging 2008; 8:125-130. Dang S, Gao X, Ma G, et al. Combination of free-breathing radial 3D fat-suppressed T1-weighted gradient-echo sequence with diffusion weighted images: potential for differentiating malignant from benign peripheral solid pulmonary masses. Magn Reson Imaging 2019; 57:271-276. Romei C, Turturici L, Tavanti L, et al. The use of chest magnetic resonance imaging in interstitial lung disease: a systematic review. Eur Respir Rev 2018; 19:27.

Prone vs supine posture differences in quantitative CT imaging-derived regional lung ventilation map and motionography in healthy subjects

C. Lee[1], J. Choi[2], K. Chae[3], E.A. Hoffman[4], S. Choi[5], A.T. Laroia[6], G. Jin[3], J. Cohen[7]; [1]Seoul/KR, [2]Iowa City/US, [3]Jeonju/KR, [4]Iowa City/US, [5]Daegu/KR, [6]Iowa City, IA/US, [7]Grenoble Cedex 9/FR

Purpose/Objectives: Prone posture provides more uniform distribution of air than supine posture, and helps to provide more effective oxygenation in lung diseases such as acute respiratory disease syndrome (ARDS). The purpose of this study is to quantitatively compare regional characteristics of normal lung functions on a lobar basis between prone and supine postures using inspiration and expiration computed tomography (CT) scans.

Methods and Materials: Normal-looking inspiration and expiration CT images were prospectively collected from 34 subjects in prone posture and retrospectively in 56 subjects in the supine posture. VIDA Apollo software (Coralville, IA, USA) and inspiration-expiration CT image matching with a non-rigid image registration technique were used to compute acinar-scale lung function distributions, including relative regional air volume change (RRAVC), three-dimensional (3D) and two-dimensional (dorsal-basal) relative displacements, and volume expansion ratio (J) between inspiration and expiration, as well as tissue fractions on inspiration (TFIN) and expiration (TFEX). The upper-to-lower-lobe ratio is computed in two way, by adding the right middle lobe (RML) to the upper (UM/L) or the lower lobes (U/ML).

Results: Compared to supine posture, RRAVC of prone posture (Figure 1) is increased in the upper lobes ($p<0.0001$) and is decreased in the lower lobes ($p<0.0001$), making the upper-to-lower-ratio nearly unity while UM/L and U/ML are 0.86 and 0.89, respectively in supine. TFIN, TFEX, and J are all decreased in the lower lobes ($p<0.01$) and increased in RML ($p<0.05$). UM/L and U/ML of TFIN, TFEX, and J are all near unity in prone, while they are smaller in supine ($p<0.0001$) even on TFIN (0.92 and 0.94, respectively) that corresponds to full alveolar recruitment in the whole lung. In motionography, regional displacement gradient, which increases toward dorsal-basal regions in supine, is reduced and shifted toward anterior regions in prone (Figure 2). U/ML, but not UM/L, of 3D and dorsal-basal displacements, were decreased ($p=0.004$ and $4.4\times10\text{-}4$, respectively). Details of quantitative comparison are provided in Figure 3.

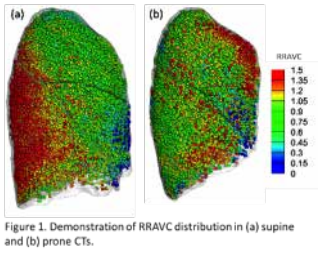

Figure 1. Demonstration of RRAVC distribution in (a) supine and (b) prone CTs.

Figure 1. Demonstration of RRAVC distribution in (a) supine and (b) prone CTs.

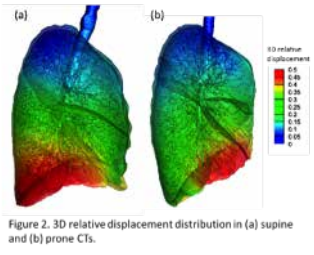

Figure 2. 3D relative displacement distribution in (a) supine and (b) prone CTs.

Figure 2. 3D relative displacement distribution in (a) supine and (b) prone CTs.

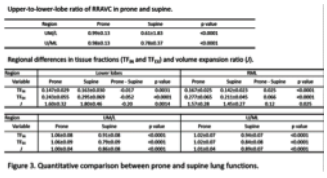
Figure 3. Quantitative comparison between prone and supine lung functions.

Figure 3. Quantitative comparison between prone and supine lung functions.

Conclusion: We observed that the prone posture demonstrated more uniform contributions of regional lung ventilation and minimized the lobar differences in lung functions compared to supine posture. These findings in normal subjects may help us to understand the benefits of the application of prone posture to the patients with ARDS or other gravitationally dependent pathologic lung diseases.

Numerical Modeling of Hyperpolarized Xenon-129 Gas Transfer in Health and COPD Subjects

O. Doganay, M. Kim, M. Chen, F. Gleeson; Oxford/UK

Purpose/Objectives: Hyperpolarized ^{129}Xe (HPX) Magnetic Resonance Imaging (MRI) using novel TS-IDEAL (Time-Series Iterative Decomposition of water and fat with Echo Asymmetry and Least-squares estimation) enables the imaging of gas transfer of xenon gas from alveolar airs sacs to the heart[1]. Although the time-series imaging approach allows for the measurement and correction of intrinsic image variations[2], the quantitative analysis of TS-IDEAL images is required to use gas transfer models similar to those developed for MR spectroscopy[3-6]. In this study, a numerical gas-exchange model is introduced for the quantitative analysis of HPX-TS-IDEAL images, as shown in Figure 1.

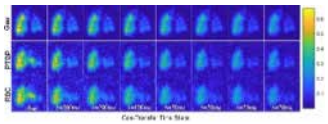

Figure 1:TS-IDEAL MRI of a COPD subject. Gas is the hyperpolarized Xenon-129 in the gas phase. PTBP and RBC correspond to the dissolved phase xenon in the Pulmonary Tissue and Blood Plasma and the Red Blood Cells in the blood plasma.

Methods and Materials: HPX-TS-IDEAL MRI was performed on 12 healthy volunteers, scanned twice 3 weeks apart, and 6 patients with Chronic Obstructive Pulmonary Disease (COPD). The diffusion of xenon gas from the alveolar into the pulmonary veins and the heart were estimated in two steps: (i) diffusion to the pulmonary tissue and (ii) diffusion from pulmonary tissue to capillaries, and capillaries to pulmonary veins and the heart using both Fick's law and Navier–Stokes equations using with COMSOL™ Multiphysics respectively, using the simulation geometry as shown in Figure 2. This model allowed measurement of two parameters: functional pulmonary tissue volume, FVPT and, functional capillary volume, FV_{Cap}, from TS-IDEAL images. The total pulmonary volume from Computed Tomography (CT) images was measured using a dedicated post-processing tool [7] and compared to the FVPT and FV_{Cap} from a healthy subject are shown in Figure 3. Calculated FVPT and FV_{Cap} from TS-IDEAL HPX imaging acquired from the healthy volunteers were compared to those from the COPD patients.

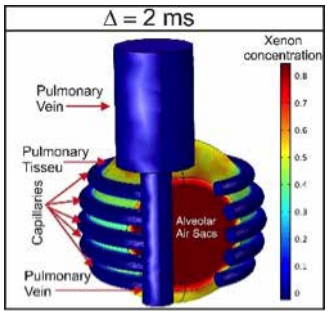

Figure 2: The simulation geometry including the map of xenon concentration for the gas transfer time point Δ = 2 ms.

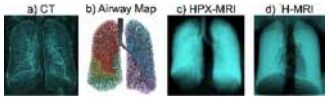

Figure 3: (a) CT, (b) Airway map, (c) Hyperpolarized 129Xe Gas ventilation and (d) 1H-MRI of a healthy subject.

Results: The volume of pulmonary tissue of the whole lung calculated from CT was found to be 873 ml and, 418 ml and 456 ml for the left and right lungs, respectively, in a healthy subject (Figure3). These measurements were in agreement with the HPX measured pulmonary tissue volume, FV_{PT}+FV_{Cap}:875 ml for the whole lung, and 389.3 ml and 485 ml for the left and right lungs from the same healthy subject. The correlation in healthy subjects between FV_{PT}+FV_{Cap} values was 0.990, p=0.005*, between repeated scans, and was 0.944, p<0.0001*, amongst all healthy subjects. The healthy cohort was statistically significantly different from the COPD cohort (p<0.0001) in Figure 4.

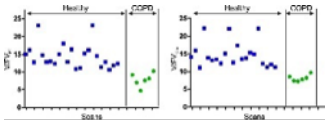

Figure 4: Comparison of the ratio of total lung volume to functional pulmonary tissue gas volume (V/FVPT) with the ratio of total lung to functional capillary gas volume (V/FVCap) in the healthy and COPD cohorts.

Conclusion: The numerical gas exchange model developed in this study can quantify functional pulmonary tissue volume and, functional capillary volume from TS-IDEAL HPX scans with demonstrated reproducibility, and distinguishes between healthy and COPD subjects.

Quantitative computed tomography in the assessment of asthma severity

M. Patyk, A. Obojski, D. Sokołowska-Dąbek, M. Parkitna-Patyk, U. Zaleska-Dorobisz; Wroclaw/PL

Purpose/Objectives: Asthma is one of the most common chronic lung diseases worldwide. It is characterised by chronic inflammation which leads initially to recurrent and subsequently to permanent airflow obstruction and airway remodelling. The clinical presentation is variable and depends on the asthma phenotype, the asthma management and severity.
The purpose of this prospective study was to evaluate the remodelling of the middle- and small-airways in patients with different degrees of asthma severity using quantitative computed tomography (QCT) imaging.

Methods and Materials: The study group was composed of 83 patients with well- defined asthma of all severity: severe refractory asthma (n=25), moderate asthma (n=28), and mild asthma (n=30). The control group included 30 healthy volunteers. All subjects were non-smokers and were examined in a stable, well-controlled condition. The chest non-contrast CT scans were performed with 128-multi-slice scanners with low dose reconstruction algorithm (SAFIRE) and were followed by pulmonary function tests. The quantitative image reconstructions of the data were done with syngo.viaPulmo3D software (syngo.via, Siemens Healthcare, Erlangen, Germany). The measurements of wall thickness (WT), outer diameter (OD), inner diameter (ID), the lumen area (LA) were taken from third to ninth generations of the bronchi in the right, lower lobe. Results of QCT were related to pulmonary function tests.

Results: Bronchial walls were significantly thicker from 3rd to the 9th generation in patients with asthma compared to the control group ($p<0.05$) for all asthma severity grades. There were no statistically significant differences between asthma subgroups ($p>0.05$). The mean lung density was significantly lower in patients with SRA compared to healthy subjects ($p<0.05$), whereas there was no difference in mild-moderate asthma group ($p>0.05$). Low attenuation value per cent (LAV%) was significantly higher in a group of patients with SRA than in other grades of asthma severity, and healthy volunteers. ($p<0.05$) There were no significant differences of LAV% between patients with mild and moderate asthma, and subsequently between mild-moderate asthma and healthy subjects ($p>0.05$).

Conclusion: Quantitative CT imaging seems to be a promising, supplementary tool in the management of asthma. Measurement of lung density provides independent data on asthma severity.

Comparison of Different Reconstruction Kernel in Quantitative Evaluation of Emphysema on CT

M. Khalil[1], Å.A. Johnsson[1], K. Cederlund[2], K. Sörensen[3], J. Brandberg[1], K. Torén[1], J.D. Vikgren[1]; [1]Gothenburg/SE, [2]Stockholm/SE, [3]Umeå/SE

Purpose/Objectives: The primary aim was to investigate the dependency of different reconstruction kernels on quantitative analysis of emphysema. The secondary aim was to evaluate the sensitivity of quantitative analysis for detection of emphysema. The third aim was to compare spirometric total lung capacity (TLC) with inspiratory lung volume on computed tomography (CT).

Methods and Materials: Participants with reported emphysema from pilotSCAPIS (n=100) and matched controls regarding; age, gender, height and weight without emphysema were included in the study.
CT images (slice thickness 0.75mm, increment 0.6mm) were reconstructed with two different reconstruction kernels; one smooth reconstruction kernel (Siemens B20f) and a sharp reconstruction kernel (Siemens B31f). The percentage of pixel attenuation values below -950 HU (LAV %) was measured on both image types using Syngo. Via CTPulmo3D software (Siemens). Two reconstructions were available for 152 examinations (76 with emphysema). A cut-off of ≥6 % of pixels less than −950 HU was used for diagnosing emphysema.
Total lung capacity (TLC) from spirometry was available for 96 participants with emphysema and 98 without emphysema: The results were compared with the inspiratory lung volume estimated by CT using Bland-Altman analysis.

Results: For the emphysema group the mean difference in LAV% between the sharp (B31f) and smooth (B20f) reconstruction kernel was 3.3 (CI 3-3.7 and SD 1.6). The control group had a mean difference of 3.9 (CI 3.5-4.3 and SD 1.9).
Using visual scoring as reference, the sensitivity of quantitative analysis was 58 % with a specificity of 39 %.
The mean difference between inspiratory lung volume estimated by spirometry and CT was 0.5 (CI 0.4-0.7, LOA -0.8-1.8) and 0.5 (CI 0.4-0.6, LOA -0.4-1.5) for the emphysema and control group respectively.

Conclusion: Based on our findings so far, we conclude that different reconstruction kernel can affect LAV%, where a sharp reconstruction kernel (B31f) results in a slightly higher LAV% than a smooth reconstruction kernel.
The performance of quantitative analysis in diagnosing emphysema was poor, regardless of reconstruction kernel.
In comparison to spirometry CT estimates of TLC leads to a slight underestimation.

Emphysema in Lung Cancer Screening Program participants - visual and automatic evaluation

A. Durawa, K. Dziadziuszko, M. Jelitto-Gorska, M. Magnus, M. Ostrowski, E. Szurowska, W. Rzyman; Gdansk/PL

Purpose/Objectives: Emphysema is a risk factor for lung cancer among smokers. The aim of the retrospective study was visual and automatic assessment of emphysema in the Second Gdansk Lung Cancer Screening Program participants.

Methods and Materials: Between 2016 and 2018, 7000 healthy volunteers aged 50-79 with 30 pack-years of smoking history were evaluated by chest Low Dose Computed Tomography (LDCT) screening. Age, gender, smoking history (pack-years) and nodule size were recorded for each person. According to the result of the diagnostic process, patients were classified into lung cancer positive (LCP) or negative (LCN) group. Eight hundred eighty-six individuals had undergone further analysis. Presence and severity of emphysema was assessed visually and automatically and noted when low attenuation regions were depicted in the lungs. Type of emphysema was determined visually.

Results: There were 326 emphysema positive (EP) and 560 emphysema negative (EN) individuals in visual assessment. Prevalence of emphysema was greater in older patients (EP - 64,8 yrs; EN - 62,9 yrs; p<0,001) with more pack-years of smoking history (EP - 46,5 p-ys; EN - 43,2 p-ys; p=0,005). Incidence of emphysema was higher in males (F/M: EP 129/197, EN 266/294; p=0,013). There was statistically significant correlation between visual and automatic assessment of emphysema prevalence and severity (mean Emphysema Index (EI) in EP patients = 4,17; in EN patients = 3,51; p=0,003). Ninety participants in the analyzed group had lung cancer (LCP) while 796 had no cancer (LCN). Prevalence of visually assessed emphysema was significantly higher in LCP patients (58,9 % vs 34,3 %; p<0,001). There was no significant association between emphysema severity and prevalence of lung cancer, neither in visual (p=0,121), nor automatic assessment (EI in LCP = 4,19; LCN = 3,70; p=0,18). Only centrilobular type of emphysema had a significant association with increased incidence of lung cancer (p=0,002).

Conclusion: Significant correlation between visual and automatic assessment of emphysema incidence and severity was observed. Presence of emphysema was associated with higher incidence of lung cancer when evaluated visually. There is no association between emphysema severity and lung cancer prevalence.

Fully automated 3D quantification of "minus" and "plus" pathology in Cystic Fibrosis using 3D-UTE MRI: A validation study

I. Benlala, J. Macey, P. Berger, F. Laurent, G. Dournes; Bordeaux/FR

Purpose/Objectives: To develop and validate a fully automated 3D quantification of lung "minus" and "plus" pathology in Cystic Fibrosis (CF) patients using 3D-MRI with ultrashort echo time (UTE).

Methods and Materials: Twenty adult patients with CF (12 males/8 females, mean age 27±7 years) were prospectively enrolled between 2015 and 2017. All patients underwent pulmonary function test, 3D-UTE MRI at submillimeter resolution and 3D-CT scan the same day. "Minus pathology" (Pminus) was meant to regroup structural alterations related to the destructive process involved in CF, leading to increased air content such as emphysema, bronchiectasis, bullae and sacculations. In addition, "plus pathology" (P_{plus}) referred to productive inflammatory processes leading to increased water content, such as mucus pluggings, wall thickening and consolisation/atelectasis. Two readers experienced in chest imaging performed the evaluation. 3D automatic quantification of relative low signal volume (LSV%) and relative low attenuation volume (LAV%) were measured as surrogate for P_{minus}. P_{plus} was quantitatively assessed by measuring the relative high signal volume (HSV%) and the relative high attenuation volume (HAV%), using 3D-UTE MRI and 3D-CT, respectively. Correlations were performed using Spearman test. Reproducibility was assessed using intra-class correlation coefficients (ICC).

Results: Both CT and MRI quantitative Pminus parameters correlated well with spirometric obstructive parameters (FEV1% with r=-0.43, p=0.04; r=-0.52, p=0.01 respectively and FEV1/FVC with r=-0.81, p=0.003; r=-0.84, p=0.002, respectively). Moreover, LSV% showed strong correlation with LAV% (r=0.78, p=0.007). High correlations were found between Pplus quantification parameters and FEV1% for both modalities with r=-0.72, p=0.01. Furthermore, high correlation was found between HSV% and HAV% (r=0.84, p=0.002). Intra and inter-observer reproducibilities of both LSV% and HSV% automatic measurements were found perfect (ICC>0.99).

Conclusion: 3D-UTE MR quantification of P_{minus} and P_{plus} is reliable and reproducible using LSV% and HSV% measurements, respectively. Therefore, both LSV% and HSV% may represent fully automated quantitative complement to conventional visual scores, to assess and follow-up CF severity, without any radiation exposure.

CT Evaluation of hyperattenuating mucus to diagnose allergic bronchopulmonary aspergillosis in the special condition of cystic fibrosis

J. Refait[1], J. Macey[1], S. Bui[1], L. Delhaes[1], F. Laurent[2], G. Dournes[1]; [1]Bordeaux/FR, [2]Pessac/FR

Purpose/Objectives: Mucus plugging (MP), central bronchiectasis (CB), and consolidation/atelectasia (CA) are conventional CT signs to diagnose allergic bronchopulmonary aspergillosis (ABPA) in cystic fibrosis (CF). Hyperattenuating mucus (HAM) has recently been described and may improve diagnostic accuracy. The goal of our study was to compare HAM versus conventional CT signs to diagnose ABPA in CF. Secondary objectives were to determine the optimal threshold of HAM quantitatively and to assess the diagnostic value of HAM using chest radiograph (CXR).

Methods and Materials: The study was retrospective and included 137 patients with CF, aged more than 6-year-old. The presence of HAM, CB, MP and CA were determined by two radiologists in consensus. HAM was quantified using an absolute mean density value (AMD) and a ratio between mucus and paraspinal muscle (DRM). Sensitivity (Se), Specificity (Sp) and Youden's J-index were calculated. The Cystic Fibrosis Conference Consensus criteria were chosen as Gold Standard.

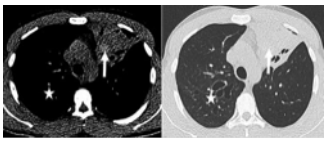

Example of a HAM (hyper attenuating mucus).

Results: 23 out of 137 CF patients had ABPA. Using CT, the most sensitive structural alteration was MP (Se=91%), followed by CB (Se=87%) and CA (Se=70%) whereas specificities were 28%, 19% and 58%, respectively. Conversely, HAM had the highest specificity (Sp=100%) whereas Se was 69%. HAM had the highest Youden's J-index (p<0.001) Quantitative optimal thresholds were AMD>78 HU (Se/Sp=71%/98%) and DRM>1.3 (Se/Sp=82%/97%). HAM was unseen using CXR (Se=0%).

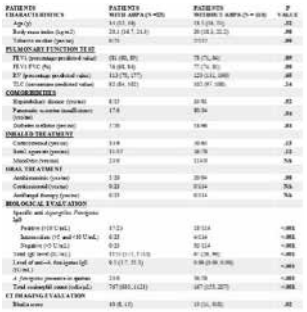

Patient characteristics

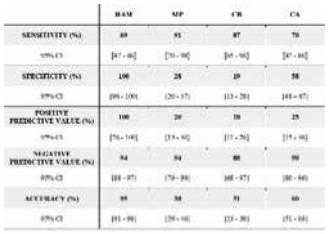

	HAM	MP	CB	CA
SENSITIVITY (%)	69	91	87	70
95% CI	[57 - 80]	[79 - 98]	[69 - 96]	[57 - 81]
SPECIFICITY (%)	100	28	19	58
95% CI	[95 - 100]	[20 - 37]	[13 - 28]	[48 - 67]
POSITIVE PREDICTIVE VALUE (%)	100	28	18	25
95% CI	[76 - 100]	[19 - 40]	[11 - 26]	[15 - 38]
NEGATIVE PREDICTIVE VALUE (%)	94	94	88	90
95% CI	[88 - 97]	[79 - 99]	[80 - 97]	[80 - 96]
ACCURACY (%)	89	38	31	60
95% CI	[81 - 94]	[29 - 48]	[23 - 39]	[51 - 68]

Diagnostic performances

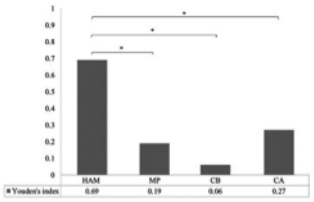

Diagnostic performance of CT biomarkers of ABPA as assessed by the Youden's J-index in 137 patients with cystic fibrosis.

Conclusion: HAM is the most specific CT biomarker of ABPA in CF, with good sensitivity. Our study suggests that routine assessment of mucus density is worth doing for the early and accurate diagnosis of ABPA.

Derivation und Validation of a Primary Ciliary Dyskinesia Computed Tomography (PCD-CT) Score in adult patients with bronchiectasis

S. Dettmer[1], M. Loebinger[2], H.-O. Shin[1], J. Fuge[1], J. Vogel-Claussen[1], A. Shah[2], P.D.T. Welte[1], F. Wacker[1], F. Ringshausen[1], D.J. Rademacher[1]; [1]Hanover/DE, [2]London/UK

Purpose/Objectives: Aim of this multicenter study was to evaluate specific features of Primary Ciliary Dyskinesia (PCD) in computed tomography and to develop and validate a CT score for PCD to facilitate diagnosis.

Methods and Materials: 121 CT in adult patients (mean age 46 years) with bronchiectasis were scored for bronchiectasis (distribution, severity, type) and associated findings (mucus plugging, consolidations, situs inversus, atelectasis, situs inversus, ect.). Patients with PCD (n=46) were compared to patients with other underlying diseases (n=75). In univariate analysis imaging findings with p<0.05 were considered for entry into a multivariate analysis. CT features contributing to the score were determined in multivariate analysis and regression coefficients were used for adjustment. Based on this score, ROC analysis (95% confidence interval) was performed. The score was validated with a cohort of another center (86 patients; 43 with and 43 without PCD).

Results: In multivariate analysis, Situs inversus (p<0.001), tree in bud pattern (p=0.001), predominance in the middle/ lower lobe (p=0.010) and atelectasis or history of resection of a middle/ lower lobe (p=0.020) have turned out to be significant different between patients with and without PCD and have been included in the score. The presence of each imaging feature contributed to the total score following adjustment of its regression coefficient values to points between 1 and 4 (figure 1); the maximum PCD-CT score was 10. ROC curve analysis revealed an AUC of 0.86. Youden-Index was the highest at a threshold of 4 with a sensitivity of 0.913 and a specificity of 0.680. In the validation cohort, CT were scored accordingly. ROC curve analysis confirmed the performance of the score with AUC of 0.86.

PCD-CT Score for adult patients with bronchiectasis	
1. Situs inversus	4 points
2. Tree in bud pattern	3 points
3. Predominance of bronchiectasis in the middle/ lower lobe	2 points
4. Atelectasis or history of resection of a middle/ lower lobe	1 point
Maximum score 10, positive if score >4	

Figure 1: PCD-CT Score for adult patients with bronchiectasis

Conclusion: PCD-CT provides the first validated CT score to help practitioners in identifying bronchiectasis patients who require a further diagnostic workup for PCD. It can help to describe the range of structural changes seen on CT scans in PCD and may improve recognition of this rare and underdiagnosed disease.

Not to be Sniffed At: Role of Diaphragm Fluoroscopy in influencing patient selection for surgical intervention in patients with Diaphragmatic Paralysis

H. Ramotar, S.-J. Choi, G.S. Roe, J. Jamieson, S. Karthik; Leeds/UK

Purpose/Objectives: Partial or complete paralysis of the hemidiaphragms can occur for many different reasons including trauma, in the post-operative setting, inflammatory conditions or neuromuscular disorders. Diaphragm fluoroscopy is a dynamic study that can offer greater clarity in suspected paralysis with regards to the presence and severity of it. It may be preferred to ultrasound assessment as ultrasound can result in a small field of view and portions of the diaphragm can be difficult to visualize due to technical reasons. It is also possible to look at both hemidiaphragms simultaneously with fluoroscopy. We evaluated the role of diaphragm fluoroscopy in investigating a radiologically raised hemidiaphragm in symptomatic patients and its impact on management.

Methods and Materials: Procedures carried out from 2007 to 2018 in adult patients included. Data obtained from Radiology Informatics System, electronic patient records and PACS. Diaphragm fluoroscopy included simultaneous views of both hemidiaphragms - frontal and lateral series of images with normal respiration, deep inspiration and sniff test.

Results: 44 symptomatic patients were included in the study who demonstrated an elevated hemidiaphragm on plain film or CT, for which no cause was established on prior cross sectional images and who underwent diaphragm fluoroscopy between 2007 and 2018 inclusive. The average age of the cohort is 69 years old. 27 (61%) demonstrated partial or complete paralysis. 11/27 (41%) of these patients were then considered for surgery; 8 went on to have diaphragmatic plication performed. 6 (75%) of the patients that were treated had an improvement in clinical symptoms and 7 (88%) demonstrated a radiological improvement. Overall, 30% of patients that demonstrated pathology on diaphragm fluoroscopy underwent surgical intervention, with a majority of them having both a clinical and radiological improvement.

Conclusion: In our centre diaphragm fluoroscopy has facilitated an appropriate case selection, from patients with diaphragmatic paralysis, for surgical intervention resulting in both clinical and radiological improvement in a significant majority of these.

Perfusion defects on dual energy CT angiogram correlate with lower survival in patients with pulmonary embolism

R. Perez Johnston[1], A.J. Plodkowski[2], S.A. Hayes[1], D. Halpenny[3], M. Capanu[1], J. Weinsaft[4], M.S. Ginsberg[1]; [1]New York, NY/US, [2]Syracuse, NY/US, [3]New York, NY/US, [4]New York/US

Purpose/Objectives: To evaluate the utility of perfusion defects on dual-energy CT angiograms (DECTA) in assessing the clinical severity of pulmonary embolism (PE).

Methods and Materials: For this Institutional Review Board-approved, Health Insurance Portability and Accountability Act-compliant study, we retrospectively reviewed 1144 consecutive DECTA exams. These were performed on 1062 patients at an oncologic referral center between January 2014 to September 2014 for the evaluation of suspected PE. The 1144 exams included 1136 diagnostic iodine maps which were reviewed for the presence and extent of perfusion defects based on a perfusion defect score. Presence and location of obstructive and non-obstructive PE, right ventricular to left ventricular ratio (RV/LV ratio) and IVC backflow were also recorded. The perfusion defect score was graded based on percentage of absent perfusion within each lung segment. These scores were correlated with clinical parameters including vital signs, ECG abnormalities, echocardiogram findings, troponin and bnp levels. Clinical information regarding primary cancer diagnosis, oncologic stage and date of death were also recorded.

Results: Of the 1136 diagnostic iodine maps, 153 patients had PE detected on CTA and 96 of these patients had perfusion defects on iodine maps. After uni- and multivariate analysis, significant correlation was found between patients with perfusion defects and RV/LV ratio (p=0.05), IVC backflow (p=0.03), elevated troponin (p=0.03) and right heart dysfunction determined on echocardiogram (p=0.05). When looking at all patients with PE, the presence of a perfusion defect was association with a higher heart rate (p=0.02)

and significant ECG changes (p=0.01). The greater the perfusion defect score, the higher the likelihood of IVC backflow (p=0.005) and obstructive PE (p= 0.002). When adjusted for oncologic stage, patients with a perfusion defect and a higher score had a higher mortality rate (p=0.005).

Conclusion: The presence of a perfusion defect correlates with several parameters evaluating PE severity. A perfusion defect and higher perfusion defect score were associated with a lower survival.

Intra-patient comparison of pulmonary nodule enhancement in subtraction CT and dual-energy CT

D. Grob[1], L.J. Oostveen[1], C. Jacobs[1], M.M. Prokop[1], C.M.M. Schaefer-Prokop[2], I. Sechopoulos[1], M. Brink[1]; [1]Nijmegen/NL, [2]Amersfoort/NL

Purpose/Objectives: Subtraction CT (SCT) is a new software-based imaging modality that has the same diagnostic performance as dual-energy CT (DECT) in pulmonary embolism (PE) detection, but its performance for other applications is not investigated yet. In this study we aimed to determine the capability of SCT in depicting benign and malignant pulmonary nodule enhancement by comparing it to that of DECT.

Methods and Materials: We identified 29 patients with solid pulmonary nodules (≥ 4 mm) in a cohort of 295 consecutive patients recruited for a prospective study on PE. Patients were worked up or followed for at least 20 months to obtain a standard of reference. In total, 96 nodules were investigated (72 malignant, 24 benign). Patients in this study had received a pre-contrast CT at 100 kV prior to a dual-energy CT angiography (CTA) at 100 and 140 kV (Siemens Definition Flash, Germany), with 60 ml of iodinated contrast (300 mg I/ml) followed by 40 ml saline flush injected at 5 ml/s. Scan acquisition was 5 s after reaching a relative threshold enhancement (60 HU) in the pulmonary trunk. For SCT, iodine maps were obtained by subtracting the pre contrast from the contrast-enhanced scan after non-rigid registration (Canon Medical Systems, Japan). Nodules were annotated and volumetrically segmented on the CTA on a lung screening workstation (CIRRUS Lung Screening, The Netherlands) and mean enhancement calculated. Student's t-test was used for statistical testing.

Results: Mean enhancement of the nodules was significantly higher for SCT than for DECT (34.6±12.7 vs 25.7±20.8 HU; p<0.001). Mean enhancement in malignant and benign nodules was 35.5±11.7 HU and 31.9±15.4 HU on SCT (p=0.24), and 26.6±20.7 HU and 22.8±21.4 HU on DECT (p=0.44), respectively. Dose-length-product was slightly lower for SCT than DECT (156 and 163 mGy·cm; p<0.001).

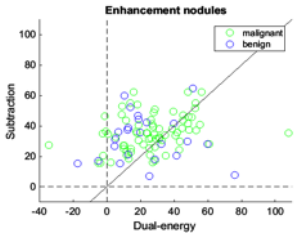

The enhancement of the nodules measured in subtraction CT and dual-energy CT. The solid black line represents equal enhancement.

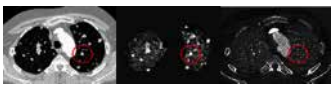

(left) Post-contrast CTA of a 50 year old male patient, (middle) subtraction CT iodine map, and (right) dual-energy CT iodine map, with a malignant nodule (red circle), whose higher enhancement with subtraction CT can be clearly seen.

Conclusion: Subtraction CT shows higher nodule enhancement compared to dual-energy CT. As expected, due to the use of early acquisition, CTA for PE cannot be used to characterize incidental nodules as benign or malignant. However, previous studies have shown the feasibility of nodule characterization with DECT with late acquisition. Therefore, given that it results in better enhancement depiction, it is expected that, SCT with optimized timing could be a promising development for improved nodule characterization at a comparable radiation dose to DECT, without the need for dedicated additional hardware.

CT angiography for pulmonary embolism in the emergency department: Diagnostic accuracy of 20 ml high-concentration contrast medium

G. Milanese[1], R. Cobelli[1], C. Manna[1], M. Silva[1], E. Rasciti[2], P. Sara[1], N. Sverzellati[1]; [1]Parma/IT, [2]Bologna/IT

Purpose/Objectives: To compare the diagnostic performance of CT pulmonary angiography (CTPA) between 20 ml and 40 ml of contrast medium (CM), in patients with suspected pulmonary embolism (PE).

Methods and Materials: CTPAs performed by 64-row multidetector scanner with 20ml (ultra-low volume: ULV) or 40 ml (low volume: LV) of high-concentration CM (Iomeprol 400 mgI/ml; iodine delivery rate 1.2 mgI/sec) were retrieved.
CTPAs were performed with reduced tube potential (100 kVp) to optimize vessel opacification from iodinated CM, and with reference tube current (150 mAs) with automatic exposure control for tube current modulation.
Inter-observer agreement for presence of PE was calculated by the weighted kappa test.
Two radiologists (blinded and independent) scored vascular enhancement and image noise by a 5-point Likert score.

Quantitative analysis was performed by densitometric parameters, including vascular contrast enhancement (CE; densitometric threshold for diagnostic CE>250 HU), and quantitative metrics for image noise, both in central and peripheral pulmonary arteries; furthermore, the overall mean CE was calculated.
Readers recorded the presence of collateral abnormalities (including pulmonary consolidations, pleural effusions and breathing artifacts).

Results: One-hundred and seventy-six CTPAs were included: 102 ULV and 74 LV were included.
Inter-observer agreement for the detection of PE was excellent (k = 0.83) when considering the overall CTPA datasets; it was excellent also after stratification of CTPAs between ULV and LV protocols (k = 0.83 and 0.82, respectively).
The qualitative score was overall sufficient by ULV, yet inferior than LV (p<0.001). Qualitative image noise was comparable between ULV and LV, though the inter-observer agreement was only fair for peripheral vessels. Non-diagnostic qualitative parameters was reported in 9/102 ULV, of which 7/9 were associated with major pulmonary abnormalities.
Quantitative image noise was not significantly different between ULV and LV. The mean CE was lower in ULV group (p<0.001), though >250 HU in both groups.

Conclusion: CTPA with 20 ml allows sufficient CE of the pulmonary arteries in patients with clinical suspect of PE.
Decreased image quality was mostly associated with massive PE or concomitant pleuro-pulmonary abnormalities.

Organ-based radiation dose reduction to breast in lung cancer screening with low-dose computed tomography (CT)

P. Franchi[1], G. Cicchetti[2], A. Del Ciello[2], A. Farchione[2], L. Bonomo[2], A.R. Larici[2]; [1]Teramo/IT, [2]Rome/IT

Purpose/Objectives: To encourage a method to reduce the amount of radiation at breast level, at least in women, in lung cancer screening CT protocols.
To evaluate image quality of chest CT in a lung cancer screening program using a specific organ dose adaption and reduction (SODAR) protocol integrated into scanners that reduce dose to the anterior aspect of the body of patients, in particular to female breast (reduced sensitive-area up to 40%).

Methods and Materials: 20 high-smoker, female subjects, aged between 55 and 74 years, who were already subjected to a low-dose chest CT for the screening of lung cancer (CT parameters: kV: 100-120; mAs: 40-60) one year before, were enrolled prospectively. All the women had a negative screening result.
After informed consent, SODAR protocol has been applied to this population at the standard screening control at one year with low-dose CT, keeping the same technical parameters.
Image quality was assessed by two chest radiologists in consensus using a scale of 1 to 4 (1, excellent; 2, good; 3, fair; 4, nondiagnostic) for the two low dose CTs performed per patient.
Moreover a 1-cm region of interest (ROI) was placed in each pulmonary lobe in a central region of the parenchyma, in particular in a homogenous portion of the lung (free from visible vessels and bronchi), in both CT examinations of each woman. The standard deviation of each measurement was recorded as an indicator for image noise.

Results: No statistical differences on image quality of pulmonary parenchyma were found between low-dose chest CTs obtained without and with SODAR protocol.
Subjective image quality ranged between 1 and 3; no scan areas were considered nondiagnostic.
No significant difference in image noise was found between the SODAR group with a mean noise of 74,3 and standard low-dose images with a mean of 77,5 (P>0.05).

Conclusion: The use of SODAR protocol in the low-dose chest CT could be encouraged in all lung cancer screening programs to reduce radiation dose to breast in smoker women (who meet the criteria for inclusion) without sacrificing image quality.

Comparison of ultra-low dose CT scanning protocols for the detection of pulmonary nodules classified according to lungrads: A phantom study

G. Milanese[1], M. Silva[1], T. Frauenfelder[2], M. Eberhard[3], N. Sverzellati[1], U. Pastorino[4]; [1]Parma/IT, [2]Zurich/CH, [3]Uster/CH, [4]Milan/IT

Purpose/Objectives: To test ultra-low dose computed tomography (ULDCT) scanning protocols for lung cancer screening, by assessing decreasing radiation dose levels for detection rate of pulmonary nodules (PN).

Methods and Materials: Single-energy volumetric CT of an anthropomorphic chest phantom containing microspheres representing PNs was performed on a third-generation dual-source CT scanner (SOMATOM® Force; Siemens Healthineers, Forchheim, Germany). One Standard dose CT scan - acting as reference standard for PN image quality - was performed at 120 kVp with 150 reference mAs using tube current modulation. Subsequently, a tin-filter for low-energy pre-filtration of X-ray beam was included for five ULDCT scans (tube voltage of 100 kVp and 120, 70, 50, 30, and 20 reference mAs by using tube current modulation). Each ULDCT

acquisition protocol was named consecutively from 1 to 5 as the current-time product decreased from 120 to 20 reference mAs and reconstructed with iterative algorithm ADMIRE at strength levels 2, 3, 4, and 5.
PNs were subjectively assessed by one reader according to a 4-point Likert scale, as follows: 0, non-detectable PN; 1, detectable PN, but very unlikely to be segmented by semi-automatic computer-aided analysis (CAD) software; 2, detectable PN and likely to be segmented by CAD software; 3, detectable PN with image quality equal to standard of reference. Nodules of uncertain score were evaluated in consensus with a second reader.
PNs qualitative scores were analysed according to nodule type and size as detailed in Lung Imaging Reporting and Data System (LungRADS), simulating baseline and incidence round.

Results: 19 solid and 11 subsolid (9 non-solid, 2 part-solid) PNs were included in the analysis.
When assigning LungRADS categories for PNs detected in a simulated baseline screening round, there were 17 LungRADS-2, 4 LungRADS-3, 8 LungRADS-4A and one LungRADS-4B PNs. They were detectable in any ULDCT protocol, with the exception of one non-detectable (qualitative score = 0) part-solid nodule only in ULDCT 1 scanning protocol reconstructed with ADMIRE 3 algorithm.
When assigning LungRADS categories for PNs detected in a simulated incidence screening round, there were 4 LungRADS-2, 14 LungRADS-3, 2 LungRADS-4A and 10 LungRADS-4B PNs. Ten out of them were non-detectable in at least one ULDCT dataset; however, they displayed a score of at least 1 (detectable PN) in ULDCT 2 (Sn100 kVp and 70 reference mAs), provided image reconstruction by ADMIRE 4 and ADMIRE 5.

Conclusion: ULDCT scanning protocols allow the detection of PNs and they can be proposed for the purpose of lung cancer screening.

Vertical off-centering in Reduced Dose Chest-CT with Automated Tube Current Modulation: Impact on effective dose and image noise

K. Martini, M. Eberhard, N. Saltybaeva; Zurich/CH

Purpose/Objectives: To assess the effect of vertical off-centering on effective radiation dose and noise in chest-CT with automated tube current modulation (TCM).

Methods and Materials: One hundred consecutive patients (36 female; mean age 56 years) were scanned on a 192-slice CT scanner with a Standard dose (SD) and a Reduced dose (RD) chest-CT protocol using TMC. Image noise was evaluated by placing circular regions of interest in the apical, middle and lower lung quadrants (Figure 1). Study population was stratified according to patient position in the gantry: positioned in the gantry iso-centre (1), higher than the gantry iso-centre (2) and lower than the gantry iso-centre (3). Pearson correlation was used to determine the correlation between effective radiation dose and vertical off-centering. Student's-t-Test was used to evaluate for significant differences in image noise between groups (1-3).

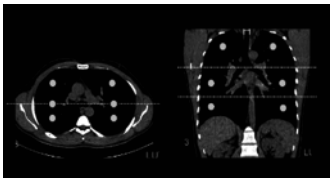

Region of interest (ROI) placement in different lung quadrants.

Results: Average vertical off-centering was of 10.6 mm below the gantry iso-center. When considering the scan iso-centre, the gantry iso-center ±20 mm, 72% of patients were positioned correctly, while 26% of patients were positioned to low and 2% of patients were positioned to high. Effective radiation dose correlated with vertical off-centering in the SD as well as in the RD protocol (r= -0.30 and r= -0.27; respectively) (Figure 2). Lowest image noise was observed where patient position was too high, and highest in patients positioned to low (SD: 74,95 HU vs. 86,45 HU – RD: 131.9 HU vs. 151.3 HU; p<0.001).

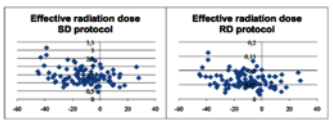

Correlation of vertical off-centering in mm with radiation dose in standard dose and reduced dose chest-CT protocol.

Conclusion: Vertical off-centering influences effective radiation dose and image noise. Efficient use of the TCM function requires accurate patient positioning in the gantry iso-centre.

Study on Radiation Dose in accordance with the Automatic Exposure Control Chamber position on Chest PA

D. Sung, E.-S. Lee, S.-Y. Shin; Seoul/KR

Purpose/Objectives: To compare the exposure dose and dose area product (DAP) according to the position of AEC activation on chest PA and to suggest the ideal position of AEC chamber for reducing radiation exposure.

Methods and Materials: For chest posteroanterior (PA) projections, film focus distance (FFD) of 180cm, field of view (FOV) of 42.5 X 40cm, grid ratio of 15:1 were used without any additional filter. Using a Rando phantom, a nano meter was attached over the center of the incident and the exposure dose was measured 5 times under the same conditions. Chest PA films were taken following

the standard protocols, using Siemens DR. Exposure dose was measured after activating right upper, left upper, both upper, central, and all of AEC chambers, 5 times each and by changing the tube voltages (96 kVp, 102 kVp, 109 kVp, and 125 kVp). Exposure doses recorded in the DICOM header were compared with DAP.

Results: At the tube voltage of 96kVP, the exposure dose with AEC activation on right upper, left upper, both upper, central chamber, and all chambers were measured as 0.159mGy, 0.158mGy, 0.156mGy, 0.335mGy, and 0.205mGy, respectively. At 102kVp, the measured doses were 0.152mGy, 0.156mGy, 0.143mGy, 0.293mGy, and 0.179mGy, respectively. At 109kVp, the measured doses were 0.129mGy, 0.128mGy, 0.130mGy, 0.267mGy, and 0.156mGy, respectively. At 125kVp, the measured doses were 0.108mGy, 0.105mGy, 0.116mGy, 0.202mGy, and 0.114mGy, respectively.
The exposure doses recorded by DICOM header were as follows; 0.169, 0.165, 0.173, 0.346, and 0.204 at the tube voltage of 96kVp; 0.162, 0.155, 0.154, 0.305, and 0.183 at 102kVp; 0.140, 0.134, 0.139, 0.283, and 0.167 at 109kVp, 0.115, 0.109, 0.117, 0.210, and 0.132 at 125kVp.
The exposure dose measured was the lowest with AEC activation on the left upper chamber at 125kVp, consistent with the information provided by the DICOM header. The DAP was the lowest when AEC was activated on the left upper chamber whereas the highest DAP was measured when AEC was activated on the central chamber.

Conclusion: In conclusion, we suggest the use of a high tube voltage such as 125kVp with AEC activation of the left upper ion chamber in order to reduce patients' radiation exposure dose in chest PA examinations.

CT-guided microcoil pulmonary nodule localization prior to video-assisted thoracoscopic surgery (VATS): Diagnostic utility and recurrence-free survival

J.C.L. Rodrigues[1], A. Pierre[2], K. Hanneman[3], M. Cabanero[2], J. Kavangh[2], T. Waddell[2], T. Chung[3], S. Keshavjee[2], K. Yasufuku[2], E. Nguyen[2]; [1]Bath/UK, [2]Toronto/CA, [3]Toronto, ON/CA

Purpose/Objectives: Identifying and resecting T1aN0M0 non-small cell lung cancer (NSCLC) offers the best chance of long-term survival in lung cancer. Whether a lobectomy is truly required for curative treatment of small, peripheral NSCLC tumors is uncertain. Such nodules are likely impalpable and hard to identify at video-assisted thoracoscopic surgery (VATS). Pre-operative CT-guided microcoil nodule localization has the potential to help. We hypothesized that CT-guided microcoil localization and VATS wedge resection would be curative for early stage lung cancer. Our aims were to quantify the diagnostic impact of CT-guided microcoil localization prior to VATS resection and determine the recurrence-free survival over a minimum of 2 years.

Methods and Materials: 124 consecutive patients with CT-guided microcoil localization (Fig.1) (2008-2016) were included. Patient demographics, nodule characteristics and histopathology were recorded. Recurrences were evaluated based on cytology or histopathology. In the absence of this, recurrence was defined when the CT abnormality developed on surveillance CT and persisted/progressed on at least 2 consecutive surveillance CT studies. The time to recurrence was defined as the interval between CT-guided microcoil localization and the CT where the recurrence was first demonstrated. Primary endpoint was recurrence-free survival at ≥2 year CT surveillance. Statistical analysis included Kaplan-Meier survival curves and Cox-regression.

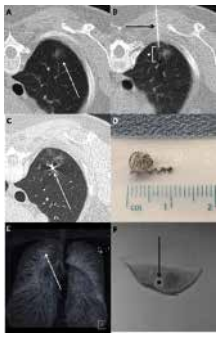

Fig.1 A) 16mm ground-glass nodule. B) Chiba needle containing a microcoil placed through a co-axial needle. C&D) Deployed micocoil. E) Post-procedure imaging. F) Resected specimen radiograph containing the microcoil.

Results: In 124 patients (35% men, 65±12 years), 126 nodules (size 13±6mm, distance to pleura 20±9mm) had microcoil localization and VATS resection. Nodules were 42% (53/126) solid, 32.5% (30/126) ground-glass, and 24% (41/126) sub-solid. It altered histologic diagnosis in 21% (5/24) of patients with diagnostic pre-microcoil CT-guided biopsy Excision pathology was 10% (12/126) benign, 22% (28/126) metastasis, 4% (5 /126) atypical adenomatous hyperplasia, 17% (21/126) adenocarcinoma-in-situ, 17% (22/126) minimally invasive adenocarcinoma, and 30% (38/126) invasive lung primary (Fig.2). After ≥2 year CT surveillance in 79 patients with malignant pathology, local recurrence occurred in 6% (5/79), intrathoracic 22% (17/79), and extrathoracic 17% (13/79). No recurrence occurred for AIS or MIA or when the nodule was <1cm in size. After multivariable adjustment, nodule location >10mm distance from the pleura was an independent predictor of time to recurrence, after adjusting for significant univariate variables of age and size (Hazard ratio 2.9 [95% confidence interval: 1.1-7.4], p=0.03).

Fig.2 A flow chart demonstrating the clinical impact of CT-guided microcoil localization and VATS resection (AAH = atypical adenomatous hyperplasia, AIS = adenocarcinoma in situ, MIA = minimally invasive adenocarcinoma)

Conclusion: CT-guided microcoil localization and video-assisted thoracoscopic sublobar resection may be curative for early stage lung cancer, showing excellent recurrence-free survival for superficial pre-malignant, minimally invasive, and small invasive lung tumors. These findings may also help inform guidelines for surveillance CT regimens in these subgroups in the future.

Air embolism - severe complication of percutaneous lung needle biopsy, which could be avoided

M. Jelitto-Gorska[1], K. Dziadziuszko[1], R. Dziedzic[1], M. Studniarek[1], T. Gorycki[1], B.J. Regent[2], E. Szurowska[1]; [1]Gdansk/PL, [2]Gdynia/PL

Purpose/Objectives: Air embolism is a very rare complication after lung tumor biopsy but could be fatal. The aim of the study is to find direct cause of air embolism and assess possible risk factors of this complication.

Methods and Materials: Between 2013-2017 in the department of radiology 1041 percutaneous lung biopsy were performed under computed tomography control. Fine aspiration needles and core needles were used according to a clinical decision. Control CT scan was performed directly after each procedure to reveal the early complications. Retrospectively, all control CT scans were checked to find intravascular air and its eventual presence was correlated with the clinical state of the patient. In the case of air embolism, we carefully analyzed the procedures to find direct cause of this complication and to assess possible risk factors.

Results: The intravascular air was found in 3 (0,29%) cases of all performed procedures. In all cases, severe clinical outcomes were noticed. In two cases cerebral stroke with hemiplegia appeared with the coexistence of general muscle stiffness. In one case a transient ischemic attack of the cervical spine with tetraplegia was confirmed on the base of clinical symptoms. No other asymptomatic air embolism was found. All three procedures were performed with the use of core needle, each different gauge. In two cases we noticed that the biopsy needle cut directly the small pulmonary vein, in which we noted air in control CT scan. In one case it was impossible to visualize the direct vein crossing due to advanced interstitial disease in the punctured lung, but it was strongly suspected because of massive hemoptysis after the procedure. Additionally, in all three cases, there was a coincidence of pneumothorax in a control CT scan and all the punctured lesions were located in the upper lobe, above the level of the left atrium.

Conclusion: Air embolism is a dangerous complication of percutaneous lung needle biopsy but could be avoided by omitting to cut a pulmonary vein with a core needle. Possible risk factors of that complication are the coexistence of pneumothorax and lesion location in the upper lobe, above the level of the left atrium.

Bronchiolocentric interstitial pneumonia: Tomographic patterns of bronchopulmonary abnormalities

C. Vb Machado, M.R Lourenco, I.B Sanches, D. T Wada, A. I Padua, T. R de Nadai, J.A. Baddini-Martinez, A. T Fabro, M.K. Santos; Ribeirao Preto/BR

Purpose/Objectives: To describe the tomographic findings in patients with bronchiolocentric interstitial pneumonia (BIP) and to correlate them with clinical data and multidisciplinary diagnosis.

Methods and Materials: This was a retrospective observational study of patients with pathological diagnosis of BIP, evaluated by high resolution computed tomography (HRCT). CT images were reviewed separately by 2 resident physicians and 2 experienced thoracic radiologists, with final decision obtained by consensus. It was evaluated: classification according to ATS/ERS 2018 (usual interstitial pneumonia - UIP, probable or undetermined for UIP, alternative diagnosis), if alternative diagnosis, which specific pattern (e.g. non-specific interstitial pneumonia - NSIP) or uncharacteristic pattern; presence of ground-glass opacities, reticulations, honeycombing, consolidations, centrilobular nodules, tree-in-bud opacities, mosaic attenuation, air trapping, "headcheese sign", bronchial impactions, non-honeycombing cysts, bronchiectasis, "elongated bronchus sign", apex-basal gradient and intra- and inter-lung distribution. Patients electronic records and registry of the multidisciplinary discussions were reviewed.

Results: 29 patients were included (17 men, age 62 ± 7 years), with 28 patients classified as „alternative diagnosis", 26 of them showing an „uncharacteristic" pattern. The most frequent findings observed in 3 or more lobes were: mosaic attenuation, air trapping, ground-glass opacities, reticulations and bronchiectasis. The sign of the elongated bronchus was observed in 16 cases. Regarding distribution, 17 had diffuse lung disease and 16 had central and peripheral abnormalities. Twenty-eight patients

were discussed at a multidisciplinary meeting, with a variety of diagnoses, including: hypersensitivity pneumonia (HP), chronic bronchoaspiration, interstitial pneumonia with autoimmune features, drug toxicity and collagen-vascular diseases. In only 8 patients, the multidisciplinary team had reached a definitive diagnosis (higher degree of confidence), including 3 HP and 3 chronic bronchoaspiration cases.

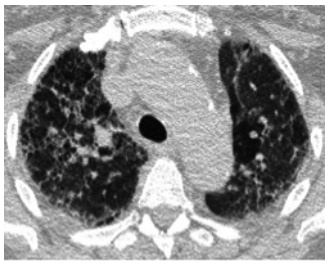

Figure 1: Axial HRCT showing the diffuse, central and peripheral distribution of the abnormalities, with mosaic attenuation, ground glass, reticulations and bronchiectasis.

Figure 2: Coronal HRCT showing the diffuse, central and peripheral distribution of the abnormalities, with mosaic attenuation, ground glass, reticulations and bronchiectasis.

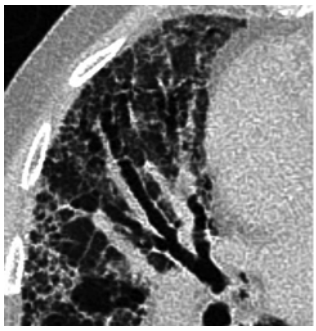

Figure 3: Elongated bronchus sign (dilated and tortuous bronchus standing from the central region to the periphery in the same axial section).

Conclusion: BIP is a form of fibrosing interstitial lung disease with only a few studies, representing a diagnostic challenge. In this study, the most characteristic tomographic pattern was diffuse disease (upper and lower lobes), involving central (peribronchial) and peripheral regions, with mosaic attenuation, ground-glass opacities, reticulations, bronchiectasis and air trapping at expiration. The elongated bronchus sign may represent a characteristic of high specificity.

The Sum of Usual Interstitial Pneumonia (UIP) and Emphysema is Equal to Combined Pulmonary Fibrosis and Emphysema (CPFE): A Study of HRCT

Z.N. Tekin; Istanbul/TR

Purpose/Objectives: The study aims to describe the prevalence of usual interstitial pneumonia (UIP) in high-resolution computed tomography (HRCT) imaging of the lung and evaluate the co-occurrence of UIP and emphysema described as combined pulmonary fibrosis and emphysema (CPFE).

Methods and Materials: The study was carried out on 252 consecutive patients over 50 years old (140 females; mean age: 65.5 years, age range: 50-93 years), who were underwent clinically indicated HRCT of the lung to assess either a certain or a potential pulmonary disease. All patients were referred to the radiology department by whole departments, especially pulmonary medicine throughout 2018.
Those patients are categorized according to age , gender and UIP patterns including subpleural basilar predominant fibrosis,reticulations and honeycombing. In addition to these findings, upper lobe predominant centrilobular emphysema occupying at least 10% of the thoracic volume to make the diagnosis were evaluated to diagnose CPFE. All examinations were retrospectively reevaluated by the same radiologist with five years experience in thoracic imaging.

Results: Subpleural basilar predominant fibrosis (61/252, 24.2 %), reticulations (64/252, 25.4 %) and honeycombing (21/252, 8.3 %), upper lobe predominant centrilobular and paraseptal emphysema (49/252, 19.4 %) and upper lobe predominant paraseptal emphysema (5/252, 2 %) and diffuse panaciner emphysema (3/252, 1.2 %) were defined.
A total of 21 patients with UIP (8.3 %) including 13 male and 8 female with a mean age 71.2 and age range between 57-83 years, were detected within 252 patients. Of those, 15 upper lobe predominant centrilobular and paraseptal emphysema (15/21, 71.4 %) so- called as CPFE, and 1 paraseptal emphysem (1/21, 4.8 %) were described.

Conclusion: CPFE is a disease characterized by both centrilobular emphysema usually in the upper lobes and fibrosis typically in the lower lobes which is important clinically because of the increased risk for lung cancer and poor overall survival. Due to the high rate of CPFE (71.4 %), it is essential for radiologists and pulmonary specialists to recognize early on and screen these patients for lung cancer which is not uncommon and can be aggressive.

Increased in- and expiratory CT Density Changes reveal possible Abnormalities in Idiopathic Pulmonary Fibrosis, Hypersensitivity Pneumonitis and Systemic Sclerosis

S.Y. Kim, M. Wittwer, M. Funke, A. Leichtle, S. Berezowska, T. Geiser, J.T. Heverhagen, A. Poellinger; Berne/CH

Purpose/Objectives: Idiopathic pulmonary fibrosis (IPF), hypersensitivity pneumonitis (HP) and systemic sclerosis (SSc) are among the most frequent diseases causing fibrosis of the lung. The fibrotic manifestations show a preponderance of peripheral basal areas to varying degree. Despite significant advances, the understanding of the pathogenesis of these diseases is still incomplete. Alveolar collapse and consequent induration is thought to lead to fibrotic transformation of lung tissue. The aim of the study was to investigate normal-appearing tissue during expiration for signs of collapsibility and differences from other diseases or controls.

Methods and Materials: The study was approved by the local ethics committee. Two readers retrospectively assessed in- and expiratory CTs of 75 patients (15 controls without lung tissue abnormalities, 15 patients with COPD or emphysema, 15 patients with IPF, 15 patients with HP, and 15 patients with SSc). Densitometry of unaffected lung tissue was performed in all lung segments with a ROI of 15 mm diameter on soft-tissue kernel reconstruction during inspiration and expiration, resulting in a total of 6000 ROI measurements. Inspiration and expiration CTs were acquired at 120 kV or 100 kV on two different CT-scanners, Siemens SOMATOM Definition Flash and Philips Brilliance 64, which were performed for routine clinical work-up.

Results: Using a linear mixed effects model significant differences in attenuation changes between inspiration and expiration of unaffected lung parenchyma were found between IPF, HP, SSc on one side and controls on the other side for all lung lobes ($p < 0.001$). There was no statistically significant difference between the attenuation changes for IPF patients and HP patients, but between IPF patients and SSc patients. No significant difference was observed between attentuation changes of controls and COPD patients in the middle lobe/lingula ($p = 0.41$). Interreader variability tested with single score interclass correlation was 0.95 (values above 0.9 indicate excellent reliability).

Conclusion: High CT attenuation changes between inspiration and expiration in IPF, HP and to a lesser degree in SSc patients might suggest altered lung parenchyma in normal-appearing tissue on CT. Higher than normal density changes during the respiratory cycle might be explained by alveolar collapse of radiologically unaffected lung tissue possibly preceding fibrosis.

Characterization of interstitial lung disease associated with anti-ribonucleoprotein (RNP) antibodies

R. Lhote, P.A. Grenier, J. Haroche, M. Miyara, S. Boussouar, A. Mathian, M. Pha, Z. Amoura, F. Cohen Aubart; Paris/FR

Purpose/Objectives: Interstitial lung disease (ILD) is a common feature of mixed connective tissue disease (MCTD). However, many patients do not meet the criteria for MCTD and thus may be diagnosed as interstitial pneumonia with autoimmune features. The aim of this study was to characterize ILD associated with anti-ribonucleoprotein (RNP) antibodies.

Methods and Materials: Chest CT-scans of patients with anti-RNP antibody who were seen between January 2011 and October 2015 were reviewed. The underlying disease was classified with international criteria using clinical and serological features.

Results: Among 544 patients with anti-RNP antibodies, 188 underwent a chest CT scan, and 48 (26%) of them had radiological features of ILD. The presence of ILD was significantly associated with dyspnea, crackles, arthritis, Raynaud's phenomenon, myositis and sicca syndrome. The most frequent pattern was non-specific interstitial pneumonia (NSIP) in 39 patients (81%). Among patients with ILD, 17(35%) had a radiological pattern consisting of cysts and ground glass attenuation not fulfilling the lymphoid interstitial pneumonia criteria. In 3 patients, cysts were related to fibrosis; in 14 patients, cysts corresponded to an original ILD pattern.

Conclusion: ILD was found in 26% of patients with anti-RNP antibodies independently of the underlying disease. Anti-RNP-associated ILD mainly corresponds to NSIP or an original pattern consisting of cysts and ground glass attenuation.

Characteristics of lung disease patterns on CT scan in patients with idiopathic inflammatory myopathies: Is CT pattern related to myositis specific autoantibodies?

A. Laporte[1], K. Mariampillai[2], Y. Allenbach[2], B. Granger[2], P. Cluzel[2], O. Benveniste[2], P. Grenier[2], S. Boussouar[2]; [1]Neuilly sur seine/FR, [2]Paris/FR

Purpose/Objectives: The study consisted in a retrospective analysis of chest computed tomography (CT) of a cohort of patients with idiopathic inflammatory myopathies (IIM).
The characteristics of CT patterns of lung disease were used for cluster analysis. The objective of the study was 1) to identify different lung patterns associated to IIM and 2) to evaluate the potential relationship between the identified CT findings of interstitial lung disease (ILD) and myositis specific auto-antibodies (MSA).

Methods and Materials: All consecutive IIM patients referred to internal medicine department between 2004 and 2018, were included. All chest CT scans were retrospectively assessed by three radiologists for the presence of 48 imaging criteria. All criteria were described by univariate then multivariate analysis to identify subgroups of patients.

Results: CT scans of 275 patients [182 (66%) women] including 68 (24.7%) inclusion body myositis (IBM), 62 (22.6%) immune-mediated necrotizing myopathy (IMNM), 59 (21.5%) dermatomyositis (DM), 54 (19.6%) antisynthetase syndrome (ASS) and 32 (11.6%) polymyositis (PM) were analyzed.
168 patients (61%) had MSA.101 patients (37%) had ILD, including 54 ASS, 16 DM, 12 PM, 15 IMNM and 4 IBM.
Cluster analysis provided 3 groups significantly different. The first group with normal CT scan (n=185) defined by absence of MSA or presence of anti-cN1A, anti-HMGCR, anti-SRP and included 94% (n=64) of overall IBM, 77.8% (n=49) of IMNM, 72.6% (n=45) of DM and 64.7% (n=22) of PM. The second group (n=69) characterized by mild extent disease (<25% of a lobe), curvilinear consolidation, peripheral ground-glass opacity (GGO), intralobular reticulations defined by anti-Jo1, anti-PL12 or anti-SRP and included 70.4% (n=38) of overall ASS, 16.1% (n=10) of IMNM and 15.2% (n= 9) of DM. The third one (n=21) is a cluster with important extent disease (> 75% of a lobe), different signs of fibrosis, peribronchovascular consolidation, panlobar GGO, pulmonary hypertension (n=8) characterizing by 45.5% of overall MDA5 (n=5) and 20.3% of overall ASS (n=11).
Subpleural microcysts were significantly more present for ASS than other IIM with ILD: RR=4 [IC95% = (3.27, 15.22)]. MDA5 had significantly more peribronchovascular consolidation compared to other antibodies: RR=7 (IC95% = [4.33; 46.79]).

Conclusion: Despite the heterogeneity of ILD observed in IIM, ILD could be split among 3 clusters according to CT-scan criteria and theses clusters were associated to MSA. The identification by radiologists of those clusters could facilitate diagnostic screening, following and prognostic value.

Diagnosis of idiopathic pulmonary fibrosis: Comparison of the new and old classification

A. Farchione, A. Ottavianelli, G. Sgalla, G. Cicchetti, M.D.E. Lo Greco, A. Del Ciello, B. Iovene, R. Manfredi, L. Richeldi, A.R. Larici; Rome/IT

Purpose/Objectives: In 2018 have been published the new ATS/ERS/JRS/ALAT Guidelines and the Fleishner Society White paper for the diagnosis of idiopathic pulmonary fibrosis (IPF). Compared to the previous 2011 ATS/ERS/JRS/ALAT guidelines, both the documents introduced the "probable UIP" and "indeterminate for UIP" patterns instead of the possible one. The aim of our work was to determine the difference in disease classification by using the 2011 and 2018 guidelines and the impact on patient's management.

Methods and Materials: 50 patients referred to our hospital between 2014-2017, which underwent a chest CT scan for a suspected interstitial lung disease (ILD), have been enrolled. CT scans have been conducted according to the suggestion of recent guidelines (sub-millimetric collimation and high-spatial-frequency-algorithm). The cases have been previously classified according to 2011 guidelines by a multidisciplinary team (MDT), afterwards a thoracic radiologist (4 year experience) reviewed the CT scans according to the more recent 2018 guidelines. The frequency of the different diagnostic categories as well as of the binary pattern score (UIP/non UIP) have been determined using both classification system, moreover the agreement for the binary CT pattern scores was calculated (Cohen's weighted k coefficient).

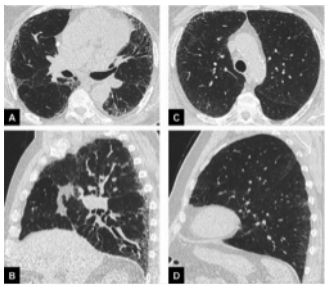

The image shows two „possibile UIP" pattern re-classified as „probable UIP" (figures a and b) and „indeterminate for UIP" (figures c and d).

Results: The frequency of "UIP" pattern resulted similar when using the two classification system (24 % and 26%, 2011 and 2018 guidelines respectively), as well as the frequency of "alternative diagnosis" and "inconsistent with UIP" pattern (26% and 22%, respectively). Among the "possible UIP" cases, 20% have been re-classified as "typical UIP pattern", 64% as "probable UIP", 12% as "indeterminate for UIP" and 4% as "inconsistent with UIP". Similar frequencies have been observed in the binary classification of the data ("typical UIP" 76% and 74%, 2011 and 2018 guidelines respectively; "other than UIP" 24 % and 26%, 2011 and 2018 guidelines respectively), however a moderate concordance has been observed (k=0,52).

Frequency of CT patterns according to the 2011 and 2018 ATS/ERS/JRS/ALAT guidelines

Conclusion: The more detailed classification introduced with the 2018 guidelines could impact on clinical management of patient with ILD. Not significant difference has been observed in answering the main question "is a UIP or not UIP pattern?". According to the 2011 guidelines the "possible UIP" pattern required a biopsy to confirm the histo-pathological disease. In our series, however, the "possible UIP" cases were mainly re-classified as "probable UIP" not requiring a biopsy for the diagnosis of IPF in the appropriate clinical context, while only a minor portion was defined as "indeterminate for UIP" requiring biopsy.

The impact of chest CT quality in the diagnosis of Usual Interstitial Pneumonia (UIP) pattern

A. Farchione, M.D.G. Sgalla, G. Cicchetti, L. Calandriello, M.D.A. Comes, M.D.N. Re, M.D.F. Varone, R. Manfredi, L. Richeldi, A.R. Larici; Rome/IT

Purpose/Objectives: In the appropriate clinical context, the presence of the usual interstitial pneumonia (UIP) pattern on high resolution CT scan (HRCT) of the chest allows a confident diagnosis of idiopathic pulmonary fibrosis (IPF). Our aim was to assess the impact of technical quality of chest CT for the identification of the UIP pattern.

Methods and Materials: 76 patients referred to our hospital between 2014-2017 and having two chest CT scans (152 exams) within a 6-month time interval performed in different centre, our hospital (a tertiary centre, hub) and the affiliated ones (spoke) respectively, were included. All the patients had a final diagnosis defined by a multidisciplinary team (MDT), among them 48 IPF diagnosis were comprised. One thoracic radiologist scored the overall image quality according to a five points scale and considering the following parameters: patient position, inspiratory and/or expiratory scan, inspiratory and/or expiratory level, slice thickness, sharp and/or standard filter, contiguous section, KV, mAs, motion artefacts. Two chest radiologists (18 and 4 years experience respectively) assessed CT scans for the classification of imaging patterns. The last ATS/ERS/JRS/ALAT guidelines for the diagnosis of IPF were applied. Intra- and inter-observer agreement for diagnostic categories and for the binary CT pattern scores (UIP/non UIP) were calculated (Cohen's weighted and unweighted k coefficient, respectively).

Results: CT quality was very poor to moderate in 48 (49%) of the scans performed at the spoke centres, high to very high in 94 (96%) CTs performed at the hub centre ($p<0.001$). In particular, 35 (27%) spoke exams used sections >1.5 mm, 17 (18%) had moderate to high motion artefacts and only 7 (7%) had expiratory scans. The UIP pattern was identified more frequently in CT scans performed at the hub centre. A greater proportion of patients with MDT diagnosis of IPF had UIP identified in hub CTs as compared to spoke CTs (43% and 33%, respectively). The level of intra-observer agreement across the diagnosis category scores and for the binary score of UIP in the hub and spoke CTs was good for the more experienced radiologist (Kw=0.7 and Kw=0.76, respectively), moderate/fair for the less experienced radiologist (Kw=0.41 and Kw=0.37, respectively).

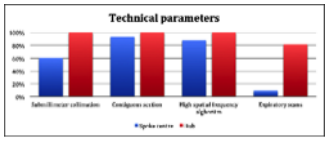

Frequencies of applied technical parameters in CT scan performed at spoke and hub centers in the same patients.

Conclusion: CT scan quality affects the identification of the UIP pattern by thoracic radiologists, especially by those less experienced. The adoption of optimal HRCT scan might speed up the diagnostic work up and avoid the costs and the radiation exposure related to additional CT scanning.

A Survey of Institutions with Sixteen Detector-Rows or More CT Scanners for the Introduction of National Lung Cancer Screening Program Using Low-Dose Chest CT in S. Korea

S.H. Paik; Deajeon/KR

Purpose: To survey medical institutions in Korea that conduct chest low-dose computed tomography (LDCT) scan prior to introduction of the national lung cancer screening (LCS) project.

Methods and Materials: From July-October 2016, a survey was conducted in 366 institutions that use CT scanner with 16 detector-rows or more. After explaining the purpose of this study to personnel of institutions or health care centers via phone, an online survey was conducted by sending a questionnaire link to personnel through e-mail or text message.

Distribution of CT Scanner with 16 Detector-rows or more

Flow Diagram of Survey

Results: Among 366 medical institutions, 282 responded to conduct LDCT scan for LCS. The most frequently used CT section thickness was 5 mm and only 29 institutions comply with Korean guidelines for LCS. The number of institutions that employ a full time radiologist was 330. LDCT scan protocols and CT radiation dose structured reporting system were established in 305 and 302 institutions, respectively. Fifty-nine institutions knew about Lung-RADS and only 14 used it.

Conclusion: Many of the institutions with 16 detector-row or more CT scanners did not meet Korean guidelines for LSC. Appropriate education and promotion is needed to improve and sustain the quality of LDCT for LCS.

Number of row	Number of CT scanner	(%)
16	83	29.4%
64	91	32.3%
80	3	1.0%
128	85	30.1%
256	14	5.0%
320	2	0.7%
Non response	4	1.4%
Total	282	100.0%

Detector Slice of CT Scanner LDCT for LCS

References: Jang SH, Sheen S, Kim HY, Yim HW, Park BY, Kim JW, et al. The Korean guideline for lung cancer screening. J Korean Med Assoc 2015;58:291-301 Kim HY. Lung cancer screening: update. J Korean Soc Radiol 2015;73:137-146 Korea Central Cancer Registry, National Cancer Center. Annual report of cancer statistics in Korea in 2013. Available at: http://www.ncc.re.kr/cancerStatsView.&searchKey=total&searchValue=&pageNum=1. Published December, 2015. Accessed March Goo JM, Chong S, Ahn MI. Are lung imaging reporting and data system categories clear to survey of the Korean Society of Thoracic Radiology members on ten difficult-to-classify Radiol 2017;18:402-40

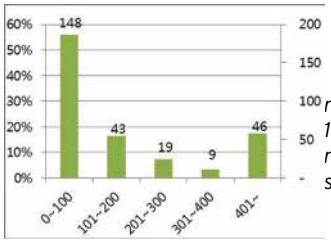

Number of Chest LDCT Scans per Month

ncc?bbsnum=358 19, 2017 Han DH, radiologists? A scenarios. Korean J

Deep Learning for Classification of a Small (≤2cm) Pulmonary Nodule on CT Imaging: A Preliminary Study

K.J. Chae[1], G.Y. Jin1, S.-B. Ko[2], Y. Wang[2], H. Zhang[2], E.J. Choi[1], H. Choi[1]; [1]Jeonju/KR, [2]Saskatoon/CA

Purpose: To propose a deep learning-based malignancy prediction model (CT-lungNET) which is more simple and faster in diagnosis of a small (≤2cm) pulmonary nodule on non-enhanced chest CT, and preliminarily evaluate its performance and usefulness for the human reviewers.

Methods and Materials: A total of 173 whole non-enhanced chest CT images containing 208 pulmonary nodules (94 malignant and 11 benign nodules) sized from 5 to 20mm were collected. Pathologic confirmed nodules or nodules not changed for more than 1 year were included, and 30 benign and 30 malignant nodules were randomly assigned into the test set. We designed CT-lungNET with 3 convolutional layers followed by 2 fully-connected layers, and compared its diagnostic performance and processing time with those of AlexNet by using the area under the receiver operating curve (AUROC). An observer performance test was conducted in the eight human reviewers of four different subgroups (medical students, physicians, radiologic residents and thoracic radiologists) before (test 1) and after (test 2) referring to the CT-lungNET's malignancy prediction rate with pairwise comparison receiver operating curve analysis.

Architecture of CT-lungNET. It consists of 3 convolutional layers followed by 2 fully connected layers.

Results: CT-lungNET showed improved AUROC (0.85; 95% CI, 0.74-0.93), than that of the AlexNet (0.82, 95% CI, 0.71-0.91). The processing speed per one image slice was about 10 times faster than AlexNet (0.90 vs 8.79s). At the observer performance test, classification performances of non-radiologists increased with the aid of CT-lungNET, (mean AUC improvement: 0.13 [range, 0.03 to 0.19]), but it was not significantly increased in the radiologists group (mean AUC improvement: 0.02 [range, -0.02 to 0.07]).

Conclusion: CT-lungNET was able to provide better classification results with a lot shorter processing time than AlexNet in diagnosis of small pulmonary nodules on non-enhanced chest CT. In this preliminary observer performance test, CT-lungNET may have a role as a second reviewer for less experienced reviewers, resulting in enhanced performance in the diagnosis of early lung cancer.

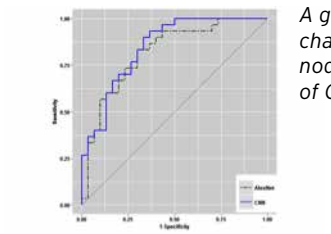

A graph shows receiver operating characteristic (ROC) curves for nodule classification performances of CT-lungNET and AlexNET.

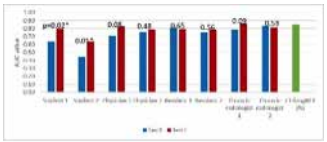

Histogram shows changes of AUC values of each reviewers before (test 1) and after (test 2) referring the result of CT-lungNET.

References: Doi K. Computer-aided diagnosis in medical imaging: historical review, current status and future potential. Computerized medical imaging and graphics: the official journal of the Computerized Medical Imaging Society. 2007;31(4-5):198-211. Song Q, Zhao L, Luo X, Dou X. Using Deep Learning for Classification of Lung Nodules on Computed Tomography Images. Journal of healthcare engineering. 2017;2017:8314740.

Significance of baseline CT assessment for predicting the pulmonary fibrosis during the course of chemotherapy-induced pneumonitis

J.-Y. Han, J.W. Baek, K.-N. Lee, S.J. Choi; Busan/KR

Purpose: The purpose of our study is to evaluate risk factors for the development of pulmonary fibrosis in the baseline CT during the course of chemotherapy-induced pneumonitis (CIP).

Methods and Materials: We retrospectively identified 80 cases of CIP by clinical, radiological, and pathological findings. When fibrosis developed during the follow-up, the extent of pulmonary fibrosis was evaluated at final follow-up CT in terms of a 5% volumetric score for 6 zones. Univariate and multivariate analyses were performed to identify the clinical and radiological risk factors for the development of fibrosis and severe fibrosis over 11% in extent.

Results: Fibrosis occurred in 26 of the 80 total patients (32.5%) during a mean 5.6 months of follow up. Risk factors for developing fibrosis were revealed as preexisting interstitial lung disease (ILD) and moderate to severe emphysema in multivariate analysis (OR = 10.12, 95% CI = 2.35-43.66, and OR = 12.85, 95% CI = 2.81-58.82, respectively). Risk factors for developing severe fibrosis over 11% in extent were revealed as a moderate to severe emphysema (OR = 5.78, 95% CI = 1.07-31.26) in multivariate analysis.

Conclusion: Moderate to severe emphysema as well as preexisting ILD visible on baseline CT are risk factors for developing pulmonary fibrosis in the course of CIP. Thin section CT maybe helpful to predict the risk of pulmonary fibrosis before administering chemotherapy.

References: Limper AH. Chemotherapy-induced lung disease. Clin Chest Med. 2004;25(1):53-64. Dimopoulou I, Bamias A, Lyberopoulos P, Dimopoulos MA. Pulmonary toxicity from novel antineoplastic agents. Ann Oncol. 2006;17(3):372-9. Vahid B, Marik PE. Pulmonary complications of novel antineoplastic agents for solid tumors. Chest. 2008;133(2):528-38. Sakurada T, Kakiuchi S, Tajima S, Horinouchi Y, Okada N, Nishisako H, et al. Characteristics of and risk factors for interstitial lung disease induced by chemotherapy for lung cancer. Ann Pharmacother. 2015;49(4):398-404. Camus P, Kudoh S, Ebina M. Interstitial lung disease associated with drug therapy. Br J Cancer. 2004;91 Suppl 2:S18-23. Muller NL, White DA, Jiang H, Gemma A. Diagnosis and management of drug-associated interstitial lung disease. Br J Cancer. 2004;91 Suppl 2:S24-30. Lee HN, Kim MY, Koo HJ, Kim SS, Yoon DH, Lee JC, et al. Thin-Section CT Characteristics and Longitudinal CT Follow-up of Chemotherapy Induced Interstitial Pneumonitis: A Retrospective Cohort Study. Medicine (Baltimore). 2016;95(2):e2460.

Pleural invasion classification of primary lung cancer by 3T MRI with contrast enhanced radial T1-wieghted 3D spoiled gradient echo sequence comparison with CT analysis

W. Kwon; Wonju/KR

Purpose: To clarify pleural invasion classification of primary lung cancer by 3T MRI with radial T1-wieghted 3D spoiled gradient echo sequence compared with computed tomography (CT)

Methods and Materials: Pathologically confirmed pleural invasion of non-small cell lung cancer between 2016 and 2018 were retrospectively reviewed. A 64-channel multidetector CT and 3T MRI equipped with radial volumetric interpolated breath-hold examination (VIBE) were compared in terms of length of contact, angle of mass margin, the relation of the lesion to pleura, ratio of the interface between tumor and neighboring structures to maximum tumor diameter, the relationship with convex border of primary lung cancer and pleural invasion, and smooth margin of interface between primary lung cancer and pleura on MR.

Results: Eighteen patients (13 men and 5 women; mean age, 74.4 years; age range, 56–88 years) were enrolled. Histologically the non-small cell lung cancers were diagnosed as 11 adenocarcinoma and 7 squamous cell carcinoma. Nine cases of pleural invasion (PL) 0, 8 cases of PL 1 and 1 PL 2 were analyzed. Tumor size was respectively 5.01 ± 2.12cm, 3.98 ± 1.72cm, and 2.7cm. MRI revealed same finding of smooth margin of interface between primary lung cancer and pleura for PL 0 and PL 1 and 100% sensitivity and specificity in all 17 cases. One case of PL 2 showed irregular margin of interface. There was no significantly different at length of contact and angle of mass margin in case of PL 0 and PL 1 on CT. There were no significantly different between MRI and CT for the relation of the lesion to pleura, ratio of the interface between tumor and neighboring structures to maximum tumor diameter, and the relationship with convex border of primary lung cancer and pleural invasion.

Conclusion: Absence or visceral pleural invasion can be classified using smooth margin of tumor interface by MRI with radial VIBE sequence and that is superior to CT analysis.

References:
1. *Use of CT to evaluate pleural invasion in non-small cell lung cancer: measurement of the ratio of the interface between tumor and neighboring structures to maximum tumor diameter. Radiology 2013;267:619-626*
2. *Pleural tags on CT scans to predict visceral pleural invasion of non-small cell lung cancer that does not abut the pleura. Radiology 2016;279:590-596*
3. *Convex border of peripheral non-small cell lung cancer on CT images as a potential indicator of pleural invasion. Medicine 2017;96:e7323*
4. *Multivariate analysis of pleural invasion of peripheral non-small cell lung cancer-based computed tomography features. JCAT 2016;40:757-762*

Long-term outcome after surgical treatment for part-solid lung cancer less than 3 cm: Single institutional experience

T.H. Kim, C.H. Park, D.H. Moon, S. Lee; Seoul/KR

Purpose: Ground glass opacity nodule (GGN) with or without part-solid portion is a common finding of early lung adenocarcinoma. There have been many studies on GGNs, but the extent and appropriate timing of surgical resection and lymphadenectomy are controversial. We report a long-term surgical outcome of GGNs with or without part-solid portion in early lung adenocarcinoma.

Methods and Materials: From march 2008 to December 2016, we retrospectively analyzed 202 patients who had undergone resection of GGNs less than 3 cm. GGNs were divided into three groups: pure-ground glass nodule (P-GGN) without solid portion, part-solid GGN with less than 5 mm of solid portion (PS-GGN < 5 mm), and part-solid GGN with greater than 5 mm of solid portion (PS-GGN > 5 mm). Solid portions were defined as areas above -400 HU on CT images. The 5-year overall survival rate and recurrence-free survival rate after surgical treatment were compared.

Results: There were 74 male and 128 female. The median age was 59 years old (range, 30-82 years). The median follow-up period was 40 months (range, 19-125 months). There were 45 P-GGNs (22.3%), 49 PS-GGNs < 5 mm (24.2%) and 108 PS-GGNs > 5 mm (53.5%). Invasive adenocarcinoma was found in 8 patients with P-GGNs (17.8%), 21 with PS-GGNs < 5mm (42.9%), and 100 with PS-GGNs ≥ 5mm (92.6%) (p < 0.01). The 5-year overall survival rate was 100% in patients with P-GGN and PS-GGN < 5 mm, and 97.2% in patients with PS-GGN ≥ 5mm. The recurrence-free survival rate was 100% for P-GGN and PS-GGN < 5 mm, and 91.7% for PS-GGN ≥ 5mm (p = 0.01).

Conclusion: Pure GGNs and PS-GGN < 5mm showed excellent long-term surgical outcome, but PS-GGN ≥ 5mm showed relatively high tumor recurrence rate. Therefore, when performing surgery for PS-GGN ≥ 5mm, adequate resection margin and lymph node dissection are needed.

References:
1. *Surgical outcome of combined subsegmentectomy in right upper lobe for GGO -dominant early stage lung cancer: Analysis of 7 cases. Okamoto K, Hanaoka J. Respir Med Case Rep. 2018;26:123-125.*
2. *The role of the ground-glass opacity ratio in resected lung adenocarcinoma. Huang TW, Lin KH, Huang HK, Chen YI, Ko KH, Chang CK, Hsu HH, Chang H, Lee SC. Eur J Cardiothorac Surg. 2018;54(2):229-234.*
3. *Radiological classification of multiple lung cancers and the prognostic impact based on the presence of a ground glass opacity component on thin-section computed tomography. Hattori A, Matsunaga T, Takamochi K, Oh S, Suzuki K. Lung Cancer. 2017;113:7-13.*

CT-derived Area and Density of Pectoralis Muscle Associated Disease Severity and Longitudinal Change in Chronic Obstructive Pulmonary Disease

S.H. Bak, S.O. Kwon, S.-S. Han, W.J. Kim; Chuncheon/KR

Purpose: The present study aimed to assess the ability of computed tomography (CT)-derived pectoralis muscle area (PMA) and pectoralis muscle density (PMD) in diagnosing chronic obstructive pulmonary disease (COPD) severity and longitudinal pulmonary function changes in patients with COPD.

Methods and Materials: Two hundred and ninety-three participants were included in this study, and 222 participants completed three additional visits after the first. PMA and PMD measurements were recorded on a single axial slice, above the aortic arch on baseline, of a chest CT. Emphysema index and bronchial wall thickness were quantitatively assessed for all scans. We used the generalized linear mixed model to examine associations between PMA and PMD measurements and pulmonary function.

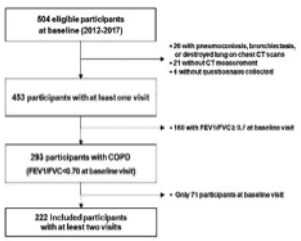

Figure 1, flowchart for study population

Results: PMA and PMD were significantly associated with baseline lung function and emphysema severity. Subjects with the greatest PMA and PMD had significantly less airflow obstruction (β, 0.064; 95% confidence interval, 0.03-0.09). PMA showed an association with CAT score. However, PMD did not show associations with either CAT score or modified Medical Research Council scores. In addition, neither PMA nor PMD was associated with changes in FEV1 over 3 years.

Conclusion: CT-derived features of the pectoralis muscle could be helpful in predicting disease severity in patients with COPD, and were not associated with longitudinal changes in lung function.

References: Marquis K, Debigare R, Lacasse Y, et al. Midthigh muscle cross-sectional area is a better predictor of mortality than body mass index in patients with chronic obstructive pulmonary disease. Am J Respir Crit Care Med 2002; 166: 809-813.
McDonald ML, Diaz AA, Ross JC, et al. Quantitative computed tomography measures of pectoralis muscle area and disease severity in chronic obstructive pulmonary disease. A cross-sectional study. Ann Am Thorac Soc 2014; 11: 326-334.
McDonald MN, Diaz AA, Rutten E, et al. Chest computed tomography-derived low fat-free mass index and mortality in COPD. Eur Respir J 2017; 50.
Cleary LC, Crofford LJ, Long D, et al. CT based muscle density predicts muscle function and health-related quality of life in patients with idiopathic inflammatory myopathies. Arthritis care & research 2015; 67: 1031.

Is it meaningful to evaluate the thyroid attenuation on unenhanced chest CT?

J.J. Woo, Y. Kim, J.K. An, R.K. Yoon; Seoul/KR

Purpose: To determine if low thyroid attenuation on unenhanced chest CT correlate with thyroid functional abnormality

Methods and Materials: This was a retrospective study of 385 patients who underwent both unenhanced chest CT and thyroid function tests performed within 1 year of the CT examination. Attenuation of the thyroid gland and of surrounding muscle was evaluated in each patient. Results of thyroid function tests were used to classify thyroid function as hypothyroid, euthyroid, or hyperthyroid. Thyroid CT attenuation of patients with abnormally low TSH and high TSH were compared to those with normal TSH. The difference of thyroid attenuation and surrounding muscle attenuation was classified into 2 group (low and high) and analysed to determine the relationship with status of thyroid function.

Results: Both high and low TSH group demonstrated significantly decreased thyroid attenuation ($p<0.014$). Low difference between thyroid and muscle attenuation group also significantly more likely to have abnormal thyroid function ($p<0.025$).

Conclusion: There is a significant correlation between thyroid attenuation on unenhanced CT and serum TSH levels. Also low density gap between thyroid and surrounding muscle is strongly associated with abnormal thyroid function. So abnormally decreased thyroid attenuation finding merits inclusion in the radiology report to suggest the possibility of abnormal thyroid function.

References: Pankow BG, Michalak J, McGee MK. Adult human thyroid weight. Health physics. 1985;49(6):1097-1103. Imanishi Y, Ehara N, Shinagawa T, et al. Correlation of CT values, iodine concentration, and histological changes in the thyroid. Journal of computer assisted tomography. 2000;24(2):322-326. Nachiappan AC, Metwalli ZA, Hailey BS, Patel RA, Ostrowski ML, Wynne DM. The thyroid: review of imaging features and biopsy techniques with radiologic-pathologic correlation. Radiographics. 2014;34(2):276-293. Maldjian PD, Chen T. Is visual assessment of thyroid attenuation on unenhanced CT of the chest useful for detecting hypothyroidism? Clinical Radiology. 2016;71(11):1199.e1199-1199.e1114. Pandey V, Reis M, Zhou Y. Correlation between computed tomography density and functional status of the thyroid gland. Journal of computer assisted tomography. 2016;40(2):316-319.

Early detection of chronic complicated bronchopleural fistula after pulmonary resection in longitudinal CT follow up

J.W. Baek, J.-Y. Han, K.-N. Lee, S.J. Choi; Busan/KR

Purpose: The purpose of our study is to evaluate risk factors for progression to chronic complicated bronchopleural fistula (BPF) after pulmonary resection in longitudinal CT follow up.

Methods and Materials: We retrospectively reviewed the 34 cases of BPF after pulmonary resection between 2010 and 2017 by longitudinal CT scans. We compared the clinical and radiologic characteristics of the group who had progressed to chronic complicated BPF (n=6) and the group who showed complete recovery from initial infection (n=20) in longitudinal CT scan. The clinical and radiologic risk factors for the chronic complicated BPF were examined by logistic regression analysis among total patients with BPF.

Results: The course of pleural cavity in follow up CT ($p=0.045$), the duration of BPF before developing complication ($p<0.001$), the thickness of cavity wall ($p=0.009$) were significantly different between the two groups. Risk factors for progression to chronic complicated BPF were revealed as the course of pleural cavity in follow up CT (OR = 21.0, 95% CI = 1.84-240.52), the duration of BPF before developing complication (over 3 months) (OR = 13.3, 95% CI = 1.05-169.56), the thickness of cavity wall over 5mm (OR = 14.7, 95% CI = 1.16-185.74) in univariate analysis.

Conclusion: Risk factors for progression to chronic complicated BPF might be identified in the follow up CT scans.

References:
1. *Khan JH, Rahman SB, McElhinney DB, Harmon AL, Anthony JP, Hall TS, Jablons DMJAC, Annals T: Management strategies for complex bronchopleural fistula. 2000, 8(1):78-84.*
2. *Uramoto H, Hanagiri T: The development of bronchopleural fistula in lung cancer patients after major surgery: 31 years of experience with 19 cases. Anticancer Res 2011, 31(2):619-624.*
3. *Varoli F, Roviaro G, Grignani F, Vergani C, Maciocco M, Rebuffat C: Endoscopic treatment of bronchopleural fistulas. Ann Thorac Surg 1998, 65(3):807-809.*
4. *Hollaus PH, Lax F, el-Nashef BB, Hauck HH, Lucciarini P, Pridun NS: Natural history of bronchopleural fistula after pneumonectomy: a review of 96 cases. Ann Thorac Surg 1997, 63(5):1391-1396; discussion 1396-1397.*
5. *Westcott JL, Volpe JP: Peripheral bronchopleural fistula: CT evaluation in 20 patients with pneumonia, empyema, or postoperative air leak. Radiology 1995, 196(1):175-181.*
6. *Mao R, Ying PQ, Xie D, Dai CY, Zha JY, Chen T, Jiang GN, Fei K, Chen C: Conservative management of empyema-complicated post-lobectomy bronchopleural fistulas: experience of consecutive 13 cases in 9 years. J Thorac Dis 2016, 8(7):1577-1586.*

The use of low dose chest CT in healthcare workers with latent pulmonary tuberculosis

Y. Choi, M.Y. Kim, K. Jin; Seoul/KR

Purpose: To investigate prevalence and image findings of tuberculosis (TB) on chest radiograph and low-dose chest CT(LDCT) in healthcare workers with latent TB infection (LTBI).

Methods and Materials: Among 1,976 hospital personnel screened for LTBI with Interferon-Gamma Release Assays (IGRAs), IGRA-positive subjects were retrospectively analyzed. On chest radiographs, clustered nodular or linear-streaky opacities of upper lung were defined as positive. LDCT findings were classified into 4 categories: active TB, indeterminate activity of TB, inactive TB, and normal. Clustered centrilobular nodules and/or cavitary consolidation were classified as active TB; tiny ill-defined nodules and minimal reticulation as indeterminate TB; fibronodular scarring as inactive TB. Medical records were reviewed to confirm whether anti-TB treatment was started in IGRA-positive subjects.

Results: IGRA was positive in 255 (12.9%). Among 144 (56.5%) IGRA-positive subjects only underwent chest radiograph, there were no positive chest radiograph. LDCT was performed in 111 (43.5%) in addition to chest radiograph. Normal was found in 103 subjects (92.7%). There was no subject with inactive TB on LDCT. Eight (0.7%) of 111 subjects were active (n=5) or indeterminate TB (n=3) on LDCT. Among those 8 subjects, chest radiograph was positive in 5 (62.5%); 3 from 5 active and 2 from 3 indeterminate. Empirical anti-TB treatment was began in 8 subjects with active or indeterminate TB on LDCT.

Conclusion: The use of LDCT for IGRA-positive subjects leads to the sensitive detection of TB-positive findings.

References: Use of low-dose computed tomography to assess pulmonary tuberculosis among healthcare workers in a tuberculosis hospital. He W et al. Infect Dis Poverty. 2017 24;6:68
Tuberculosis contact investigation using interferon-gamma release assay with chest x-ray and computed tomography. Fujikawa et al. PLoS One. 2014; 14;9:e85612
Diagnostic accuracy of chest radiography for the diagnosis of tuberculosis (TB) and its role in the detection of latent TB infection: a systematic review. Piccazzo R et al. J Rheumatol Suppl. 2014;91:32-40
Tuberculosis screening using IGRA and chest computed tomography in patients with inflammatory bowel disease: A retrospective study. Song DJ et al. J Dig Dis. 2017;18:23-30

Therapeutic and monitoring devices in the thorax: Radiographic evaluation of findings and complications

Y.-H. Kim[1], J.E. Lee[1], K.N. Lee[2]; [1]Gwangju/KR, [2]Busan/KR

Learning objectives: Describe the clinical indications and physiology of the therapeutic and monitoring devices in the thorax Describe and illustrate the appropriate position for the devices on chest radiographs Describe and illustrate the complication associated with the devices

Background: We frequently encountered therapeutic and monitoring devices in the thorax, especially with patients of poor clinical condition. It is imperative that we have to realize correct and incorrect position of the therapeutic and monitoring devices for patient care.

Imaging findings OR Procedure details: Describe the correct positions of bronchopulmonary devices, esophageal devices, cardiac devices, endovascular devices, Illustrate the incorrect positions of the devices Illustrate and describe complications associated with the devices.

Conclusion: Chest radiographs are frequently used to confirm placement of devices. Radiologist plays a vital role and have to familiarize with correct or abnormal position of these devices on chest radiographs & identifying complications in a timely fashion.

References:
1. *Stone DJ, Gal TJ. 6th ed. Philadelphia: Elsevier Churchill Livingstone; 2005. Airway Management: In Miller's Anesthesia; 1431–2.*
2. *Metheny NA. Preventing respiratory complications of tube feedings: evidence-based practice. Am J Crit Care. 2006;15:360–9.*
3. *Durai, R., Hoque, H., & Davies, T.W. Managing a chest tube and drainage system. AORN, 91(2), 275-283.*
4. *Wang L, McFadden S, Ruetz L, Feasibility of monitoring thoracic congestion with impedance measured from an ICD lead system in a chronic heart failure dog model, PACE 2000;23(4): p. 612.*
5. *Sigakis CJG, Mathai SK, Suby-Long TD, Restauri NL, Ocazionez D, Bang TJ, Restrepo CS, Sachs PB, Vargas D. Radiographic Review of Current Therapeutic and Monitoring Devices in the Chest. Radiographics. 2018;38(4):1027-1045*
6. *Marik PE. Noninvasive cardiac output monitors: a state-of the-art review. J Cardiothorac Vasc Anesth. 2013;27(1):121–134.*

Pattern approach of mosaic attenuation: Radiological anatomy and strategy for differentiation

E.-J. Kang, K.-N. Lee, T.-H. Ham; Busan/KR

Learning objectives:
1. To review the radiological anatomy of mosaic attenuation on chest CT
2. To categorize various etiology and pathophysiology of mosaic attenuation
3. To discuss how to differentiate the underlying cause of mosaic attenuation

Background: Mosaic attenuation is commonly encountered imaging pattern on chest computed tomography (CT), however the differential diagnosis is broad. The main causes of the mosaic attenuation can categorized to disease affecting small airways, pulmonary vasculature, and interstitium (alone or combination). The major difficulty of differential diagnosis is which areas of lung attenuation are normal and which area abnormal. Moreover, the parenchymal heterogeneity of lung can occur in even though normal individuals.

Imaging findings OR Procedure details:
(1) Radiological anatomy of mosaic attenuation
  A. Normal lung attenuation on chest CT
  B. Parenchymal heterogeneity in normal individuals
(2) Etiology and pathophysiology
  A. Air airway disease
  B. Pulmonary vascular disease
  C. Parenchymal lung disease
(3) Strategy for differentiation

Conclusion: In this educational exhibition, we are going to describe radiological anatomy of mosaic attenuation on chest CT, and discuss how to differentiate the underlying cause of them.

References:
1. *Kligerman SJ, Henry T, Lin CT, Franks TJ, Galvin JR. Mosaic Attenuation: Etiology, Methods of Differentiation, and Pitfalls. Radiographics. 2015;35:1360-80.*
2. *Ridge CA, Bankier AA, Eisenberg RL. Mosaic attenuation. AJR Am J Roentgenol. 2011;197:W970-7.*
3. *Abbott GF, Rosado-de-Christenson ML, Rossi SE, Suster S. Imaging of small airways disease. J Thorac Imaging. 2009;24:285-98*

Comorbidities of Lung Emphysema

C.H. Park, Y.T. Kim, S.S. Jou; Cheonan/KR

Learning objectives: The purpose of presentation is to describe the radiologic findings underlying pulmonary emphysema with pulmonary comorbidities including infection, fibrosis, primary lung cancer, hemorrhage, and other rare conditions.

Background: Emphysema is a type of chronic obstructive pulmonary disease that causes permanent enlargement of the alveolar process due to the destruction of the alveolar wall. Chronic obstructive pulmonary disease accounts for the fourth leading cause of adult mortality in the United States and is expected to be the third leading cause of death in 2020. Some reports evaluating the cause of death in patients with chronic obstructive pulmonary disease suggest that patients are more likely to die of comorbidities rather than chronic obstructive pulmonary disease. Emphysema may be accompanied by various complications or concurrent disease, such as pulmonary infection, lung cancer, pneumothorax, pulmonary arterial hypertension, cor pulmonale, chest deformities such as barrel chest, and saber sheath trachea. If pulmonary emphysema is accompanied by these comorbidities, it may show different and unique findings according to the change of lung parenchyme due to underlying emphysema.

Imaging findings OR Procedure details: Comorbidities of underlying pulmonary emphysema
1. Infection
2. Combined fibrosis
3. Lung cancer
4. Pulmonary hemorrhage
5. Other rare conditions

Conclusion: Pulmonary emphysema can combined with various pulmonary comorbidities. Various radiologic findings can be seen according to changes of lung parenchyme due to underlying pulmonary emphysema. Understanding these radiological findings may help to diagnose and treat these comorbidities.

References:
1. Cavailles A, Brinchault-Rabin G, Dixmier A, et al. Comorbidities of COPD. Eur Respir Rev 2013;22:454-475.
2. Chatila WM, Thomashow MB, Minai OA et al. Comorbidities in chronic obstructive pulmonary disease. Proc Am Thorac Soc 2008;5:549-555.
3. Friedman PJ. Imaging studies in emphysema. Proc Am Thorac Soc 2008;5:494-500.

Comparison of digital tomosynthesis and chest radiography for prediction of calcification in pulmonary nodule: A phantom study

S. You, J.S. Sun, K.J. Park, Y.-H. Jang, T. Ha, S. Heo; Suwon/KR

Purpose: To compare the effectiveness of digital tomosynthesis (DTS) with chest radiography (CXR) to predict calcification in solitary pulmonary nodules (SPNs) according to the nodule size and location.

Methods and Materials: Synthetic three different sizes (8, 12, and 15 mm) and densities (40, 250 HU) of SPNs (0~4 nodules/1 exam) were inserted into 8 different area of lung phantom classified as danger or non-danger zone. DTS and CXR were all performed at the same time for every 60 examinations. Two sets of image data were randomly arranged and five observers independently reviewed all images in a random order. Five observers were asked to identify nodule and score confidence for calcification on SPN with 4 scales. They also recorded interpretation time. The jackknife alternative free-response receiver operating characteristic (JAFROC) was used to analyze overall diagnostic performance for two modalities in terms of ability to detect SPNs and to predict calcification of SPNs.

Results: Among all observers, nodule detection performance was better in DTS (AUC = 0.91) than in CXR (AUC=0.52). Overall, the sensitivity and specificity of calcification prediction in CXR were 61.1% and 89.2%, respectively, and those in DTS were 98% and 99.9%, respectively. Also the positive predictive value and negative predictive value of DTS (99.1%, 98.9%) were higher than that of CXR (90.3%, 58.8%). In DTS, diagnostic performance of calcification prediction was better in both danger zone nodules and non-danger zone nodules. On CXR, the predictability of calcification in danger zone nodules was less than in non-danger zone nodules, but there was no significant difference of calcification predictability between in danger zone nodules and in non-danger zone nodules on DTS exam. AUC value in DTS was also significantly higher than in CXR, regardless of nodule size.

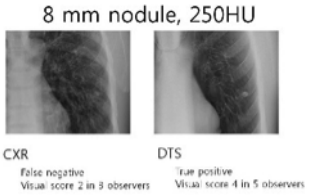

There is calcific nodule in Lt lung. 3 observers readed this nodule as noncalcified nodule. But all 5 observers readed this nodule as calcified nodule on DTS

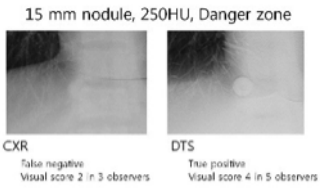

There is calcific nodule in Rt lung danger zone, which is obscured by dyaphragm. 3 observers readed this nodule as noncalcified nodule. But all 5 observers readed this nodule as calcified nodule.

Conclusion: The DTS significantly improved the diagnostic performance to predict calcification of SPNs than CXR, especially nodules located in danger zone that easily obscured by superimposed vascular structure and bone structure.

Radiographic Findings of Intrapulmonary Hemorrhage as a Complication of Clopidogrel Use in a Patient with Acute Coronary Syndrome

D. Sung, E.-S. Lee, S.-Y. Shin; Seoul/KR

Purpose: Clopidogrel is an effective antiplatelet agent that is used as an adjuvant to percutaneous coronary intervention (PCI) with promising antithrombotic effects. Intrapulmonary hemorrhage following PCI is a rare complication. We report a case of bleeding in a patient treated with a clopidogrel immediately after PCI.

Methods and Materials: A 53-year-old man visited the emergency department with continuous, severe substernal chest pain associated with sweating, radiating to both shoulders and the back. Laboratory tests revealed elevated heart and liver enzymes. An emergency coronary angiogram showed total occlusion in the middle segment of the left anterior descending (LAD) artery, severe stenosis of the proximal segment of the LAD, severe stenosis of the mid to distal segment of the left circumflex artery and proximal segment of the right coronary artery (RCA), and moderate stenosis of the middle segment of the RCA. Percutaneous transluminal coronary angioplasty (PTCA) was done and followed by maintenance doses of aspirin 100 mg and clopidogrel 75 mg. Three days later, the patient presented with hemoptysis and nasal bleeding with dyspnea.

Results: The chest radiograph obtained at admission showed haziness of the central lung zones and blurring of the hilar shadows, suggesting mild pulmonary edema. A follow-up chest radiograph revealed worse bilateral alveolar infiltration in both lungs, prominent upper lobes, and bilateral pleural effusion. In a chest radiograph obtained 5 days after PTCA, the bilateral infiltrations and pleural effusions were increased slightly. Chest computed tomography revealed diffuse patchy ground-glass opacity with a crazy-paving pattern in both lungs and relative sparing of both lower lobes. Focal areas of airspace consolidation were seen in both upper lobes.

Conclusion: Patients who undergo PTCA and are given antiplatelet agents such as clopidogrel can develop hemoptysis and dyspnea. If alveolar infiltrates are seen on chest radiographs, the possibility of intrapulmonary hemorrhage must be considered. Clinicians and radiologists need to be aware of this life-threatening bleeding complication of clopidogrel

References:
1. *Fernandex-Perez GC, Vazquez M, Delgado C, et al. Pulmonary hemorrhage in a patient with acute coronary syndrome. AJR 2007;189:W135-W137*
2. *Gill DS, Ng KS. Massive pulmonary hemorrhage complicating the treatment of acute coronary syndrome. Heart 2004;90:e15*
3. *Kalra S, Bell MR, Rihal CS. Alveolar hemorrhage as a complication of treatment with abciximab. Chest 2001;120:126-131*
4. *Kilaru PK, Schweiger MJ, Kozman HA, Weil TR. Diffuse alveolar hemorrhage after clopidogrel use. J Invas Cardiol 2001;13:535-537*

Phantom Experimental study on Radiation dose to Doctors using an ambu-bag during head CT scan: Comparison study with non-Pb apron

D. Sung, E.-S. Lee, S.-Y. Shin; Seoul/KR

Purpose: For breathless or unconscious patients, head CT is often taken with a doctor using an Ambu-bag to sustain patient's respiration. In such situations, the doctor will be exposed to CT radiation even if he or she wears a radiation protection suit. By using a phantom manikin, the authors tried to report the dose the doctor would receive in various situations of head CT scan and also compare the doses depending on the thickness of the protective suit.

Methods and Materials: The doses were measured during pre-contrast CT and angiography 3D CT using a systematic phantom (Kyoto Kagaku PBU-50). Assuming the ambu-bag situation, lead-free aprons corresponding to 0.3 mm Pb and 0.5 mm Pb were placed on the back of the CT gantry. Three dosimeters were placed inside of each apron. The dosimeters used were photomultiplier fluorescent dosimeters. Both pre-contrast CT and angiography 3D CT scans were repeated 5 times each with using in 0.3 mm non-Pb and 0.5 mm non-Pb aprons. Thus, we compared the radiation doses expected to be received by doctors with 0.3mm non-Pb and 0.5mm Non-pb aprons.

Results: The mean radiation dose was 0.023 mGy with 0.3 mm Non-Pb apron and 0.010 mGy with 0.5 mm Non-Pb apron after 5 scans of pre-contrast CT. The mean doses during angiographic 3D CT were 0.062 mGy for 0.3 mm Non-Pb apron and 0.025 mGy for 0.5 mm Non-Pb apron. In all situations, the voltage was 135kVP and the current was 170mA. The mean DLP values were 1652.52 mGy * cm with 0.3 mm Non-Pb apron and 1836.05 mGy * cm with 0.5 mm Non-Pb apron during pre-contrast CT, and 3084.53 mGy * cm with 0.3 mm Non-Pb apron and 3261.87 mGy * cm with 0.5 mm Non-Pb apron during angiographic 3D CT

Conclusion: In the ambu-bag situation, the exposure radiation dose when wearing a 0.5mm Non-Pb apron is reduced to less than 1/2 compared to when wearing a 0.3mm Non-Pb apron during both pre-contrast CT and and angiography 3D CT scans. Thus, wearing a 0.5mm non-Pb protective suit is an efficient way to reduce individual exposure dose.

Diverse clinical and radiologic manifestations of Tuberculosis in unusual human body parts from A to Z: Nobody shall sneak out of the white death

B.G. Choi[1], C. Kim[2], Y.H. Lee[1], S.K. Yeom[3], S.H. Hwang[2], B.-K. Je[1], K.Y. Lee[1], K.Y.Y. Lee[1]; [1]Ansan/KR, [2]Seoul/KR, [3]Ansan-si, Gyeonggi-do/KR

Learning objectives: To update and describe radiologic findings of tuberculosis (TB) in various human body parts. To review pathogenic and pathologic features of TB. To outline the imaging and clinical findings of TB in various human body parts. To suggest the differential points of TB in various human body parts.

Background: TB is one of the top 10 causes of death and the leading cause from a single infectious agent (above HIV/AIDS). Millions of people continue to fall sick with TB each year. In 2017, TB caused an estimated 1.3 million deaths (range, 1.2–1.4 million) among HIV-negative people. Because the symptoms of tuberculosis are nonspecific, it is not easy for clinicians to diagnose tuberculosis. Therefore, in this educational exhibition, we want to present the images of tuberculosis that are not typical from head to toe.

Case 1. F/17. Miliary nodules in both lungs and mediastinal lymphadenopathy including right paratracheal, subcarinal and both hilar area. Cystic change occurs after 2months. These cystic lesions significantly improved after 2 years.

Case 2. F/65. 6cm sized heterogeneously enhancing mass in Rt. frontal bone with bone destruction, mimicking primary skull origin tumor.

Case 3. M/51. 8cm sized mass-like lesion in the hepatic S4 and S2 with diffuse hepatomegaly. The lesion has multiple low-attenuation lesions.

Case 4. M/29. 7.0cm sized large cystic lesion including intracystic numerous nodules showing T1/T2 intermediate to low SI within tendon sheath along the biceps tendon. Bony erosion at volar aspect of proximal radius is also accompanied.

Cystic Change in military TB

Case 1

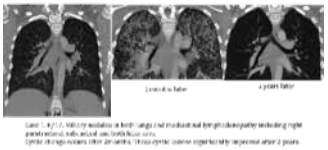

Skull tuberculosis

Case 2

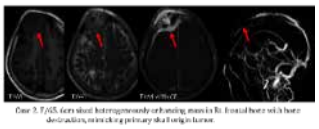

Hepatic Tuberculosis

Case 3

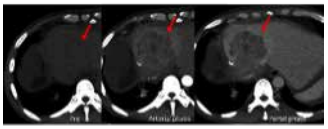

Tuberculous Tenosynovitis

Case 4

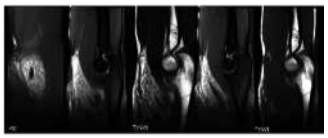

Imaging findings OR Procedure details: We will show imaging findings of atypical tuberculosis from head to toe including the following contents.

The pathogenic and pathologic features of tuberculosis (TB).

(1) Primary and recurrent (post-primary) infection
(2) Extrapulmonary tuberculosis and classic pulmonary tuberculosis.

Clinical history and radiologic findings of TB.

(1) TB in Head and Neck including calvarial tuberculosis
(2) TB in Chest, except pulmonary TB.
(3) TB in Liver
(4) TB in Kidney
(5) TB in Intestine
(6) TB in Anus
(7) TB in Spine

Conclusion: Tuberculosis presents a wide spectrum of clinical and imaging findings, and may affect many different organs in different ways.
The diagnosis requires a high degree of suspicion and, it is important that the radiologist recognizes the imaging findings allowing for the establishment of a more effective strategy to confirm the diagnosis and to institute the appropriate treatment as soon as possible.

References:

1. *Pulmonary Tuberculosis: Role of Radiology in Diagnosis and Management. Nachiappan AC, Rahbar K, Shi Xiao, et al. RadioGraphics 2017 Jan-Feb;37(1):52-72*
2. *Mycobacterial infection in immunocompromised patients. Washington L, Miller WT Jr. J Thorac Imaging. 1998 Oct;13(4):271-81.*
3. *Application of ultrasound-guided core biopsy to minimize the non-diagnostic results and the requirement of diagnostic surgery in extrapulmonary tuberculosis of the head and neck. Hvo UC, Chen CN, Lin CY, et al. Eur Radiol. 2016 Sep;26(9):2999-3005*
4. *Calvarial tuberculosis: an unusual presentation. O'Brien J, Buckley O, Persaud T, Colhoun E. Eur Radiol. 2007 Nov;17(11):3014-5.*
5. *Acute hepatobiliary tuberculosis: a report of two cases and a review of the literature. Hickey N, McNulty JG, Osborne H, Finucane J. Eur Radiol. 1999;9(5):886-9*

Tumoral and peritumoral CT radiomics for the prediction of ALK (anaplastic lymphoma kinase) and EGFR (epidermal growth factor receptor) mutation in lung adenocarcinoma

J. Choe, S.M. Lee, J.B. Seo, H.N. Noh; Seoul/KR

Purpose: To investigate the ability of tumoral and peritumoral radiomic features to predict anaplastic lymphoma kinase (ALK) and epidermal growth factor receptor (EGFR) mutation status of lung adenocarcinoma in Asian cohort patients.

Methods and Materials: Total 506 patients (M:F = 290:216, median 62 years) with pathologically proven lung adenocarcinoma were retrospectively analyzed. Within the tumoral and peritumoral regions of contrast enhanced CT scan, radiomic features were extracted from segmented volumes of each tumor. We developed radiomic signatures capable of distinguishing between mutation status, ALK+, EGFR+ or wild type (ALK– and EGFR–) using a multinomial logistic LASSO regression model in a discovery cohort (N = 350) and verified them in a temporal validation cohort (N = 156). The classification performance of the radiomics signature and combining this signature with clinical parameters were explored by using the Obuchowski index.

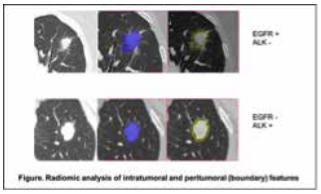

Figure 1 radiomic analysis

Results: Comparing wild type and non-wild type, there were significantly more male patients and smoker with wild-type group. The smoking pack-year was higher in the wild type compared to non-wild type group. Comparing ALK mutant and EGFR mutant group, patients with ALK mutation showed younger age (ALK+ vs EGFR+, median age 56 vs 63; P < 0.0001).
The 5 radiomics features (4 intratumoral and 1 peritumoral features) were independent predictor for classifying wild type, ALK+ and EGFR+ mutation tumors. The diagnostic performance of three classification model was 0.683 (unweighted Obuchowski C index) for tumor radiomic signature alone and 0.696 for both tumor and peritumoral radiomic signature. Combined model using clinical factors (age, sex, smoking) and radiomic signature was 0.754 in the discovery cohort and 0.634 on validation cohort. Regarding the binary classification of ALK+ and EGFR+ tumors, radiomics signature alone showed high diagnostic performance in both discovery and validation cohort (pairwise C index; 0.762 in discovery cohort and 0.705 in validation cohort).

Table

Conclusion: EGFR positive and ALK positive lung adenocarcinomas show distinct radiologic features that can be predicted by radiomic approach.

References:
1. *Braman NM, et al. Intratumoral and peritumoral radiomics for the pretreatment prediction of pathological complete response to neoadjuvant chemotherapy based on breast DCE-MRI. Breast Cancer Research. 2017;19:57-71.*
2. *Liu Y, et al. Radiomic features are associated with EGFR mutation status in lung adenocarcinomas. Clin Lung Cancer. 2016 September;17(5): 441–448.*
3. *Velazquez ER, et al. Somatic Mutations Drive Distinct Imaging Phenotypes in Lung Cancer. Cancer Res. 2017;77(14):3922-3930.*

EDUCATIONAL POSTER

P-0009 **Unusual primary lung tumors: Approach to diagnosis**
F. Ufuk[1], F. Kaya[2]; [1]Denizli/TR, [2]Afyonkarahisar/TR

P-0011 **Lung diseases presenting with multiple cysts: A diagnostic approach**
F. Ufuk; Denizli/TR

P-0012 **The many faces of Lymphangitic carcinomatosis**
F. Ufuk, G. Yavas; Denizli/TR

P-0013 **Pleural appendages, a new cause of lung nodules**
A. Villanueva Marcos[1], A. Villanueva[2], R. Ahmed[1], G. Yogarajah[1], J. Etxano[3]; [1]Redhill/UK, [2]Vigo/ES, [3]Vitoria-Gasteiz/ES

P-0015 **Differential diagnosis of infectious diseases, drug toxicity, and pulmonary infiltration due to underlying malignancy in non-AIDS immunocompromised patients using HRCT**
N. Tanaka, T. Kobayashi, Y. Kunihiro, T. Matsumoto; Ube, Yamaguchi/JP

P-0016 **Pulmonary arteriovenous malformations - A pictorial review of radiographic appearances**
N. Jawad, G.J. Robinson; Hull/UK

P-0017 **The Thorax Beyond the Lung - Pleural Neoplasms**
J. G. Santos[1], S. L. Rodrigues[1], L. Samouco[2], M. Gouvêa[1], L.F.P. Gonçalves[3]; [1]Porto/PT, [2]Porto/PT, [3]Braga, BR/PT

P-0018 **Thymus: A journey through normal and pathological imaging manifestations**
L. Samouco[1], S.L. Rodrigues[2], D.F. Soares[3], D. Fonseca[4], M.J. Magalhães[2], M. Gouvêa2; 1Porto /PT, [2]Porto/PT, [3]Braga/PT, [4]Senhora da hora/PT

P-0021 **Esophageal Lymphatic Drainage - A Pictorial Review**
J.G. Santos[1], C.A. Baraças[2], L.H.C.B. Samouco[1], S.L. Rodrigues[1], N. Costa[1], L.F.P. Gonçalves[3], M. Gouvêa[1]; [1]Porto/PT, [2]Pedrouços-Maia/PT, [3]Braga, BR/PT

P-0022 **Pulmonary infections: A pictorial essay of the main imaging signs**
G. Meirelles[1], J. Capobianco[1], P.R.P. Santana[2], V.B. Antunes[1], A.V.B. Pavani[1], V. Lajarin[1], C. Figueiredo[1], C.A.Y. Verrastro[1], I. Missrie[1], T. Franquet[3]; [1]Sao Paulo/BR, [2]Sao Paulo, SP/BR, [3]Barcelona/ES

P-0024 **Thoracic imaging findings in patients with primary humoral immunodeficiency**
P. Patel, I. Karafotias, S.D. Tran, N. Mulholland, G. Yusuf, K. Stefanidis; London/UK

P-0025 **Smoking-related Interstitial Lung Diseases: HRCT findings and pathological correlations**
S. Caruso, G. Marrone, R. Liotta, F. Crinò, A. Di Piazza, G. Gentile, V. Carollo, G. Mamone, M. Milazzo, E. Oddo; Palermo/IT

P-0028 **Only diffuse cystic lesion of the lung**
S. Caruso, G. Marrone, F. Crinò, A. Di Piazza, V. Carollo, G. Mamone, G. Gentile, L. Maruzzelli, R. Miraglia, M. Milazzo; Palermo/IT

P-0030 **CT findings of Pulmonary Nocardiosis**
R.S.S. AL Umairi[1], S. AL Tai[2], F. AL Kindi[2]; [1]119074/SG, [2]Muscat/OM

P-0040 **The Role of Interventional Radiologist in the Treatment of Complications after Lung Transplantation**
S. Caruso, R. Miraglia, L. Maruzzelli, P. Vitulo, A. Di Piazza, G. Marrone, V. Carollo, F. Crinò; Palermo/IT

P-0042 **Complications from ablative therapy for atrial fibrillation**
J. P. Kanne[1], T. Henry[2], H. Mann[3], S. kligerman[4], D. Godwin[5]; [1]Madison, WI/US, [2]San Francisco/US, [3]Salt Lake City, UT/US, [4]San Diego/US, [5]Seattle, WA/US

P-0043 **Pleuroparenchymal fibroelastosis - Imaging features of a rare and under-recognised disorder**
K. Kwan; Singapore/SG

P-0044 **Asbestos - forbidden, but not forgotten**
L. Tamkevičiūtė[1], A. Tumenas[1], J. Zaveckiene[1], M. Arzanauskaite[2]; [1]Kaunas/LT, [2]Liverpool/UK

P-0046 **Vulnerable Coronary Plaques - Imaging Findings on Coronary CTA That I Should I Know!**
J. Noschang, R. Caruso Chate, W.Y. Ishikawa, P. Netto, H. Shoji, G.B.S. Teles, R. Neto, B. Freitas, M.B.D.G. Funari, G. Szarf; São Paulo/BR

P-0048 **Imaging of the Pericardium**
G. Szarf, G. Meirelles, C. Verrastro, V.B. Antunes, I. Missrie, A. Marchini da Silva, C. Figueiredo, A.V.B. Pavani, V. Lajarin, J. Capobianco; Sao Paulo/BR

P-0049 **Imaging of lung transplantation and common postoperative complications**
Y. Choi, W.H. Cho, D.H. Kim; Yangsan/KR

P-0050 **Clinicoradiologic significance of Late-Onset Noninfectious Pulmonary Complications (LONIPCs) after allogenic hematopoietic stem cell transplantation (HSCT)**
K.E. Shin[1], J.S. Park[2], J.W. Lee[3]; [1]Bucheon-si, Gyeonggi-do/KR, [2]Bucheon/KR, [3]Seoul/KR

P-0053 **Seeing through the fog - A review of adenocarcinoma spectrum lesions in the lung and their staging according to TNM 8**
A. Leandru, V. Halai, L. Chen, A. Wallis; Portsmouth/UK

P-0054 **Chest Magnetic Resonance Imaging: Current Applications and Future Perspectives**
Y.J. Jeong, Y. Lee, J.W. Lee, S.M. Park, G. Lee; Busan/KR

P-0057 **Comorbidities of Lung Emphysema**
C.H. Park, Y.T. Kim, S.S. Jou; Cheonan/KR

P-0058 **„Reality TB": An educational imaging case series of pulmonary and extra-thoracic tuberculosis initially misdiagnosed as malignancy**
S. Mahboobani, D. Olakunbi, C. Ross, M. Berry, M. Coleman, N.H. Strickland; London/UK

P-0059 **Health Effects of Electronic Cigarettes**
I. Willekens, J. de Mey; Brussels/BE

P-0060 **Imaging review of the spectrum of thoracic manifestations in rheumatoid arthritis**
V. Quintana Checa, P. Olmedilla, S. Hernandez Muniz, E. Gonzalez-Cardenas, P. Muñoz Hernandez, J. Fernandez-Garcia; Madrid/ES

P-0061 **A pictorial review of incidental cardiac findings in a non- cardiac dedicated CT**
J. Todd, M. Arzanauskaite; Liverpool/UK

P-0063 **Behçet disease: A rare and fatal cause of massive haemoptysis**
D. Cozzi[1], C. Moroni[1], M.C. Bonini[1], C. Fattorini[1], A. Bindi[2], E. Cavigli[2], M. Bartolucci[1], V. Miele1; [1]Florence/IT, [2]Firenze/IT

P-0065 **Imaging of Collagen Vascular Diseases: Spectrum of the Intrathoracic Manifestations**
V.B. Antunes, J. Capobianco, G. Meirelles, I. Missrie, C. Verrastro, A.V.B. Pavani, G. Szarf, A. Marchini da Silva, V. Lajarin, C. Figueiredo; Sao Paulo/BR

P-0066 **Multimodality imaging in connective tissue disease-related interstitial lung disease**
C.A.S. Ruano[1], M.F. Moraes-Fontes[1], S. Pinheiro[1], A. Borba[1], O. Fernandes[1], S.I.C. Silva[1], T. Bilhim[1], K.L. Irion[2]; [1]Lisbon/PT, [2]Manchester/UK

P-0067 **Intracranial manifestations in diffuse parenchymal lung diseases, a pictorial review**
R.-I. Milos, F. Prayer, M.T. Schmook, F. Oberndorfer, D. Prayer, H. Prosch; Vienna/AT

P-0068 **The four targets in malignant pleural mesothelioma (MPM)**
A. Villanueva Marcos[1], J. Broncano[2], M.J. Garcia-Velloso[3], R. Ahmed[1], K. Sabarwal[1]; [1]Redhill/UK, [2]Córdoba/ES, [3]Pamplona/ES

P-0069 **Primary Pulmonary Meningioma: A Rare Entity with Diagnostic Challenge**
K. Peldschus, D.S. Steurer, D.I. Apostolova, T. Frenzel; Hamburg/DE

P-0071 **Lungs of stone – A review of pulmonary calcification and other causes of high attenuation lesions in the lungs**
L. Chen[1], V. Halai[2], A. Leandru[3], A. Wallis[1]; [1]Portsmouth/UK, [2]Waterlooville/UK, [3]Portsmouth/UK

P-0072 **Get it off your chest! A no-nonsense guide to intrathoracic venous anomalies**
A. Vahedi[1], M. Arzanauskaite[1], A. Ganguly[2], S. Hesni[2]; [1]Liverpool/UK, [2]London/UK

P-0073 **‚A Narrow Escape' - An unusual complication of cement embolisation after vertebroplasty**
S. Hesni[1], A. Vahedi[2], M. Roddie[1], M. Naik[1]; [1]London/UK, [2]Liverpool/UK

P-0074 **‚Caught in the Middle' - An interesting cause of bowel obstruction visible on chest radiography**
S. Hesni[1], A. Vahedi[2], M. Roddie[1], A. Tamimi[3]; [1]London/UK, [2]Liverpool/UK, [3]Basildon/UK

P-0075 **The benign pulmonary nodule – So it's not cancer, what now?**
L. Chen[1], V. Halai[2], A. Leandru[3], A. Wallis[1]; [1]Portsmouth/UK, [2]Waterlooville/UK, [3]Portsmouth/UK

P-0076 **Imaging findings and follow-up in thoracic amyloidosis**
M. Lacroix[1], J.S. Rech[2], C. De Margerie-Mellon[1], H. Nunes[2], Y. Uzunhan[2], B. Arnulf[1], P.-Y. Brillet[3]; [1]Paris/FR, [2]Bobigny/FR, [3]Bobigny/FR

P-0080 **Ground-Glass Opacities in Patients Diagnosed with Chronic Hypersensitivity Pneumonitis**
M. Radeljak Protrka, M. Vukelic Markovic, R. Huzjan Korunic, M. Simic, J. Tekavec-Trkanjec, B. Brkljacic; Zagreb/HR

P-0082 **Imaging findings of central venous catheters related complications: a pictorial review**
P.R.P. Santana, M.O. Coelho, G.R. Oki, B.L. Moreira, A.K. Medeiros, I. Missrie, C.A.Y. Verrastro, G. Meirelles, A.C.P. Gomes; Sao Paulo/BR

P-0083 **Pattern approach of mosaic attenuation: Radiological anatomy and strategy for differentiation**
E.-J. Kang, K.-N. Lee, T.-H. Ham; Busan/KR

P-0084 **Differential Diagnosis of Bronchiectasis**
P.R.P. Santana, J.W.M. Trindade Jr., B.B. Libânio, P.R. Almeida, A.K. Medeiros, B.L. Moreira, V.B. Antunes, J. Capobianco, G. Meirelles, A.C.P. Gomes; Sao Paulo/BR

P-0086 **Heterotaxy syndrome with laevocardia and abdominal inversion (HLAI): An uncommon anomaly?**
C. Vila[1], A. Villanueva Marcos[2], O. Persiva Morenza[1], R. Vidal[1], R. Ahmed[3]; [1]Barcelona/ES, [2]Huntingdon/UK, [3]Redhill/UK

P-0087 **The various etiologies of the "pulmonary vein sign"**
C.F. Munoz-Nunez, D. Veiga-Canuto, L.F. Londoño-Villa, M.P. Calvillo, C. Fonfria, L. Trilles, A. Carreres; Valencia/ES

P-0088 **Diverse clinical and radiologic manifestations of Tuberculosis in unusual human body parts from A to Z: Nobody shall sneak out of the white death**
B.G. Choi[1], C. Kim[2], Y.H. Lee[1], S.K. Yeom[3], S.H. Hwang[2], B.-K. Je[1], K.Y. Lee[1], K.Y. Lee[1]; [1]Ansan/KR, [2]Seoul/KR, [3]Ansan-si, Gyeonggi-do/KR

P-0091 **Imaging in Lung Cancer Staging – A Review of TNM 8 and Treatment Implications**
V. Halai, L. Chen, A. Leandru, A. Wallis; Portsmouth/UK

P-0092 **Imaging in Idiopathic Pulmonary Fibrosis (IPF) - Review of the Revised International Guidelines and Implications on Management**
V. Halai, L. Chen, A. Leandru, A. Wallis; Portsmouth/UK

P-0093 **Cardiac devices on chest radiograph: A pictorial review**
C. Salem Ramakumaran, O. Bebb, D. Schlosshan, A.L. Johnstone; Leeds/UK

P-0094 **Pathologies of the Large Airways: Tumors and tumorslike**
L. Mazzamurro, C. Valdesi, S. Conte, L. Fabrizio, M. Scutti, R.L. Patea, M. Mereu, A.R. Cotroneo; Chieti/IT

P-0095 **Nodules Gone Wild: A Case Review of Tiny (Sub-6mm) Pulmonary Nodules Which Develop into Lung Cancer**
D. Dressler, D.J. Borgaonkar, K. Greenlaw, D. Manos; Halifax/CA

P-0096 **Thoracic and systemic complications in oncologic patients: Main imaging findings**
C. Valdesi[1], L. Fabrizio[2], M. Scutti[3], L. Mazzamurro[4], M. Mereu[1], R.L. Patea[1], A.R. Cotroneo[1]; [1]Chieti/IT, [2]San Salvo/IT, [3]Guardiagrele/IT, [4]Pescara/IT

P-0097 **CT findings of pulmonary metastatic disease**
C. Valdesi[1], S. Conte[1], L. Fabrizio[2], M. Scutti[3], L. Mazzamurro[4], M. Mereu[1], R.L. Patea[1], A.R. Cotroneo[1]; [1]Chieti/IT, [2]San Salvo/IT, [3]Guardiagrele/IT, [4]Pescara/IT

P-0100 **Eosinophilic lung diseases: Allergies, infections and vasculitis; what we need to know**
J. Capobianco, G. Meirelles, V.B. Antunes, G. Szarf, C. Verrastro, A.V.B. Pavani, P.R.P. Santana, C. Figueiredo; Sao Paulo/BR

P-0101 **Alveolar opacities in critically ill patient: A confusing or a helpful finding?**
L. Fabrizio[1], S. Conte[1], A. Travaglini[1], M. Scutti[2], L. Mazzamurro[3], M. Mereu[1], R.L. Patea[1], A.R. Cotroneo[1]; [1]Chieti/IT, [2]Guardiagrele/IT, [3]Pescara/IT

P-0102 **Radiological features of patients with cryptogenic organizing pneumonia (COP) diagnosis: Onset and follow-up radiological patterns**
F. Tiralongo[1], M. Palermo[2], G. Distefano[3], F. Libra[1], S.E. Torrisi[1], G. Sambataro[1], L.A. Mauro[1], A. Basile[1], C. Vancheri[1], S. Palmucci[1]; [1]Catania/IT, [2]Catania/IT, [3]Ragusa/IT

P-0103 **Bronchial Arteries – A practical approach for the general radiologist**
J.M. Almeida, J.M. Veiga, C.A.S. Ruano, C. Leal, O. Fernandes, L. Figueiredo; Lisbon/PT

P-0105 **Pulmonary Infections in Immunocompromised Patients: HRCT findings**
S. Conte, M. Scutti, L. Fabrizio, C. Valdesi, L. Mazzamurro, M. Mereu, R.L. Patea, A.R. Cotroneo; Chieti/IT

P-0106 **Between two lungs: Cardiac findings in non-gated CT**
M.N.C.D. Silva[1], A.T. Vilares[2], A. Carvalho[1], I. Portugal[1], M.S.C. Rodrigues[1], A.J.B.S. Madureira[1]; [1]Porto/PT, [2]Espinho/PT

P-0107 **Therapeutic and monitoring devices in the thorax: Radiographic evaluation of findings and complications**
Y.H. Kim[1], J.E. Lee[1], K.N. Lee[2]; [1]Gwangju/KR, [2]Busan/KR

P-0108 **Clinical and radiological features of chest calcifications: Distribution, appearance and underlying causes**
F. Libra[1], M. Palermo[2], G. Distefano[3], F. Tiralongo[1], S. Torrisi[1], A. Libra[1], A. Vancheri[1], A. Basile[1], C. Vancheri[1], S. Palmucci[1]; [1]Catania/IT, [2]Catania/IT, [3]Ragusa/IT

P-0111 **The great pretender – pulmonary inflammatory pseudotumour. Imaging findings with pathologic correlation**
V. Buroviené[1], M. Arzanauskaite[2], J. Zaveckiene[1]; [1]Kaunas/LT, [2]Liverpool/UK

P-0112 **Diagnosing Idiopathic Pulmonary Fibrosis according to updated 2018 diagnostic criteria guidelines: A case-based pictorial review**
M. Benegas Urteaga, M. Sanchez, I. Vollmer, F. Hernandez, C. Lucena, J. Ramirez, J. Sellares; Barcelona/ES

Abstracts appear as submitted to the abstract/poster submission system and have not been checked for correctness and completeness.

SCIENTIFIC POSTER

P-0001 **Aspergilloma in Honeycomb Cysts**
F. Ufuk, M. Demirci; Denizli/TR

P-0002 **Transthoracic rebiopsy for mutation analysis in lung adenocarcinoma: Outcomes and risk factors for non-diagnostic specimen in 199 patients**
B. Nam, T.J. Kim, K. Park, M.-J. Ahn, Y.-L. Choi, M.J. Chung, T.S. Kim, K.S. Lee; Seoul/KR

P-0003 **Thoracic calcifications on magnetic resonance imaging: Correlations with computed tomography**
J. Zampieri[1], G. Pacini[1], M. Zanon[2], S. Altmayer[1], G. Watte[1], G. Meirelles[3], E. Marchiori[4], A.S. Souza Jr.[5], B. Hochhegger[1]; [1]Porto Alegre/BR, [2]Porto Alegre, RS/BR, [3]Sao Paulo/BR, [4]Rio de Janeiro/BR, [5]Sao Jose do Rio Preto/BR

P-0004 **Quantitative computed tomography phenotypes, spirometric parameters, and episodes of exacerbation in heavy smokers: An analysis from South America**
M. Barros[1], B. Hochhegger[1], S. Altmayer[1], G. Watte[1], M. Zanon[2], A.P. Sartori[1], G. Pacini[1], J.M. Chatkin[1]; [1]Porto Alegre/BR, [2]Porto Alegre, RS/BR

P-0005 **18F-FDG PET/CT and Whole-body MRI Diagnostic Performance in M staging non-small cell lung cancer: A Systematic Review**
T. Medeiros[1], G. Watte[1], G. Pacini[1], M. Zanon[2], S. Altmayer[1], M. Barros[1], G. Meirelles[3], K.L. Irion[4], E. Marchiori[5], B. Hochhegger[1]; [1]Porto Alegre/BR, [2]Porto Alegre, RS/BR, [3]Sao Paulo/BR, [4]Manchester/UK, [5]Rio de Janeiro/BR

P-0006 **Bronchiolocentric interstitial pneumonia: Correlation with signs of esophageal disease and possible bronchoaspiration**
M.R. Lourenco, C.V.B. Machado, D.T. Wada, I.B Sanches, L.R. Alves, F. EG Cipriano, A. T Fabro, J.A. Baddini-Martinez, M.K. Santos; Ribeirao Preto/BR

P-0007 **Correlation between the SUVmax and CT texture features determined by FDG-PET/CT of lung adenocarcinoma and squamous cell carcinoma using free research software**
Y. Tomori, S. Murayama, K. Ishigami, T. Yamashiro, H. Tomita, M. Tsubakimoto; Nishihara-cho, Okinawa/JP

P-0008 **Deep Learning for Classification of A Small (≤2cm) Pulmonary Nodule on CT Imaging: A Preliminary Study**
K.J. Chae[1], G.Y. Jin[1], S.-B. Ko[2], Y. Wang[2], H. Zhang[2], E.J. Choi[1], H. Choi[1]; [1]Jeonju/KR, [2]Saskatoon/CA

P-0010 **Relation between peripheral to central pulmonary artery diameter ratio with chronic obstructive pulmonary disease severity**
V.F. Ilyas, A.G. Icksan, R. Wihastuti, A. Fuady, J. Prihartono; Jakarta/ID

P-0019 **Evaluation of the impact of Ultra Low Dose Chest Computed Tomography in the antibiotics prescription in patients with suspected community-acquired pneumonia - Preliminary data**
D.P. Bianco, T. Accorsi, R. Caruso Chate, G.B.S. Teles, H. Shoji, R. Sasdelli Neto, R.B.D. Passos, W.Y. Ishikawa, M.B.D.G. Funari, G. Szarf; São Paulo/BR

P-0020 **Diagnostic Accuracy of CT and Pathologic Correlation of Lung Adenocarcinoma Spectrum Lesions**
K. Greenlaw[1], A. Sedlic[2], J.R. Mayo[3]; [1]Halifax, NS/CA, [2]Vancouver/CA, [3]Vancouver, BC, BC/CA

P-0023 **Lung cancer detected through CT surveillance of incidental lung nodules**
H.R. Alomaish[1], A. Suhail[2], C. Crocker[2], V. Luong[2], D. Manos[3]; [1]Toronto, ON/CA, [2]Halifax/CA, [3]Halifax, NS/CA

P-0026 **Comparison of digital tomosynthesis and chest radiography for prediction of calcification in pulmonary nodule: A phantom study**
S. You, J.S. Sun, K.J. Park, Y.-H. Jang, T.Y. Ha, S. Heo; Suwon/KR

P-0027 **Testing of different scoring methods of lung HRCT in patients with scleroderma**
J. Vanasek, E. Kocova, M. Hyrsl, E. Cermakova, T. Soukup, P. Elias; Hradec Králové/CZ

P-0029 **Long-term outcome after surgical treatment for part-solid lung cancer less than 3 cm: Single institutional experience**
T.H. Kim, C.H. Park, D.H. Moon, S. Lee; Seoul/KR

P-0031 **Thoracic CT Findings Predictive of Treatment in Drowning**
N. Tsuchiya[1], Y. Ohno[2], Y. Nakano[3], T. Yamashiro[1], S. Gibo[4], M. Schiebler[5], S. Murayama1; [1]Okinawa/JP, [2]Kobe/JP, [3]Shiga/JP, [4]Urasoe, Okinawa/JP, [5]Madison, WI/US

P-0032 **Chest HRCT findings in former cigarette smokers**
E. Detorakis[1], M. Raissaki[2], K. Antoniou[2], I. Papadopoulou[2], R. Illing[3]; [1]Iraklion/GR, [2]Heraklion/GR, [3]Budapest/HU

P-0033 **Unveiling image findings in secondhand smokers – The role of chest HRCT**
E. Detorakis[1], M. Raissaki[2], K. Antoniou[2], I. Papadopoulou[2], R. Illing[3]; [1]Iraklion/GR, [2]Heraklion/GR, [3]Budapest/HU

P-0037 **Is it meaningful to evaluate the thyroid attenuation on unenhanced chest CT?**
J.J. Woo, Y. Kim, J.K. An, R.K. Yoon; Seoul/KR

P-0038 **Diagnostic outcome and safety of CT-guided core needle biopsy for mediastinal mass: A Systematic review and meta-analysis**
H.N. Lee; Seoul/KR

P-0041 **HRCT findings after balloon pulmonary angioplasty (BPA)**
E. Rasciti, F. Niro, D. Attinà, N. Galiè, F. Monteduro, L. Lovato; Bologna/IT

P-0045 **LDCT lung cancer screening in populations at different risk for lung cancer**
G.B.S. Teles, A.C. Macedo, R. Caruso Chate, G. Szarf, M.B.D.G. Funari; Sao Paulo/BR

P-0047 **Ciliated muconodular papillary tumor of the lung: thin-section CT findings of 16 cases**
M. Kusumoto, Y. Onishi, H. Watanabe, S. Watanabe, N. Motoi; Tokyo/JP

P-0051 **Atypical patterns of sarcoidosis on thoracic HRCT: A retrospective analysis from a regional reference center**
G. Distefano, M. Palermo, F. Libra, F. Tiralongo, S.E. Torrisi, A. Vancheri, G. Sambataro, A. Basile, C. Vancheri, S. Palmucci; Catania/IT

P-0052 **The use of low dose chest CT in healthcare workers with latent pulmonary tuberculosis**
Y. Choi, M.Y. Kim, K. Jin; Seoul/KR

P-0055 **Significance of baseline CT assessment for predicting the pulmonary fibrosis during the course of chemotherapy-induced pneumonitis**
J.-Y. Han, J.W. Baek, K.-N. Lee, S.J. Choi; Busan/KR

P-0056 **Early detection of chronic complicated bronchopleural fistula after pulmonary resection in longitudinal CT follow up**
J.W. Baek, J.-Y. Han, K.-N. Lee, S.J. Choi; Busan/KR

P-0062 **Lung ultrasound in pulmonary tuberculosis: Preliminary results**
D. Cozzi, F. Giannelli, C. Moroni, E. Cavigli, A. Bindi, F. Rinaldi, P.G. Rogasi, M. Bartolucci, V. Miele; Florence/IT

P-0064 **Ultrasound in Scalen Lymph Node Biopsies: Correlation with Pathologic Findings**
A. Guner Akbıyık, Z.N. Tekin; Istanbul/TR

P-0070 **Diagnostic value of CT – guided transthoracic core, fine needle and the combination of these two biopsy techniques - the study on the base of 993 procedures**
M. Jelitto-Gorska[1], K. Dziadziuszko[1], M. Studniarek[1], T. Gorycki[1], B.J. Regent[2], A. Durawa[1], E. Szurowska[1]; [1]Gdansk/PL, [2]Gdynia, Pomorskie/PL

P-0077 **CT-derived Area and Density of Pectoralis Muscle Associated Disease Severity and Longitudinal Change in Chronic Obstructive Pulmonary Disease**
S.H. Bak, S.O. Kwon, S.-S. Han, W.J. Kim; Chuncheon/KR

P-0078 **Diagnostic accuracy of CT-guided core biopsy of thin-walled cavitary pulmonary lesions**
K.E. Shin[1], J.S. Park[2], J.W. Lee[3]; [1]Bucheon-si, Gyeonggi-do/KR, [2]Bucheon/KR, [3]Seoul/KR

P-0079 **A Survey of Institutions with Sixteen Detector-Rows or More CT Scanners for the Introduction of National Lung Cancer Screening Program Using Low-Dose Chest CT in S. Korea**
S.H. Paik; Deajeon/KR

P-0081 **Academic Involvement of Radiology Trainees With an Interest in Thoracic and Cardiovascular Imaging: International Survey**
M. Arzanauskaite[1], E. Terrazas[2], E. Estades[3], F. Vernuccio[4]; [1]Liverpool/UK, [2]Distrito federal/MX, [3]Wilmington/US, [4]Palermo/IT

P-0085 **CT-guided transthoracic fine needle aspirations of 781 pulmonary lesions: Risk factors for pneumothorax including the attending radiologist and cytologist**
K. Rasmark, E. Radecka, S. Nyren, P. Lindholm; Stockholm/SE

P-0089 **CT-based computational model to assess pulmonary ventilation in COPD patients: Comparison with 129Xe-MRI and SPECT images**
M. Kim, O. Doganay, T.N.H. Matin, T. Povey, F.V. Gleeson; Oxford/UK

P-0090 **Pleural invasion classification of primary lung cancer by 3T MRI with contrast enhanced radial T1-wieghted 3D spoiled gradient echo sequence comparison with CT analysis**
W. Kwon; Wonju/KR

P-0098 **Radiographic Findings of Intrapulmonary Hemorrhage as a Complication of Clopidogrel Use in a Patient with Acute Coronary Syndrome**
D. Sung, E.-S. Lee, S.-Y. Shin; Seoul/KR

P-0099 **Phantom Experimental study on Radiation dose to Doctors using an ambu-bag during head CT scan: Comparison study with non-Pb apron**
D. Sung, E.-S. Lee, S.-Y. Shin; Seoul/KR

P-0104 **Tumoral and peritumoral CT radiomics for the prediction of ALK (anaplastic lymphoma kinase) and EGFR (epidermal growth factor receptor) mutation in lung adenocarcinoma**
J. Choe, S.M. Lee, J.B. Seo, H.N. Noh; Seoul/KR

P-0109 **Lung involvement in Destombes-Rosai-Dorfman disease: Clinical and radiological features, and response to the MEK inhibitor cobimetinib**
Q. Moyon, S. Boussouar, F. Cohen Aubart, P. Maksud, N. Aladjidi, G. Prévot, J. Donadieu, Z. Amoura, P.A. Grenier, J. Haroche; Paris/FR

P-0110 **Correlation of Texture Analysis with Thymic Neoplasm Classifications: Preliminary Results**
C. Blüthgen, M. Patella, I. Schmitt-Opitz, W. Weder, T. Frauenfelder; Zurich/CH

Abstracts appear as submitted to the abstract/poster submission system and have not been checked for correctness and completeness.